



UNIVERSITEIT VAN PRETORIA
UNIVERSITY OF PRETORIA
YUNIBESITHI YA PRETORIA

*PREDICTING STAGE PERFORMANCE OF A MULTI-STAGE
CENTRIFUGAL COMPRESSOR USING THE OVERALL
COMPRESSOR PERFORMANCE CHARACTERISTIC*

SUBMITTED IN PARTIAL FULFILMENT OF THE REQUIREMENTS FOR THE DEGREE

OF

MASTER OF ENGINEERING

IN

THE DEPARTMENT OF MECHANICAL AND AERONAUTICAL ENGINEERING

UNIVERSITY OF PRETORIA

BY

DIRK HUMAN

DECEMBER 2019

Supervisor: Dr. Ghazi Mahmood (University of Pretoria)

Co-supervisor: Prof. Johan van der Spuy (University of Stellenbosch)

ABSTRACT

The reliable operation of Integrally Geared Centrifugal Compressors (IGCCs), used in the coal-fired power generation industry of South Africa, is essential for economic, environmental and safety considerations. However, due to the unavailability of individual stage performance curves, the ability of a compressor owner to identify underperforming stages to maintain these compressors proactively remains limited.

This study addresses the stage performance prediction of an IGCC when only the compressor's overall performance characteristic, in conjunction with the impeller diameters and tip speeds, are known. The study is limited to IGCCs used in the coal-fired power generation industry of South Africa.

Based on the limited inputs, two performance modelling methods were considered for this application, namely stage stacking and 1-dimensional modelling. However, stage stacking requires known operating points on each stage performance curve from which the rest of the curve can be extrapolated while 1-dimensional models require detailed stage design information to model stage performance.

This study developed a revised stage stacking procedure which in contrast to the traditional stage stacking procedure, does not require a known operating point on each stage's performance curve, for it assesses the relative stage performance at the compressor's surge flow rate. The relative maximum pressure ratio of each stage is acquired through the application of similarity principles while a simplified 1-dimensional impeller analysis model is used to assess relative impeller head coefficients.

The modelling process was developed based on performance and design data for IGCCs obtained from a compressor manufacturer. Performance data of four IGCCs, consisting of 13 stages, were obtained, including the design data for ten impellers.

Hence, the IGCCs satisfy the requirements of geometric and aerodynamic similarity, unveiling a linear relationship between the stage impeller tip speed and maximum pressure ratio. A simplified 1-dimensional performance model was used to assess relative impeller head coefficients. A verification procedure ensured the integrity of the findings of the 1-dimensional model was maintained by comparing the model results to findings obtained using commercial compressor performance modelling software. A sensitivity analysis was conducted on the 1-dimensional performance model to ascertain which input parameters could be scaled as a function of the impeller tip diameter.

For the four IGCCs for which data were obtained, the stage-discharge pressure and isentropic efficiency curves were calculated using the developed model. The maximum variation between the


measured and calculated pressure and isentropic efficiency curves equaled 8.20% and 10.84%, respectively. The prediction accuracy of the developed modelling procedure is similar to map-based models found in literature and is considered adequate for identifying an underperforming stage. Thus, the developed model could serve as a valuable conditioning monitoring tool for site-based compressor owners.

Keywords: IGCC, stage performance, stage stacking, Aungier, sensitivity analysis, similarity principles, parameterised, non-dimensional

DECLARATION

I, the undersigned, hereby declare that:

- I understand what plagiarism is and I am aware of the University's policy in this regard;
- the work contained in this dissertation is my own original work;
- I did not refer to work of current or previous students, lecture notes, handbooks or any other study material without proper referencing;
- where other people's work has been used, this has been properly acknowledged and referenced;
- I have not allowed anyone to copy any part of my dissertation;
- I have not previously in its entirety or in part submitted this dissertation at any university for a degree.

Signature of student: 

Name of student: Dirk Human

Student number: 28053347

Date: 05/12/19

TABLE OF CONTENTS

ABSTRACT	II
DECLARATION	IV
TABLE OF CONTENTS	V
LIST OF FIGURES	VIII
LIST OF TABLES	X
NOMENCLATURE	XI
INTRODUCTION	15
1.1. STUDY BACKGROUND	15
1.2. RESEARCH PROBLEM STATEMENT	18
1.3. MAIN STUDY OBJECTIVES	18
1.4. CHAPTER OUTLINE	18
LITERATURE STUDY	20
2.1. INTRODUCTION	20
2.2. INTEGRALLY GEARED CENTRIFUGAL COMPRESSORS	21
2.3. COMPRESSOR AERO-THERMODYNAMICS	24
2.3.1. Compressor flow analysis	24
2.3.2. Similarity principle	27
2.4. MAP-BASED COMPRESSOR PERFORMANCE MODELS	31
2.4.1. Stage stacking	31
2.4.2. Polynomial regression	33
2.5. 1-DIMENSIONAL COMPRESSOR PERFORMANCE MODELS	34
2.5.1. Impeller Performance	37
2.6. CONCLUSION	40
DEVELOPED STAGE STACKING PROCEDURE	43

3.1. INTRODUCTION	43
3.2. PARAMETERIZED PERFORMANCE CURVES	44
3.2.1. Pressure ratio curves	45
3.2.2. Maximum pressure ratio	47
3.2.3. Head coefficient curves	48
3.2.4. Maximum head coefficient	49
3.3. Stage stacking	50
3.3.1. Discharge pressure	51
3.3.2. Head coefficient	53
3.4. CONCLUSION.....	55
SIMPLIFIED 1-DIMENSIONAL IMPELLER ANALYSIS MODEL	57
4.1. INTRODUCTION	57
4.2. VALIDATION OF 1-DIMENSIONAL ANALYSIS MODEL	58
4.2.1. Validation approach	58
4.2.2. Results and discussion	60
4.3. SENSITIVITY ANALYSIS	62
4.3.1. Analysis approach.....	62
4.3.2. Results and discussion	63
4.4. COMPARATIVE IMPELLER DESIGN	65
4.4.1. Design approach.....	65
4.4.2. Design inputs	66
4.5. CONCLUSION.....	69
STAGE STACKING PROCEDURE ILLUSTRATION AND VALIDATION	70
5.1. INTRODUCTION	70
5.2. STAGE STACKING PROCEDURE ILLUSTRATED	70
5.2.1. Obtaining stage pressure curves	71
5.2.2. Obtaining stage efficiency curves	75
5.3. VALIDATION RESULTS AND DISCUSSION	83

5.4. CONCLUSION.....	84
SUMMARY AND CONCLUSION	85
6.1. EXECUTIVE SUMMARY.....	85
6.2. CONCLUSION.....	86
6.3. RECOMMENDATIONS FOR FURTHER RESEARCH.....	87
BIBLIOGRAPHY	88
APPENDIX A: IMPELLER PERFORMANCE MODELLING	xcii
APPENDIX B: MEASURED COMPRESSOR PERFORMANCE DATA	ciii
APPENDIX C: COMPAERO® STAGE DESIGN AND ANALYSIS.....	cxii
APPENDIX D: IMPELLER GEOMETRY.....	cxv
APPENDIX E: IMPELLER PERFORMANCE MODEL SENSITIVITY ANALYSIS	cxx
APPENDIX F: STAGE STACKING PROCEDURE VALIDATION	cxvii

LIST OF FIGURES

Figure 1: Pneumatic conveying plant	15
Figure 2: TA-3000 Integrally geared centrifugal compressor (Courtesy of Kriel Power Station).....	16
Figure 3: Horizontal cross-section of an Integrally Geared Compressor, image adapted from Gas Processing & LNG	21
Figure 4: Schematic of an IGCC's process flow	21
Figure 5: S-type impeller (left) and channel diffuser (right).....	22
Figure 6: Standard overall performance characteristic supplied with an IGCC, adapted from performance map of a TA3000 IGCC (Courtesy of Kriel Power Station)	23
Figure 7: Impeller inlet velocity diagram assuming no pre-swirl is present (left). Impeller tip velocity diagram (right).	24
Figure 8: Mollier diagram for a complete centrifugal compressor stage, adapted from (Dixon and Hall, 2010)	26
Figure 9: Non-dimensional impeller tip velocity diagram (Ludtke, 2004). A typical S-shaped and R-shaped impeller tip is indicated with the symbol S and R respectively.	30
Figure 10: Effect of different stage' damage mechanisms on the overall performance of a compressor, adapted from Mathioudakis and Stamatis (1994)	32
Figure 11: Stage curves calculation flow chart Mathioudakis and Stamatis (1994).....	32
Figure 12: Pressure ratio (left) and isentropic efficiency (right) of the Eckardt O impeller modelled with different loss correlation sets (Oh et al., 1997)	35
Figure 13: Total pressure ratio and efficiency modelled for the HPCC impeller (Li et al., 2015)	35
Figure 14: Impeller performance modelling employing the model of Aungier (2000)	37
Figure 15: Flow chart of the iterative procedure, adapted from Aungier (2000)	40
Figure 16: Stage total-to-total pressure ratio at the compressor surge flowrate.....	45
Figure 17: Compressor 3, stage total-to-total pressure ratio as a function of the dry air mass flow rate.....	46
Figure 18: Compressor 3, stage total-to-total pressure ratio as a function of the change in dry air mass flow rate	46
Figure 19: Stage maximum pressure ratio as a function of the impeller tip speed.....	48
Figure 20: Compressor 3, stage head coefficient as a function of dry air mass flowrate.....	49
Figure 21: Compressor stations when implementing the stage stacking procedure	51
Figure 22: Pressure ratio stage stacking procedure	53

<i>Figure 23: Head coefficient stage stacking procedure.....</i>	<i>55</i>
<i>Figure 24: Impeller geometry in the $r-\theta$ plane (left) and impeller inlet geometry (right)</i>	<i>58</i>
<i>Figure 25: Impeller geometry in the $r-Z$ plane</i>	<i>59</i>
<i>Figure 26: Impeller pressure ratio comparison</i>	<i>60</i>
<i>Figure 27: Impeller head coefficient comparison</i>	<i>61</i>
<i>Figure 28: Impeller discharge pressure approximation.....</i>	<i>66</i>
<i>Figure 29: Non-dimensional impeller tip velocity diagrams at surge flow rate.....</i>	<i>68</i>
<i>Figure 30: Overall performance curves of Compressor 3.....</i>	<i>70</i>
<i>Figure 31: Stage discharge pressure before minimization of the pressure cost function</i>	<i>72</i>
<i>Figure 32: Stage discharge pressure after the minimization of the pressure cost function</i>	<i>73</i>
<i>Figure 33: Stage discharge pressure calculated with known inter cooler pressure drop values.....</i>	<i>74</i>
<i>Figure 34: Isentropic head coefficient curves of Compressor 3.....</i>	<i>75</i>
<i>Figure 35: Head coefficients curves of Compressor 3 before minimization of the power cost function</i>	<i>78</i>
<i>Figure 36: Calculated coupling power before minimization of the cost function</i>	<i>78</i>
<i>Figure 37: Calculated coupling power after the minimization of the power cost function</i>	<i>79</i>
<i>Figure 38: Head coefficient curves of Compressor 3 after minimization of the power cost function</i>	<i>80</i>
<i>Figure 39: Stage isentropic efficiency curves</i>	<i>81</i>
<i>Figure 40: Stage isentropic efficiency calculated with known intercooler pressure drop and CTD values.....</i>	<i>82</i>
<i>Figure 41: Relative error of calculated stage total discharge pressure</i>	<i>83</i>
<i>Figure 42: Absolute error of calculated stage isentropic efficiency</i>	<i>83</i>

LIST OF TABLES

Table 1: Measured performance parameters of IGCCs.....	44
Table 2: Validation stage inlet conditions and required performance parameters.....	58
Table 3: Validation stage impeller geometry	59
Table 4: Total-to-total pressure ratio comparison.....	60
Table 5: Head coefficient comparison.....	61
Table 6: Effect of varying input parameters on the prediction accuracy of Aungier's (2000) impeller analysis model.....	63
Table 7: Impeller design input parameter contribution to total calculation uncertainty.	64
Table 8: Effect on prediction accuracy using average values for all parameters excluding the main tip parameters.....	64
Table 9: Impeller non-dimensional tip values	69
Table 10: Calculated initial maximum pressure ratio values.....	71
Table 11: Initial values and bounds of the pressure ratio curve parameters.....	72
Table 12: Final values of the pressure ratio curve parameters.....	73
Table 13: Pressure loss across stage intercoolers.....	74
Table 14: Approximated impeller discharge pressure of Compressor 3.....	76
Table 15: Relative impeller head coefficients of Compressor 3.....	76
Table 16: Initial values and bounds calculated for stage head coefficients.....	77
Table 17: Final values of the head coefficient curve parameters.....	79
Table 18: CTD across intercoolers.....	82
Table 19: Relative assessment of maximum impeller head coefficients.....	84

NOMENCLATURE

Latin – Lowercase

Symbol	Description	Unit
a	Sonic velocity	m/s
b	Blade width	m
c	Constant	-
c_{fl}	Laminar skin friction coefficient	-
c_f	Transitional skin friction coefficient	-
c_{ft}	Turbulent skin friction coefficient	-
d	Diameter	m
d_H	Hydraulic diameter	m
f_c	Entropy correction factor	-
g	Gravitational constant	m/s ²
h	Specific enthalpy	J/kg
i	Stage number	-
k_m	Means streamline curvature	rad/m
\dot{m}	Mass flow	kg/s
m	Number of measured flow points	-
n	Number of compressor stages	-
p	Pressure	kPa
s	Specific entropy	J/kgK
r	Radius	m
t	Blade thickness	m
u	Impeller design parameter	-
wp	Wetted perimeter	m
y	Specific head	J/kg
z	Effective number of blades	-

Latin – Uppercase

A	Area	m ²
A_R	Throat tip area ratio	-
B_2	Impeller tip blockage factor	-

C	Absolute velocity	m/s
C_p	Isobaric specific heat	J/kgK
C_r	Contraction ratio	-
C_{U_2}'	Hypothetical tangential velocity component	m/s
C_M	Impeller disc torque coefficient	-
D_{eq}	Equivalent diffusion factor	-
F	Cost function	-
I	Work input factor	-
L	Length	m
M_a	Mach number	-
M	Torque	kgm ² /s ²
P	Power	Watt
\dot{Q}	Volumetric Flow	m ³ /s
R	Specific gas Constant	J/kgK
RH	Relative humidity	-
Re	Reynolds number	-
R_{rot}	Rothalpy	J/kg
S_D	Impeller disc clearance	m
S_{CL}	Impeller tip clearance	m
T	Temperature	K
U	Tangential Velocity	m/s
W	Relative velocity	m/s

Greek

α	Absolute angle	°
β	Relative angle	°
ε	Radius ratio	-
Δ	Difference/Change	-
ρ	Density	kg/m ³
ϕ	Flow coefficient	-
ψ	Head coefficient	-
γ	Isentropic expansion coefficient	-
λ	Impeller tip distortion factor	-
η	Efficiency	-
Π	Pressure ratio	-

μ	Kinematic viscosity	m^2/s
ω	Angular velocity	rad/s
ϖ	Pressure loss coefficient	-
σ	Slip factor	-

Subscripts

<i>app</i>	Approximate
<i>B</i>	Blade property
<i>BL</i>	Blade loading
<i>calc</i>	Calculated
<i>c</i>	Overall compressor property
<i>cr</i>	Critical Mach number loss
<i>ch</i>	Choke
<i>COR</i>	Corrected
<i>CS</i>	Cross-sectional
<i>cooler</i>	Property of intercooler
<i>cw</i>	Cooling water
<i>D</i>	Hydraulic
<i>DF</i>	Disk friction
<i>est</i>	Estimated value
<i>exit</i>	Overall compressor discharge property
<i>ext</i>	External property
<i>FB</i>	Full blade
<i>g</i>	Gas
<i>h</i>	Hub
<i>HS</i>	Hub to shroud
<i>in</i>	Overall compressor inlet property
<i>inc</i>	Incidence
<i>L</i>	Leakage
<i>Lim</i>	Limit
<i>m</i>	Meridional component
<i>max</i>	Maximum
<i>mix</i>	Mixing
<i>min</i>	Minimum
<i>mech</i>	Mechanical
<i>meas</i>	Measured
<i>MF</i>	Mean
<i>R</i>	Recirculation
<i>r</i>	Relative property
<i>ref</i>	Reference condition

s	Isentropic
SB	Splitter blade
sf	Skin friction
sh	Shroud
th	Throat
U	Tangential component
0	Total condition
1	Impeller inlet
2	Impeller outlet
3	Intercooler inlet
4	Intercooler outlet

Superscripts

*	Critical condition or property
---	--------------------------------

Mathematical

-	Average
Σ	Sum
Π	Product
$ $	Absolute value

Abbreviations

a	Absolute
BOV	Blow off valve
C	Compressor
CTD	Cold temperature difference
CFD	Computational Fluid Dynamics
EES	Engineering Equation Solver
cd	Condensate drain
cw	Cooling water
da	Dry Air
g	Guage
IGCC	Integrally geared centrifugal compressor
IGV	Inlet Guide Vane
NIST	National Institute of Standards and Technology
s	Stage

INTRODUCTION

1.1. STUDY BACKGROUND

The coal-fired power generation industry of South Africa uses compressed air for the operation of its pneumatic conveying plant (Figure 1). The conveying plant transports fly-ash produced during the



Figure 1: Pneumatic conveying plant

coal combustion process. Fly-ash is removed from flue gas exiting the boiler with an electrostatic precipitating or fabric filter plant and stored in large storage structures (hoppers). From the hoppers, the fly-ash is pneumatically conveyed to a downstream plant for further processing. Pneumatic conveying entails the collection of fly-ash into vessels beneath the hoppers, which are then pressurized using compressed air. Using specialised sealing valves opening and closing in a pre-set sequence, the vessel content is conveyed to the next plant. The fly-ash is separated from the air-

stream and once again collected in a hopper while the air is vented into the atmosphere through additional smaller fabric filter plants.

The conveying plant requires a constant supply of compressed air at specific flow rates and pressures to operate. When compressed air is supplied outside these parameters, the conveying plant cannot perform according to its design, negatively impacting upstream and downstream processes. In such an instance, the conveying system cannot remove fly-ash at the required rate. Hence, the boiler combustion rate must be reduced to prevent damage to the upstream plants, resulting in less electricity generation. In downstream processes, fluctuating pressures cause increased wear and plant equipment failure. When a component fails, fly-ash is released into the atmosphere where it poses a risk to plant personnel health (especially when inhaled), impairs visibility, restricts the ability of plant operators to safely operate the plant and damages surrounding equipment accumulating on electrical components. The reliability of the conveying plant and hence the compressor plant remain essential for economic, environmental and safety considerations.

Although designs vary based on the power plant considered, a 3000 MW power plant typically requires compressed air at a rate of 30000 Nm³/hr at a pressure of 7 bar(g). Across the coal-fired power generation industry in South Africa, approximately 100 centrifugal compressors with a combined shaft power of over 70 MW are installed. These compressors depict an integrally geared type (Figure 2), with some having been in operations since the mid-1970s and others installed as



Figure 2: TA-3000 Integrally geared centrifugal compressor (Courtesy of Kriel Power Station)

recently as 2010. Integrally geared compressors consist of multiple stages. The repair cost of a stage can amount to 30% of the total cost of a new compressor of similar capacity and duty point. This cost

remains significant, considering it excludes the losses associated with plant downtime (up to six months depending on the compressor model), and that a single compressor can consist of up to four stages.

The manufacturer, as standard practice, supplies the compressor owner with an overall compressor performance curve when installing the compressor. However, individual stage performance curves are not readily available. For older stages (manufactured between 1975 and 1990), these curves might no longer exist while for newer stages (manufactured after 1990), they are not easily obtainable due to their proprietary nature. Without stage performance curves, the compressor owner cannot immediately identify an underperforming stage when the performance of a compressor deteriorates. The compressor keeps operating until its performance degrades to a point where it can no longer yield the required pressure and throughput. The damaged stage is subsequently identified through visual inspection, which entails opening the compressor casing. After identifying the damaged stage, the compressor remains offline while the stage components required for repairs are ordered or manufactured.

The ability of the compressor owner to monitor the performance of each compressor stage in conjunction with compressor performance as a unit is required to plan maintenance activities proactively. If a compressor owner can compare the compressor stage performance against benchmark performance characteristics, the stage deterioration can be discovered before the compressor needs to be opened for inspection. This monitoring would allow the compressor owner to obtain the necessary components required for repairs in advance while the compressor keeps operating.

Various software packages exist for modelling and trending of a centrifugal compressor's operating range, but they remain limited in they require highly detailed inputs regarding the compressor's design, or they only monitor the compressor's overall performance (total suction to discharge conditions). Detailed design information is usually proprietary and difficult or impossible to obtain, while software monitoring the compressor's overall performance does not allow for the monitoring of individual stage performance.

Furthermore, obtaining the IGCC stage performance directly from measurements taken on-site is not economically feasible. To reduce costs, site-based IGCCs are not installed with the instrumentation required for detailed performance mapping, such as mass flow meters. Instead, the installed equipment remains sufficient for general performance trending and protection of stage integrity, like tripping the compressor when a stage temperature reaches the metallurgical limit. The cost of retrofitting existing site-based compressors with the instrumentation required to produce detailed stage performance characteristics makes this approach impractical.

1.2. RESEARCH PROBLEM STATEMENT

This study investigates the feasibility of producing stage performance curves for the IGCCs used in the coal-fired power generation industry of South Africa using inputs reasonably available to compressor owners on-site, namely:

- Compressor overall performance curves for both discharge pressure and power (manufacturer supplied).
- Impeller diameter of each stage.
- Tip speed of each impeller.

1.3. MAIN STUDY OBJECTIVES

It is proposed that a method allowing compressor owners to model the performance of individual stages, should be developed for a range of compressors similar in design, application, and operating range to the ones used within the coal-fired power generation industry.

The method will use a compressor's overall performance curve in conjunction with minimal design information of each stage (stage impeller tip-speed and diameter) to deduce the individual stage performance curves.

Compressor owners could use these individual performance curves to predict the stages' required operating points and compare it to the measured operating points. This evaluation will indicate if the stage's performance is decaying, permitting proactive maintenance and operating decisions.

1.4. CHAPTER OUTLINE

Following this introductory chapter, Chapter 2 presents a literature survey regarding IGCCs, compressor aero-thermodynamics, map-based compressor performance models, and 1-dimensional compressor performance models.

Chapter 3 focuses on the modelling approach developed to model stage performance, using the overall compressor performance characteristic in conjunction with impeller tip speeds and diameters.

Chapter 4 illustrates how a simplified 1-dimensional compressor analysis model, based on scaled input parameters, can be used to acquire relative impeller performance traits. A verification process ensues, whereby the results of the 1-dimensional model are compared to the results of a commercial

compressor analysis software package. A sensitivity analysis is subsequently conducted to understand the influence of design parameters on the prediction accuracy of the 1-dimensional model.

Chapter 5 applies the developed modelling approach of Chapters 3 and 4 to compressors, where the stage performance is known.

Chapter 6 summarizes the study and provides concluding remarks and recommendations for future work.

2

LITERATURE STUDY

2.1. INTRODUCTION

This thesis objective is to develop a compressor modelling methodology requiring minimal geometrical input to deduce stage performance from the overall compressor performance characteristic. Hence, this literature study scope will be limited to 1-dimensional and empirical compressor models, focusing on:

- Layout and design of integrally geared centrifugal compressors installed at coal-fired power stations in South-Africa
- Similarity principle as applied to turbomachines
- Empirical compressor models
- 1-Dimensional compressor models

2.2. INTEGRALLY GEARED CENTRIFUGAL COMPRESSORS

IGCCs offer several advantages over other compressor concepts (Simon, 1987). A distinct characteristic of an IGCC (Figure 3) is it consists of multiple pinion shafts arranged around a speed-

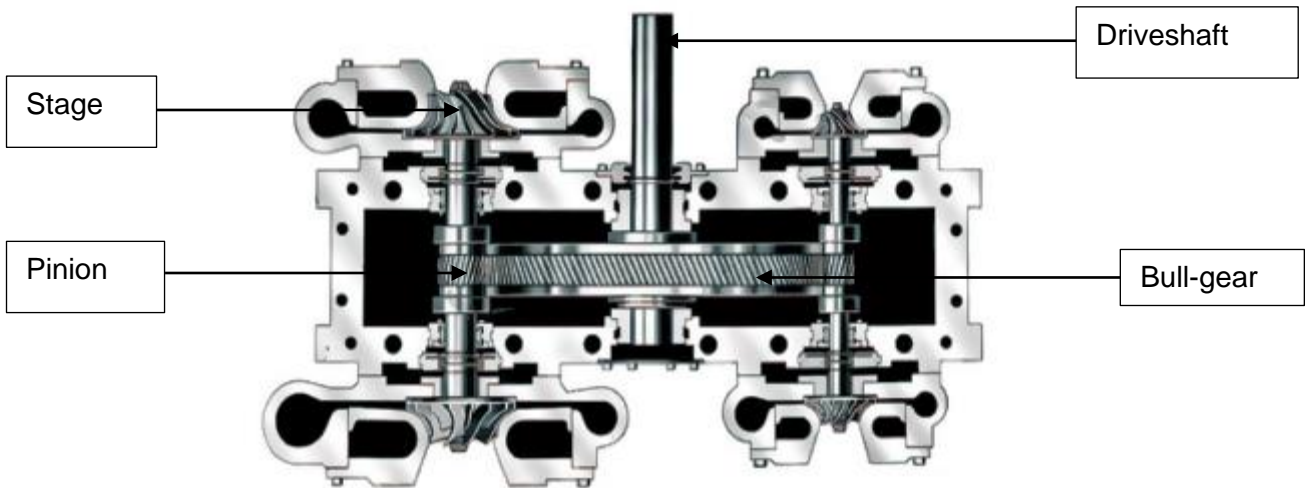


Figure 3: Horizontal cross-section of an Integrally Geared Compressor, image adapted from Gas Processing & LNG

increasing gear (bull gear). This configuration enables each impeller mounted to the end of a pinion shaft to operate at a different rotational speed selected to match the impeller's peak aerodynamic efficiency. Since these compressors operate at constant speeds, their operation is regulated through a combination of inlet guide vanes (IGV) and a blow-off valve. The IGVs are situated upstream of the first stage inlet, while the blow-off valve is located between the last stage and the compressor

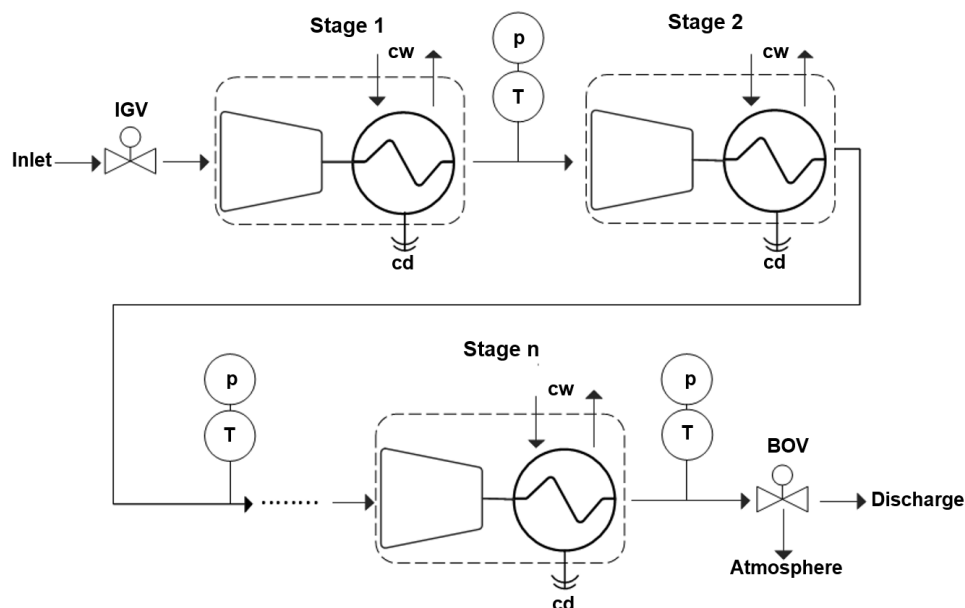


Figure 4: Schematic of an IGCC's process flow

discharge (Figure 4). The IGCC's configuration allows for intercooling of each compressor stage, improving the efficiency of the overall compression process. Protecting equipment downstream from compressor discharge, an aftercooler is usually installed downstream of the last stage. Condensation forming as the flow passes over the intercooler heat exchangers is drained to prevent carry-over and damage to the subsequent stage.

The primary compressor stage components encompass the impeller and the diffuser. The impeller-diffuser combination is designed to be aerodynamically compatible, as mismatching these elements reduces operating range and efficiencies. Several engineering disciplines determine impeller size and rotational speed setting: aero-thermodynamics determines the volume flow rate, head, efficiency and operating range; stress analysis ensures static and dynamic integrity; rotor dynamics warrant smooth running and production engineering enabling economic manufacture (Ludtke, 2004). IGCCs utilize 3-D semi-open impellers with an S-shaped blade profile and channel diffusers (Figure 5). These



Figure 5: S-type impeller (left) and channel diffuser (right)

impellers operate with high tip speeds allowing for increased volume flow rate and pressure capability when compared to traditional 3-D or 2-D impellers (Ludtke, 2004). Reducing the centrifugal load associated with these higher rotational speeds, the 3-D semi-open impeller does not have a cover disc and is referred to as semi-open (Ludtke, 2004). A diffuser is the stationary component of the compressor stage, converting the kinetic energy imparted on the fluid through the impeller into potential energy. Vaned diffusers increase the overall stage efficiency by reducing the flow field unsteadiness, which consequently reduces associated flow losses throughout the compressor (Boyce, 2003).

The IGCCs currently operating in coal-fired power plants in South-Africa were designed and manufactured between 1975 and 2010. These compressors consist of three to four stages producing compressed air at flow rates of 2400 - 8400 Nm³/hr with total-to-total pressure ratios up to 12. Since for specific applications, compressor manufacturers have pre-engineered stages and impellers with scalable geometry (Ludtke, 2004), it is reasonable to expect that for a compressor designed in a specific era all the individual stages would be aerodynamically similar. Simon (1987) and Fingerhut *et al.* (1991) presented aeronautically similar stages with impeller families designed to fit stage configurations depending on the compressor application.

It is standard practice for IGCCs to be supplied with overall compressor performance maps, such as the one depicted in Figure 6. The compressor's discharge pressure is plotted as a function of the

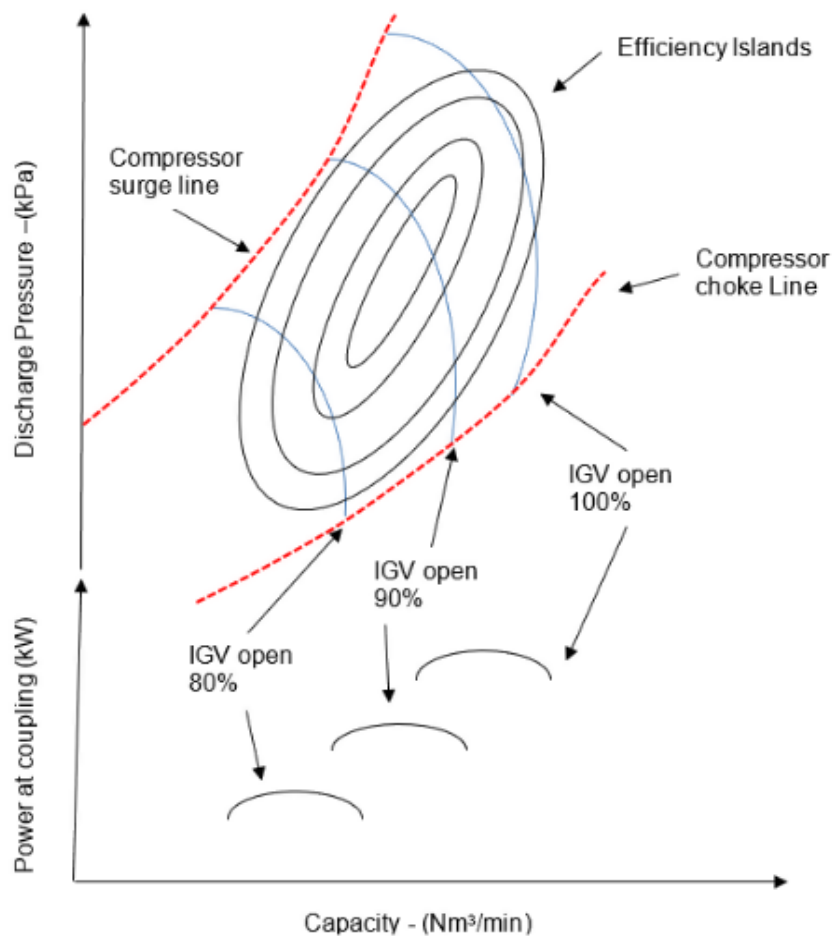


Figure 6: Standard overall performance characteristic supplied with an IGCC, adapted from performance map of a TA3000 IGCC (Courtesy of Kriel Power Station)

normalized inlet capacity of the compressor while the efficiency (normally isentropic) is plotted as a series of isometric rings, commonly known as efficiency islands. For a specific IGV position, the compressor's operating range is bounded by the surge line at one end and the choke line at the other. Similarly, the compressor coupling power is indicated as a function of the normalised inlet capacity of the compressor at each IGV setting.

2.3. COMPRESSOR AERO-THERMODYNAMICS

Aero-thermodynamics form the foundation of any compressor model, and numerous sources describe these principles, such as Dixon and Hall (2010), Ludtke (2004) and Rogers (1996). Hall and Dixon (2010) offer the theoretical reference used to discuss the concepts of section 2.3.1 while Ludtke (2004) and Balje (1981) provide the basis for the concepts discussed in section 2.3.2.

2.3.1. Compressor flow analysis

When analysing the flow through a compressor, stage velocity diagrams (Figure 7) illustrate the

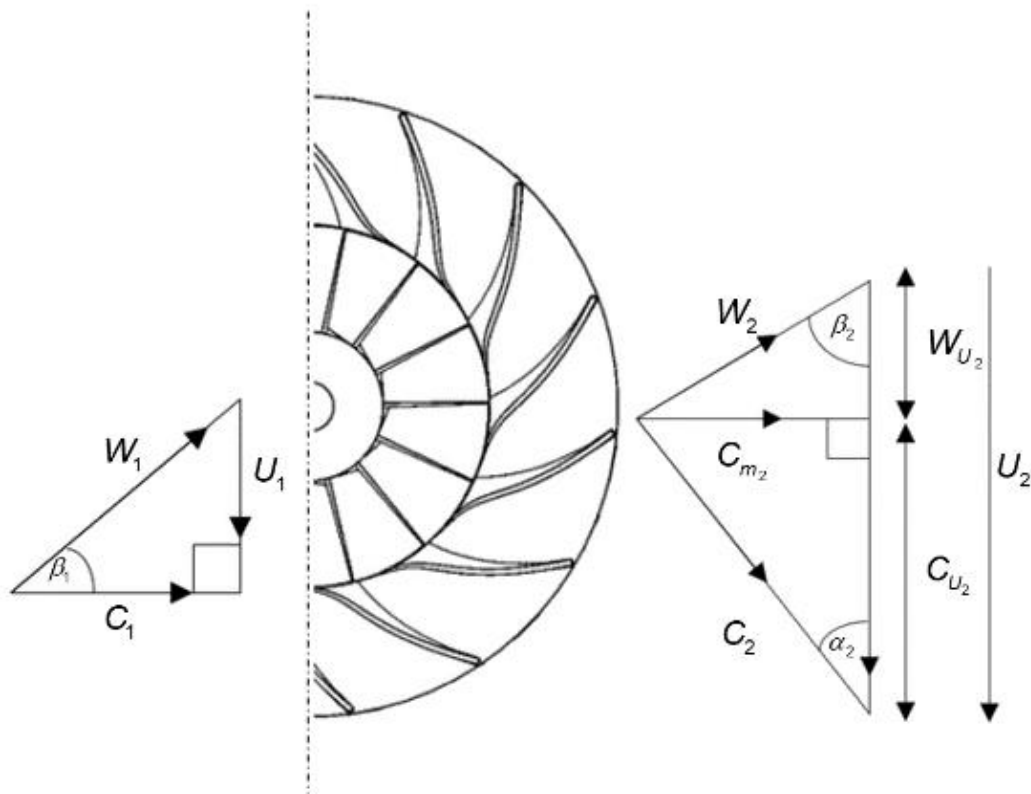


Figure 7: Impeller inlet velocity diagram assuming no pre-swirl is present (left). Impeller tip velocity diagram (right).

relationship between the absolute and relative frames of reference related to the stationary and rotating components. The torque required to impose a change in angular momentum on the fluid as it moves from the impeller inlet to impeller tip is calculated as:

$$\Sigma M = \dot{m}(r_2 C_{U_2} - r_1 C_{U_1}) \quad (2.1)$$

Notably, for no pre-swirl at the impeller inlet, the second term in the equation will be zero. The power required for an impeller revolving at a set angular velocity, and the total enthalpy change in the fluid, is therefore given by the well-known Euler Turbomachinery equation as:

$$P = \omega \Sigma M = \dot{m}(U_2 C_{U_2} - U_1 C_{U_1}) = \dot{m} \Delta h_0 \quad (2.2)$$

The relative flow leaving the impeller will receive less than perfect guidance, and the flow is said to slip (Dixon and Hall, 2010). A slip factor may be defined as:

$$\sigma = \frac{C_{U_2}}{C_{U_2}'} \quad (2.3)$$

with equation 2.2 re-written as:

$$P = \omega \Sigma M = \dot{m}(U_2 \sigma C_{U_2}' - U_1 C_{U_1}) \quad (2.4)$$

The second form of the Euler turbomachinery equation describes the energy transfer in terms of static and kinetic enthalpy rise and can be represented as:

$$\Delta h_0 = \frac{U_2^2 - U_1^2}{2} + \frac{W_1^2 - W_2^2}{2} + \frac{C_2^2 - C_1^2}{2} \quad (2.5)$$

The first two terms of equation 2.5 constitute the static and the third the dynamic enthalpy rise such that:

$$\Delta h = h_2 - h_1 = \frac{U_2^2 - U_1^2}{2} + \frac{W_1^2 - W_2^2}{2} \quad (2.6)$$

From equation 2.6, a thermodynamic property known as rothalpy can be defined as:

$$R_{rot} = h + \frac{W^2}{2} - \frac{U^2}{2} = h_{0,r} - \frac{U^2}{2} \quad (2.7)$$

Equation 2.7 depicts the difference between the total enthalpy in the relative frame of reference (relative total enthalpy), and the impeller tangential speed remains constant throughout the impeller. Rothalpy represents a useful relation in impeller analysis and will be used in the subsequent study sections.

Assessing the compression work quality requires a reference process definition. The relation between the actual process and the reference process will define the quality of the compression work.

Depending on the specific application, various reference processes can be defined: polytropic, isentropic or isothermal. Compressors utilizing intercooling normally employ an isentropic process as

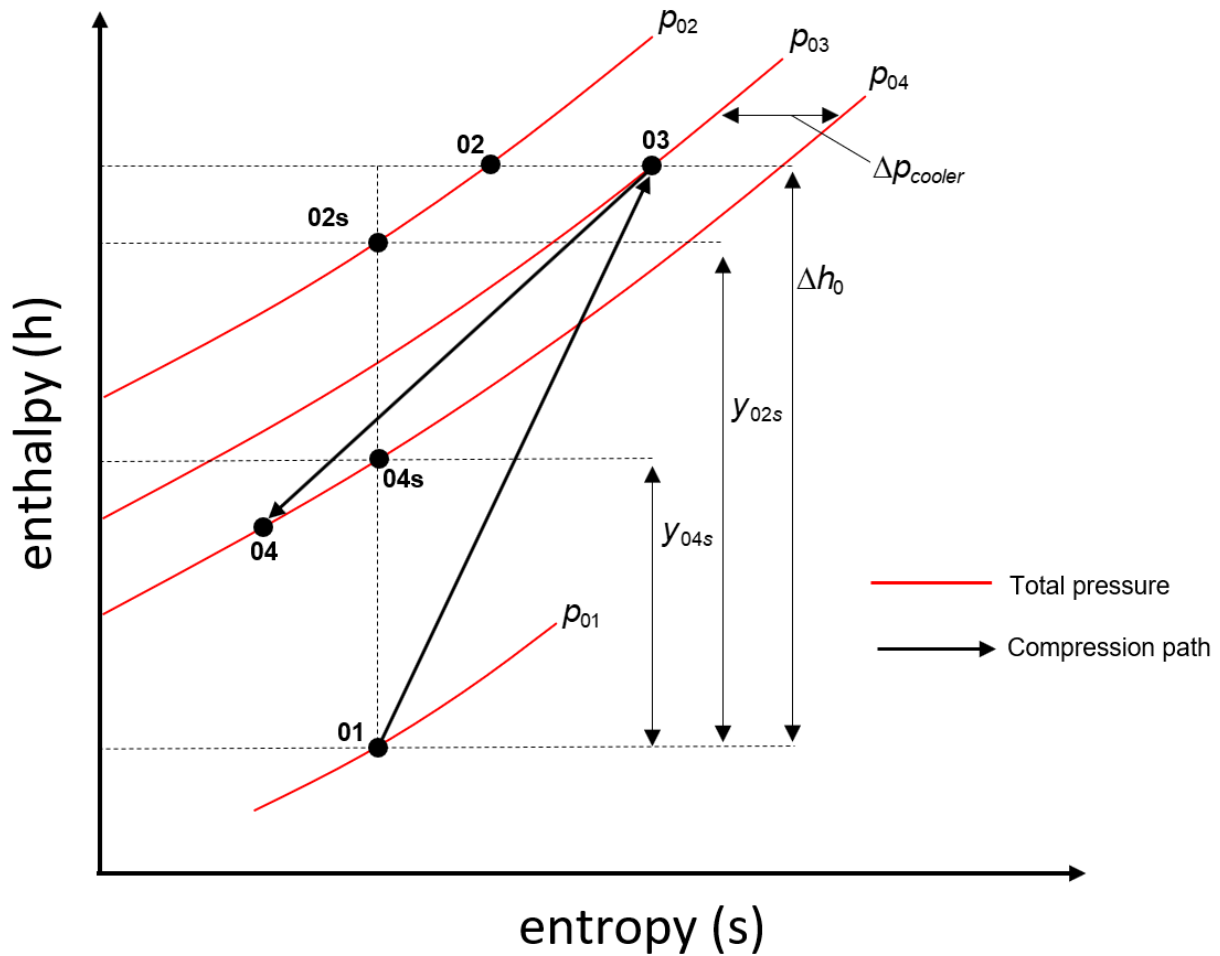


Figure 8: Mollier diagram for a complete centrifugal compressor stage, adapted from (Dixon and Hall, 2010)

reference (Ludtke, 2004). Figure 8 displays a Mollier diagram for a complete compressor stage, with intercooling (from point 03 to point 04).

The enthalpy change between states 01 and 02s defines the isentropic impeller head as:

$$y_{02s} = h_{02s} - h_{01} \quad (2.8)$$

whereas the enthalpy difference between points 01 and 02 demarcates the actual head or Euler's head:

$$\Delta h_0 = h_{02} - h_{01} \quad (2.9)$$

The isentropic total-to-total impeller efficiency is defined as:

$$\eta_{02s} = \frac{y_{02s}}{\Delta h_0} \quad (2.10)$$

Similarly, the isentropic efficiency for the stage is denoted as:

$$\eta_{04s} = \frac{y_{04s}}{\Delta h_0} \quad (2.11)$$

The stage total-to-total pressure ratio is calculated as:

$$\Pi = \frac{p_{04}}{p_{01}} \quad (2.12)$$

2.3.2. Similarity principle

Similarity considerations offer a convenient method to characterise turbomachinery. The essence of this characterisation is geometrically similar machines have similar velocity triangles at similar points in the flow path, have the same ratio of gravitational to inertial forces acting on the flow path and operate with fluids that have the same thermodynamic quality; thus, they will have equal fluid dynamic traits (Balje, 1981). The similarity principle is based on dimensional analysis (Pi theorem) used to derive non-dimensional parameters describing the relationship between variables.

2.3.2.1. Non-dimensional parameters

Numerous non-dimensional parameters characterising compressors exist in the literature. This section discusses the parameters employed for this study, namely flow coefficients (inlet and impeller tip), tip speed Mach number, and head coefficients.

Flow coefficients

The inlet flow coefficient relates the actual volume flow at the stage inlet to the impeller tip diameter and speed. A large inlet flow coefficient implies a small impeller tip diameter with a large inducer area, necessitating higher impeller rotational speeds. The inlet flow coefficient is defined as:

$$\phi_1 = \frac{\dot{Q}_1}{\frac{\pi}{4} d_2^2 U_2} \quad (2.13)$$

The most considerable flow coefficient significance engenders its effect on stage efficiency (Ludtke, 2004). A small flow coefficient value implies a small inlet hydraulic diameter to the stage, resulting in a dramatic increase in wall friction breaking down efficiency and head. For large flow coefficient

values, $\phi_1 > 0.1$, the efficiency and head deteriorate due to secondary flows and flow separation in the impeller blade channel (Ludtke, 2004).

Ludtke (2004) emphasized the usefulness of the impeller tip flow coefficient for analysing the impeller tip flow conditions. The outlet flow coefficient is depicted as:

$$\phi_2 = \frac{C_{m2}}{U_2} \quad (2.14)$$

The significance of the outlet flow coefficient is discussed in section 2.3.2.2.

Head coefficients

The stage head coefficient is computed as:

$$\psi_{04} = \frac{\Delta h_0}{U_2^2} \quad (2.15)$$

The isentropic stage head coefficient represents the isentropic head across the stage rendered non-dimensional by the impeller tip speed and is calculated as:

$$\psi_{04s} = \frac{y_{04s}}{U_2^2} = \frac{h_{04s} - h_{01}}{U_2^2} \quad (2.16)$$

Similarly, the impeller isentropic head coefficient is calculated as:

$$\psi_{02s} = \frac{y_{02s}}{U_2^2} = \frac{h_{02s} - h_{01}}{U_2^2} \quad (2.17)$$

The stage head and isentropic head coefficient are related through equation 2.18:

$$\psi_{04} = \frac{\psi_{04s}}{\eta_s} \quad (2.18)$$

Tip speed Mach number

The impeller tip speed Mach number is calculated as the impeller tip speed over the inlet stagnation sonic velocity:

$$Ma_{U_2} = \frac{U_2}{a_{01}} \quad (2.19)$$

The significance of the tip speed Mach number entails its impact on the impeller pressure ratio through its relationship with the relative inlet Mach number (Ludtke, 2004). The tip speed Mach number relates to the relative inlet Mach number through equation 2.20:

$$Ma_{W_1} = M_{U_2} \frac{W_1}{U_2} \quad (2.20)$$

where $\frac{W_1}{U_2}$ portrays a fixed relation at the design point of any given impeller (Ludtke, 2004). The relative Mach number reflects the flow compressibility; thus, an increasing Mach number will result in an increasing pressure ratio.

2.3.2.2. Non-dimensional tip velocity diagram

Ludtke (2004) asserted the non-dimensional impeller tip velocity diagram as a critical tool to characterize and classify impellers (Figure 9). In this diagram, the tip velocity triangles of impellers,

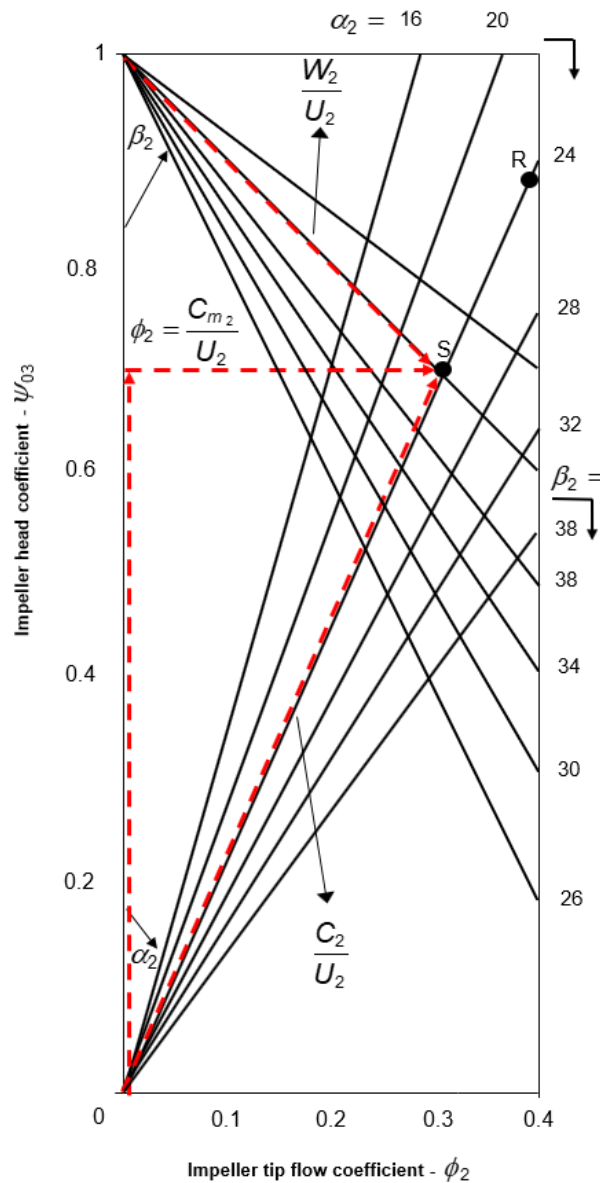


Figure 9: Non-dimensional impeller tip velocity diagram (Ludtke, 2004). A typical S-shaped and R-shaped impeller tip is indicated with the symbol S and R respectively.

which are similar (as per section 2.3.2), will be clustered around a specific region. Producing the non-dimensional impeller tip velocity diagram, the impeller tip velocity triangle is scaled using the impeller tip speed. In this form, the vertical axis signifies the impeller head coefficient while the horizontal axis portrays the impeller tip outlet flow coefficient. The relative and absolute flow angles remain unchanged when the diagram is scaled.

2.4. MAP-BASED COMPRESSOR PERFORMANCE MODELS

Map-based performance models parameterise compressor performance curves using empirical performance data based on generalized relationships, polynomial regression, scaling factors, stage stacking and artificial neural networks. Of the representations, polynomial regression represents the most widely used method due to its simple structure and low computational requirement (Cicciotti, 2015).

This study will focus on models based on stage stacking and polynomial regression, discussing these two concepts further.

2.4.1. Stage stacking

The overall performance map of a multi-stage compressor represents a combination of individual stage performance with output conditions of one stage, encompassing the inlet conditions of the subsequent one. When the individual stage performance curves are mathematically combined to produce the overall compressor performance curve, the term stage stacking is used. Equations 2.21-2.23 present stage stacking as multi-stage compressors compressing an ideal gas without intercooling:

$$\Delta T_0 = \frac{1}{C_p} \sum_{i=1}^n \frac{\psi_i}{\eta_i} U_{2,i}^2 \quad (2.21)$$

$$\Pi_c = \prod_{j=1}^n \left(\frac{\psi_j U_{2,j}^2}{C_p T_{0,in} + \sum_{k=1}^j \left(\frac{\psi_k}{\eta_k} \right)} \right) \quad (2.22)$$

$$\eta_{c,s} = \frac{\Pi^{\frac{\lambda-1}{\lambda}} - 1}{\frac{T_{0,exit}}{T_{0,in}} - 1} \quad (2.23)$$

Massardo (1991) used an inverse stage stacking, or diagnostic approach to determine the effect of stage fouling on the overall performance curve of an axial compressor. Mathioudakis and Stamatidis (1994) expanded on this technique to determine the impact of additional damage mechanisms on the overall performance of an axial compressor with similar geometry to an eight-stage compressor of the GE J-85 jet engine. First, they simulated the influence of various damage mechanisms on the

compressor's overall performance curve (Figure 10). Using the overall performance curve, illustrating a specific damage mechanism as input, they then developed a method based on stage stacking to

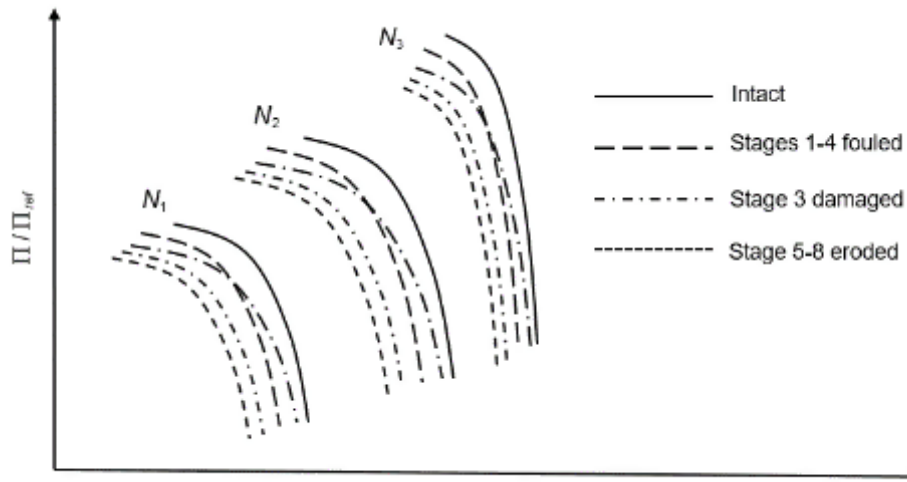


Figure 10: Effect of different stage' damage mechanisms on the overall performance of a compressor, adapted from Mathioudakis and Stamatis (1994)

identify the damaged stage and mechanism. This thesis focuses on stage stacking to produce individual stage performance curves; therefore, the Mathioudakis and Stamatis (1994) damage mechanisms representation will not be discussed further. Figure 11 displays the stage stacking algorithm Mathioudakis and Stamatis (1994) employed.

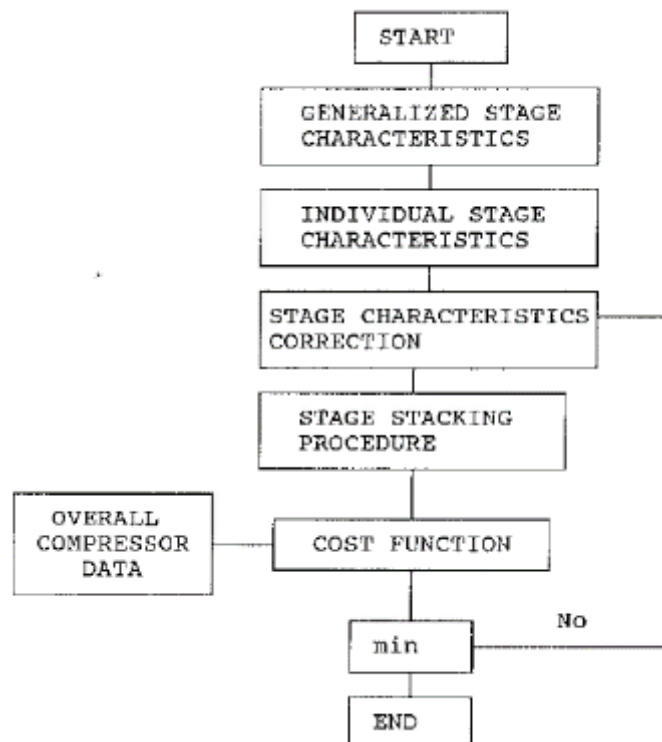


Figure 11: Stage curves calculation flow chart Mathioudakis and Stamatis (1994)

For each stage, a generalized performance curve is fitted to a point with known operating conditions. These fitted curves are then combined to produce an overall performance curve. The difference between the measured and produced overall compressor curve is then derived as a cost function. Using a numerical search algorithm, updating the shape of the generalized stage performance curves minimises the cost function.

2.4.2. Polynomial regression

Polynomial regression, especially for demonstrating compressor maps, represents the most common data-driven modelling described in the literature. For example, Müller et al. (1998) used a polynomial representation to simulate the compressors of spark-ignition engine turbochargers. The impeller head coefficient was modelled as a second-order polynomial function of the corrected inlet flow coefficient (equation 2.24):

$$\psi = A_1 + A_2\phi_c + A_3\phi_c^2 \quad (2.24)$$

with the coefficients A_1 , A_2 and A_3 exhibited as polynomial functions of the impeller tip speed. At all impeller tip speeds, the approach Müller (1998) used predicted the impeller head within $\pm 10\%$. Sieros *et al.* (1997) employed the following equations to depict centrifugal compressor efficiency in jet engines:

$$(\Pi + \eta)^2 = a_1 + a_2 X \quad (2.25)$$

$$X = (\Pi + \eta + 1 / \Pi)(\Pi + \eta) \quad (2.26)$$

The representation was applied to various compressor maps, including the ATAR and J85 aero-engines with a mean relative error between 0.75-1.20% (Sieros *et al.*, 1997).

Fang *et al.* (2014), using polynomial compressor models, compared numerous compressor mass flow rate and efficiency computations developed for vehicle engine turbocharger compressors in terms of their prediction accuracy. Fang *et al.* (2014) assessed their suitability for use with refrigeration centrifugal compressors, revealing the prediction accuracies varied substantially when applied to refrigeration compressors. They concluded since the model's accuracy varies with the compressor being assessed, careful assessment should be made in selecting a specific model.

Although map-based models are commonly used to model compressor performance, limitations regarding prediction accuracy remain pertinent. The following factors influence the prediction accuracy of map-based models (Odom and Muster, 2009):

- Manufacturer-supplied performance curves represents a new unit in clean condition. The actual performance of a site-based compressor varies from the factory provided curves by as much as 4%. Odom and Muster (2009) commented that this performance difference results from factors like the installation process of a site-based compressor and the interaction between the compressor and the process itself.
- Deviation in the predicted performance from the measured performance is expected due to measurement uncertainties.

Hence, the process of modelling centrifugal compressor performance holds only accurate to within +/- 5 % at best (Odom and Muster, 2009). When these models are used for performance monitoring, it is generally sufficiently accurate to identify performance gaps of 10% and higher (Brown and Rahman, 2002).

2.5. 1-DIMENSIONAL COMPRESSOR PERFORMANCE MODELS

One-dimensional flow analysis entails reducing the complex 3-dimensional flow inside the compressor to a mean flow condition, analysed along the various compressor components. This approach relies on fluid dynamics in conjunction with empirically developed loss correlations to model mean flow properties (Aungier, 2000).

The results obtained with these analysis models are directly dependent on the validity of the empirical loss correlations employed. Numerous empirical correlations exist, for example, Galvas (1973), Coppage *et al.* (1956), and Aungier (2000). Loss correlations vary widely in terms of complexity and the detail required while the analysis models vary regarding the respective losses considered or excluded. Numerous attempts to obtain an optimum combination of loss correlations that would produce the best performance prediction accuracy for centrifugal compressors can be found in the literature. Oh, *et al.* (1997) used three loss sets to demonstrate the performance (total pressure ratio and isentropic efficiency) of impellers including the Eckhardt A, B and O impellers. Figure 12 display the modelling results applied to the Eckhardt impeller O.

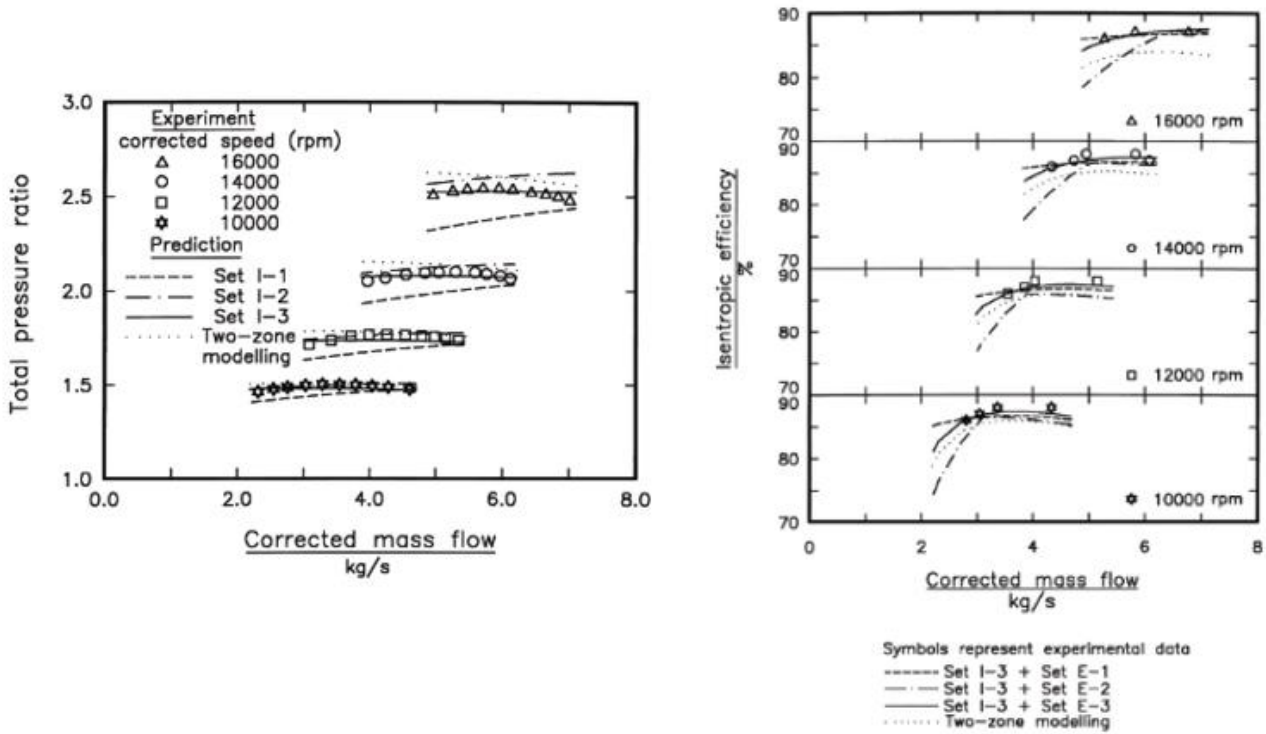


Figure 12: Pressure ratio (left) and isentropic efficiency (right) of the Eckardt O impeller modelled with different loss correlation sets (Oh et al., 1997)

Li et al. (2015) assessed the prediction accuracy of the loss sets Oh et al. (1997) developed to examine HPCC impeller performance (Figure 13). They asserted the optimum loss correlation set Oh

Losses	Galvas	Oh	New
Incidence	Galvas [1]	Conrad [11]	Aungier[2]
Skin friction	Galvas [1]	Jasen [12]	Jasen [11]
Blade loading	Coppage [12]	Coppage [13]	Coppage [13]
Clearance	None	Jasen [12]	Jasen [12]
Mixing	None	Johnston and Dean [16]	Johnston and Dean [16]
Disk Friction	Galvas [12]	Daily and Nece [14]	Daily and Nece [14]
Recirculation	Jasen [13]	Oh [3]	Japikse [4]
Slip factor	Wiesner [18]	Wiesner [18]	Qiu [19]
Vaneless diffuser loss	Stanitz [24]	Stanitz [24]	Stanitz [24]

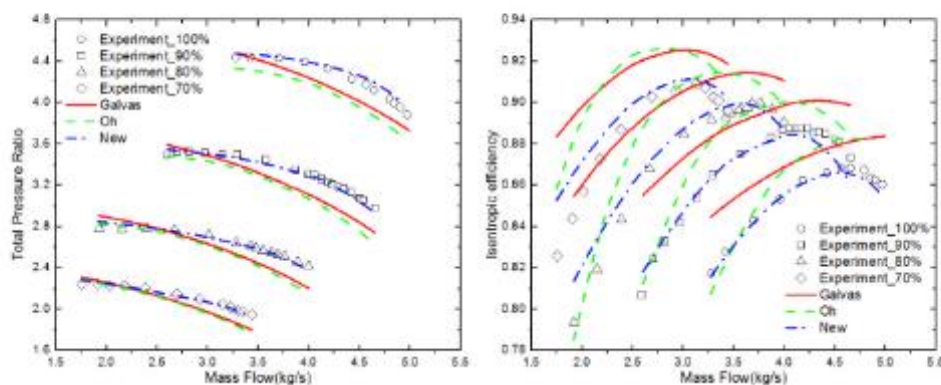


Figure 13: Total pressure ratio and efficiency modelled for the HPCC impeller (Li et al., 2015)

et al. (1997) proposed held unsatisfactory when applied to this compressor. Li *et al.* (2015) updated the loss set of Oh *et al.* (1997) through the replacement of the incidence-, recirculation- and slip factor models.

Since the analysis models are validated experimentally, no unique empirical rendition can forecast with the best accuracy for all compressors, especially when attempting to simultaneously obtain prediction accuracy for older and modern stage designs (Aungier, 2000). Older stages, designed without the aid of modern, multidimensional flow analysis, differ significantly from their modern counterparts.

This study implements the Aungier (2000) analysis model developed using experimental data from more than 100 stages with flow coefficients ranging between 0.001-0.16 and pressure ratios up to 3.5. De Wet *et al.* (2012) used this model to examine the performance of the Ziegler (2003) Radiver open CFD test case. The model predicted the static-to-static pressure ratio and total-to-total isentropic efficiency with maximum errors of 3.78% and 1.72%, respectively. De Wet *et al.* (2012) commented on the criticality of correctly calculating the impeller and diffuser throat areas when implementing the performance model of Aungier (2000) because Aungier (2000) included a choke loss in his model (Appendix A-4, equations A.4.4 - A.4.7). The choke loss is implemented when a conditional operating state, based on a critical throat area, is reached. When the criteria for incorporating the choke loss have been satisfied, the choke loss model dominates the shape of the predicted stage performance curve.

Aungier's (2000) model is valid for the complete compressor stage, namely the impeller, vaneless annular passage (vaneless space between impeller exit and diffusor entrance) and the return channels. However, since, for this thesis, only the stage diameters and tip speed are known, a modelling method requiring the stage head coefficient as input is developed in subsequent chapters. The stage head coefficient depicts an exclusive impeller property (equation 2.15); thus, only Aungier's (2000) impeller performance evaluation model is discussed in the subsequent section.

2.5.1. Impeller Performance

For this thesis, the impeller analysis model is implemented using real gas equations of state (Appendix A-1). A Mollier diagram (Figure 14) illustrates the primary impeller analysis methodology. The

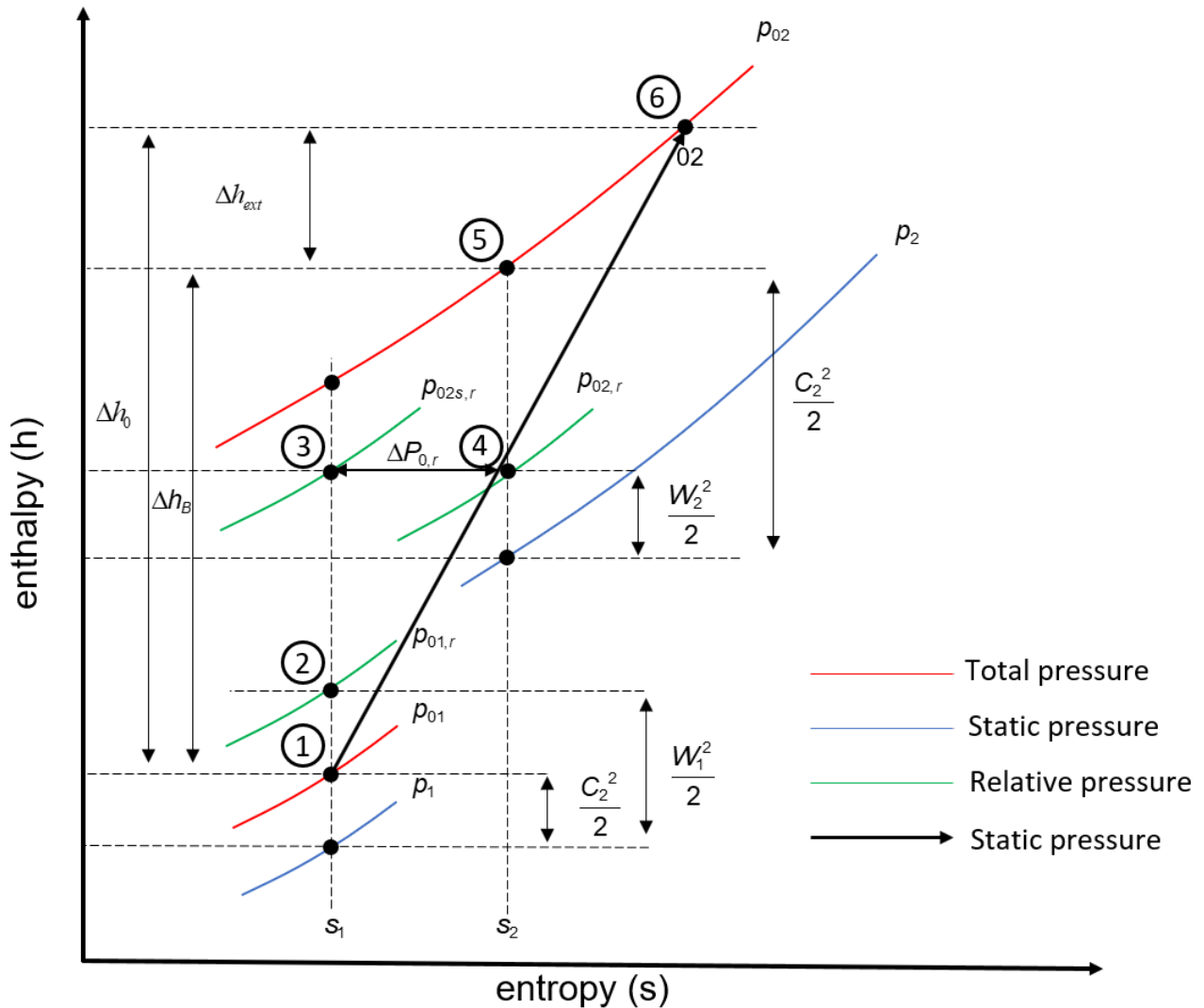


Figure 14: Impeller performance modelling employing the model of Aungier (2000)

correlations depicting individual losses, as well as the slip factor, are discussed in Appendix A.

As a first step, the known total and static inlet properties at the impeller inlet (point 1), together with the inlet velocities, define the relative total inlet properties (point 2). The total relative inlet enthalpy is calculated as:

$$h_{01,r} = h_1 + \frac{W_1^2}{2} \tag{2.27}$$

Since the inlet entropy remains the same in both the stationary and rotating frames of reference, all other total relative properties, such as pressure and temperature, can be computed as a function of

the total relative inlet enthalpy and the entropy, $p_{01,r}, T_{01,r} = f(s_1, h_{01,r})$. Relative total enthalpy at the impeller tip (point 3) is denoted as:

$$h_{02,r} = h_{01,r} + \frac{U_2^2 - U_1^2}{2} \quad (2.28)$$

All other total ideal relative properties at the tip (point 3) are once again derived as a function of enthalpy and entropy $p_{02s,r}, T_{02s,r} = f(s_1, h_{02,r})$.

The total actual relative pressure (point 4) is now calculated as:

$$p_{02,r} = p_{02s,r} - f_c (p_{01,r} - p_1) \sum_i \bar{\omega}_i \quad (2.29)$$

where f_c is the entropy correction factor defined as:

$$f_c = \frac{\rho_{02,r} T_{02,r}}{\rho_{01,r} T_{01,r}} \quad (2.30)$$

The loss summation term, $\sum_i \bar{\omega}_i$, represents the internal losses Aungier (2000) used to analyse impeller performance. Internal losses refer to the losses affecting impeller outlet pressure. Aungier (2000) modelled ten losses when examining impeller performance, explicitly: incidence-, entrance diffusion-, choking-, blade loading-, skin friction-, hub-to-shroud loading-, distortion-, blade clearance-, mixing- and supercritical Mach number losses. The correlations used to derive these losses as well as a discussion around what each loss entails is provided in Appendix A-4. With the relative pressure at point 4 ($p_{02,r}$) calculated and noting the total relative outlet enthalpy is equal for both ideal and actual cases, all other relative values at point 4, as well as the impeller outlet entropy, can be derived, $T_{02,r}, s_2, \rho_{02,r} = f(p_{02,r}, h_{02,r})$.

Based on an assumed value of the outlet flow coefficient, the meridional outlet velocity is reflected.

$$\phi_2 = \frac{C_{m_2}}{U_2} \quad (2.31)$$

If no cover seal leakage exists, the blade work input factor is presented as:

$$I_B = \sigma (1 - \lambda \phi_2 \cot \beta_{2b}) - U_1 C_{U_1} / U_2^2 \quad (2.32)$$

The correlations used to calculate the impeller tip distortion- and slip factor are provided in Appendix A-3 through equations A.3.5 and A.3.10, respectively. Using the blade work input factor, with zero swirl tangential velocity upstream of the rotor, the tangential absolute velocity component, C_{U_2} , can be computed:

$$C_{U_2} = I_B U_2 \quad (2.33)$$

With C_{U_2} , U_2 and C_{m_2} known, the absolute and relative outlet velocity components are determined using the relations of the outlet velocity triangle (Figure 7). The impeller blade work is calculated as:

$$\Delta h_B = I_B U_2^2 \quad (2.34)$$

The static flow properties remain the same in both frames of reference and using equations of state, all total absolute properties at the impeller discharge can be derived (point 5). The mass flow at the impeller outlet is portrayed as:

$$\dot{m}_2 = \rho_2 C_{m_2} A_2 \quad (2.35)$$

with the impeller tip flow area, A_2 , illustrated through equation 2.36.

$$A_2 = b_2(2\pi r_2 - z_2 t_2) \quad (2.36)$$

The outlet flow coefficient, ϕ_2 , is iterated until the impeller inlet mass flow equals the outlet mass flow. At this point (point 5), the impeller mass flow, static tip conditions, and total discharge pressure have been calculated. To obtain the impeller discharge temperature (point 6), the impeller's total work input is modelled. Aungier (2000) defined an external work input factor, I_{ext} , which together with the blade work, I_B , represents the total impeller work input:

$$I = I_B + I_{ext} \quad (2.37)$$

Aungier (2000) derived the external work input factor through the calculation of parasitic losses affecting the impeller discharge temperature without changing its discharge pressure. The external work input factor is computed as:

$$I_{ext} = I_{DF} + I_L + I_R \quad (2.38)$$

The parasitic losses Aungier (2000) considered comprise disk friction-, recirculation and clearance gap losses. The correlations defining these losses, as well as a description of each loss, are provided in Appendix A-3. The external head loss is calculated as:

$$\Delta h_{ext} = I_{ext} U_2^2 \quad (2.39)$$

The total enthalpy at the impeller exit (point 6) is derived as:

$$h_{02} = h_{01} + \Delta h_B + \Delta h_{ext} \quad (2.40)$$

from which T_{02} can be calculated as:

$$T_{02} = f(h_{02}, s_2) \quad (2.41)$$

The iterative procedure used by Aungier (2000) is shown in Figure 15.

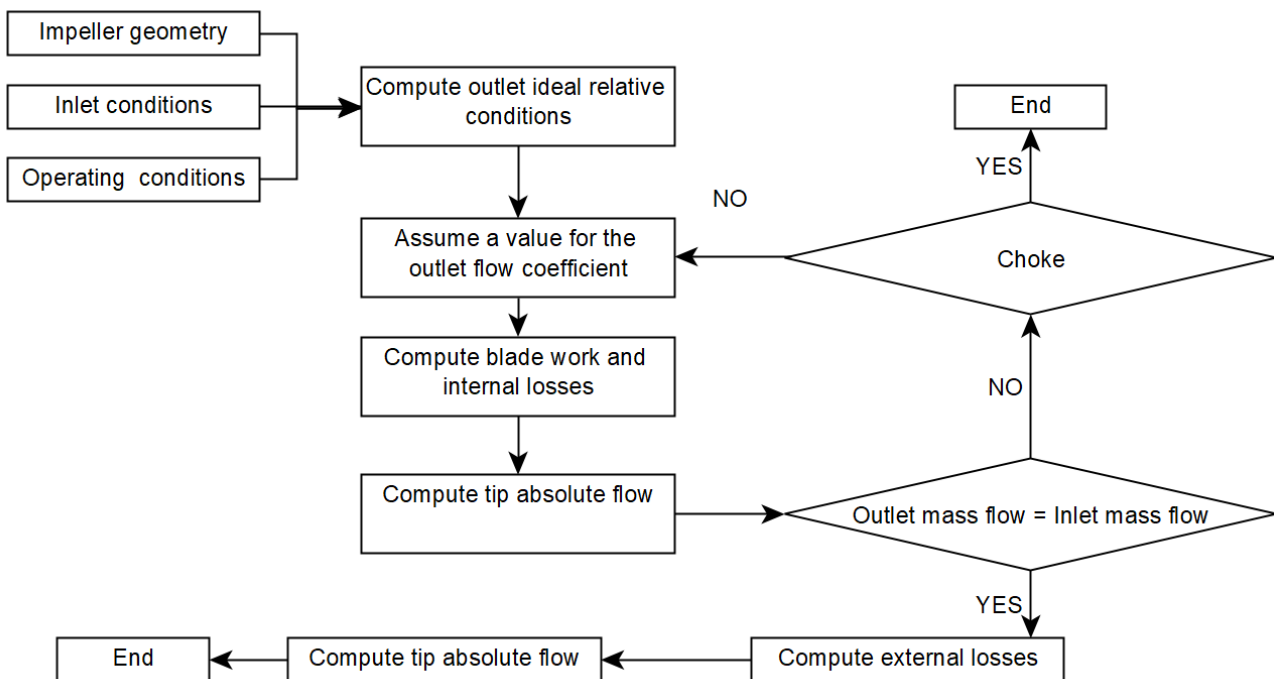


Figure 15: Flow chart of the iterative procedure, adapted from Aungier (2000)

2.6. CONCLUSION

This thesis objective is to develop a compressor modelling methodology that can be used to deduce stage performance from the overall compressor performance characteristic when only the overall compressor performance curve in conjunction with the diameter and tip speed of each impeller is known.

Aero-thermodynamics form the foundation of any compressor model (section 2.3) with the similarity principle (section 2.3.2 and 2.3.3), offering a convenient way to characterise the performance of turbomachinery. Since the IGCC stages studied in this thesis possess a similar design (section 2.2), the similarity principle, as applied to turbomachines, could be used to simplify the proposed modelling methodology.

Map-based performance models refer to the process of parameterizing compressor performance curves using empirical performance data (section 2.4). These models require the least stage design data in comparison to other performance methods, such as 1-dimensional or CFD models, illustrating a well-suited choice for achieving the study objectives. Map-based models remain sufficiently accurate in forecasting performance deficiencies of 10% and higher (Brown and Rahman, 2002).

In the literature, numerous examples of compressor performance parameterization exist (section 2.4.2). The complexity of these models increases when they have to predict compressor performance at various operating speeds. The effect of the operating speed on compressor performance is similar to the effect of the IGV position on the performance of a fixed speed compressor in the sense that for each position of the IGV, a new overall performance curve exists (Figure 6). In the context of the IGCCs considered in this thesis, the problem in predicting compressor performance at different IGV positions is further exacerbated when no mass flow meters are installed on site-based compressors. To ensure the overall performance curve used to develop the modelling methodology can be replicated for site based IGCCs without mass flow meters, the performance curves of the IGCCs forming part of this thesis will be parametrized with their IGVs in a 100% open position.

Mathioudakis and Stamatis (1994) implemented stage stacking (section 2.4.1) to derive the stage performance curves from the overall compressor performance curves of an axial compressor. Their method requires a single operating point on each stage's performance curve to be known before a parameterized curve shape is fitted through each point. Mathioudakis and Stamatis (1994) did not allude to how to obtain these operating points. For this thesis, similarity principles and a simplified 1-dimensional model is used to obtain relative operating points for each of the stage's performance curves.

One-dimensional compressor analysis models (section 2.5) employ a combination of aerothermodynamic principles and empirically derived correlations to model the compression process. A weakness of these models in the context of this thesis is 1-dimensional models require detailed geometrical compressor design input, not readily available. A general weakness of these models is the accuracy of their prediction is only as good as the accuracy of the correlations on which they are based (Aungier, 2000). Hence, no single 1-dimensional model can produce accurate performance analysis results for all compressors. This limitation is especially apparent when

attempting to obtain prediction accuracy for older and modern stage designs simultaneously (Aungier, 2000). In this study, this presents an obstacle since the study objective is to develop a modelling methodology compatible with old and new (1975 – current) IGCCs found in the coal-fired power generation industry of South Africa.

Similarity principles could be used to develop a simplified 1-dimensional model requiring less compressor design input. Accounting for the variation in prediction accuracy of 1-dimensional models when applied to older and modern stage designs, the 1-dimensional model can be used to assess relative stage performance. If the IGCCs stages are assessed in terms of their relative performance, it is assumed any weakness in prediction accuracy would be distributed proportionally between stages; thus, not affecting the relative performance analysis.

3

DEVELOPED STAGE STACKING PROCEDURE

3.1. INTRODUCTION

This chapter discusses the modelling methodology developed to obtain stage performance curves of an IGCC using the overall compressor performance curve in conjunction with the stage's impeller diameters and tip speeds. The developed method modifies the stage stacking procedure of Mathioudakis and Stamatis (1994). Mathioudakis and Stamatis (1994) used the following inputs to model the performance curves of compressor stages through a stage stacking procedure:

- Overall compressor performance curve.
- Parameterized performance curves of each stage.
- Known operating points on the performance curve of each stage.

In this thesis, operating points on the performance curve of each stage are not available, necessitating an alternative methodology to implement a stage stacking procedure.

Instead of known stage operating points, the developed model employs a stage stacking procedure based on expected stage performance. The maximum total-to-total pressure ratio and head coefficient of each stage are assessed relative to other stages at the compressors' surge flowrate. The relative stage performance then serves as a conditional requirement imposed when implementing stage stacking.

In sections 3.2.1 and 3.2.3, the total-to-total pressure ratio and stage head coefficients curves for IGCCs used in the coal-fired power generation industry of South Africa are parameterized. In section

3.2.2, similarity principals are used to relate the maximum pressure ratio of a stage to its impeller tip speed.

Section 3.2.4 discusses the maximum stage head coefficient. Maximum stage head coefficients are obtained through first designing and then assessing an impeller using a simplified version of the impeller performance analysis model of Aungier (2000). Chapter 4 illustrates how the maximum stage head coefficients are obtained.

Section 3.3 depicts how the modified stage stacking procedure is implemented via parameterised stage performance curves in conjunction with expected relative stage performance (maximum pressure ratios and stage head coefficients).

3.2. PARAMETERIZED PERFORMANCE CURVES

Performance data for four multi-stage IGCCs consisting of 13 stages between them were obtained from a compressor manufacturer (Appendix B). For each compressor, with the IGV in the 100% open position, the individual stage performance points were measured between the compressor's surge and choke operating points by systematically closing the compressor's blow-off valve. Since the data are proprietary, the compressors are assigned generic titles. For instance, C1s1 denotes compressor 1 stage 1. Table 1 lists the primary performance parameters of each compressor and its associated stages, and the complete performance data are provided in Table B-1.

Table 1: Measured performance parameters of IGCCs

Compressor no.	Stage no.	Impeller Tip Diameter [cm]	Tip Speed [m/s]	Max pressure ratio [-]	Max stage head coefficient [-]	Operating mass flowrate [kg/s dry air]	Operating coupling power [kW]
1	1	22.10	414.14	2.38	0.55	1.64	535.30
	2	14.99	408.51	2.30	0.58		
	3	13.97	380.82	2.32	0.69		
2	1	26.92	416.17	2.45	0.59	2.25	759.41
	2	18.78	419.22	2.41	0.61		
	3	17.27	385.64	2.22	0.69		
3	1	22.86	346.96	2.06	0.76	1.15	386.71
	2	17.32	353.59	1.98	0.62		
	3	12.42	294.09	1.64	0.64		
	4	11.81	303.97	1.79	0.75		
4	1	39.37	398.64	2.26	0.63	3.60	1183.73
	2	27.94	404.14	2.34	0.62		
	3	19.18	388.34	2.27	0.63		

The pressure ratio refers to the total-to-total stage pressure ratio calculated using equation 2.12. The operating range of each stage is bounded by the operating range of the overall compressors. For this thesis, the maximum pressure ratio and stage head coefficient is defined as the values each stage yields at the compressor surge mass flow rate. Thus, a stage might or might not have reached its actual maximum pressure ratio value when the compressor is at its surge point. The concept of the maximum stage pressure ratio is illustrated in Figure 16. The operating range of the compressor is

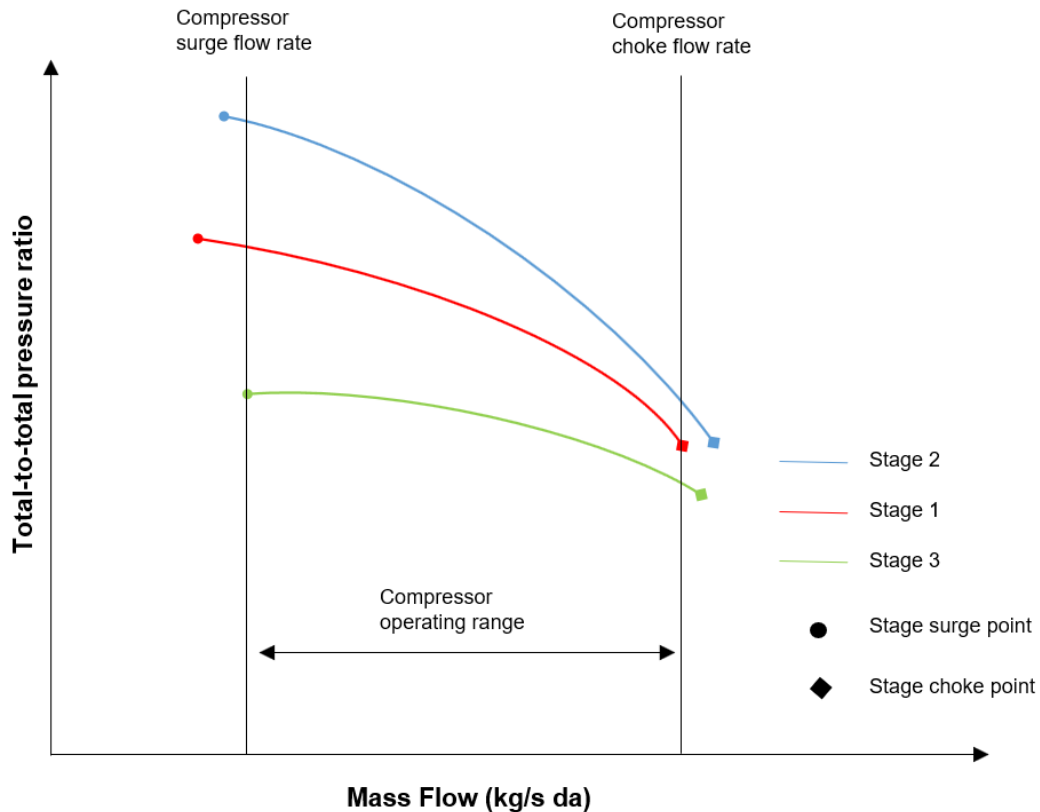


Figure 16: Stage total-to-total pressure ratio at the compressor surge flowrate.

defined as the mass flow range between the highest stage surge flow rate and the lowest stage choke flow rate.

3.2.1. Pressure ratio curves

The performance curves of Compressor 3 (Appendix B-1) illustrate parameterising the stage pressure ratio curves. Figure 17 shows the measured pressure ratio for the four stages of compressor 3 as a function of the dry air mass flow rate.

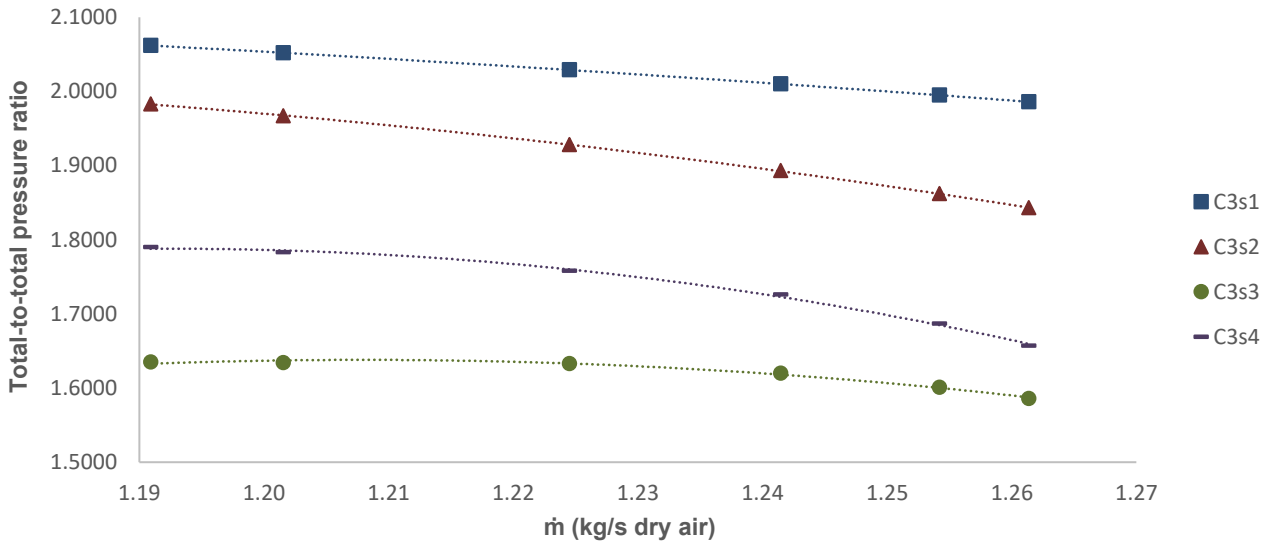


Figure 17: Compressor 3, stage total-to-total pressure ratio as a function of the dry air mass flow rate

The pressure ratio can be parameterized as a second-order polynomial with the form:

$$\Pi_i = a_i \dot{m}^2 + b_i \dot{m} + c_i \quad (3.1)$$

where a_i , b_i and c_i represent the coefficients of the polynomial that have to be determined for each stage. Parameterized in this form, the number of coefficients to be determined during the stage stacking procedure equals $3n$, where n defines the number of compressor stages.

To reduce the number of coefficients, the pressure ratio is instead parameterized as a function of the change in mass flow rate (Figure 18), with the change in mass flow rate calculated using equation 3.2.

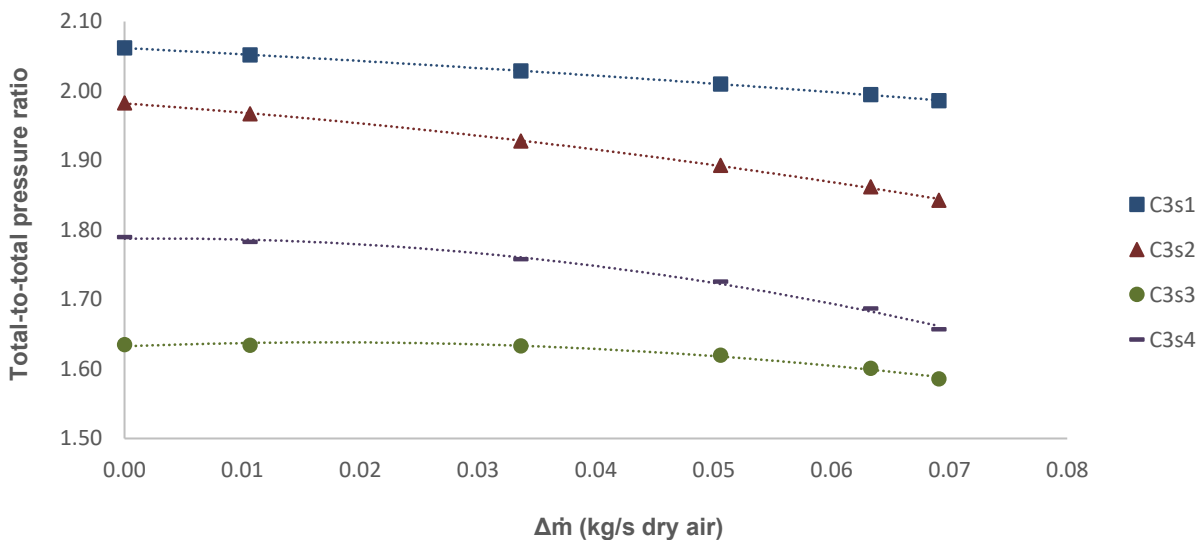


Figure 18: Compressor 3, stage total-to-total pressure ratio as a function of the change in dry air mass flow rate

$$\Delta\dot{m} = \dot{m} - \dot{m}_{\min} \quad (3.2)$$

Parameterized in this form, the polynomial representing each stage is translated horizontally on the horizontal axis, and the last coefficient is replaced by the maximum pressure ratio of each stage:

$$\Pi_i = a_i \Delta\dot{m}^2 + b_i \Delta\dot{m} + \Pi_{\max,i} \quad (3.3)$$

In this form, the number of coefficients to be determined during the stage stacking procedure reduces to $2n$.

3.2.2. Maximum pressure ratio

With the shape of the stage pressure ratio curves determined, a single operating point on each curve is required to employ the stage stacking procedure Mathioudakis and Stamatidis (1994) used. To implement the modified stage stacking procedure, the maximum pressure ratio of each stage in comparison to the other stages is estimated through the application of similarity principals.

The ratio of the relative inlet velocity and tip speed velocity, $\frac{W_1}{U_2}$, represents a fixed relation at the design point of any given impeller (Ludtke, 2004). The stages forming part of a specific IGCC are all similar in design (section 2.2), and they all operate under similar conditions. Based on this, it is assumed the stage's tip flow conditions are approximately similar at the overall compressor's design flow rate. If the tip flow conditions at the compressor design flow rate are similar, then it is further assumed the stage tip flow conditions are also similar at the compressor's surge flow rate.

In other words, if all the impellers of an IGCC are similar as per section 2.3.2, the ratio of the relative inlet velocity and tip speed velocity at the compressor's surge flow rate, $(W_1 / U_2)_{\Delta\dot{m}=0}$, is a constant value. Equation 2.20 can then be written as $Ma_{W_1,i} = cMa_{U_2,i}$. The stage pressure ratio is a function of the relative inlet Mach number (equation 2.20), which in turn, is a function of the tip speed Mach number (equation 2.19): $\Pi_{\max,i}(Ma_{W_1,i}) = cf(Ma_{U_2,i})$. Intercooling is used between subsequent stages, and the result is the difference between the inlet temperatures of the different stages varies only a few degrees. With similar inlet temperatures, the stagnation sonic velocity at the inlet of each stage is nearly equal, and the tip speed Mach number of each stage is thus predominantly a function of the impeller tip speed: $Ma_{U_2,i} = f(U_{2,i})$. The stage maximum pressure ratio is then a function of the impeller's tip speed only: $\Pi_{\max,i} = cf(U_{2,i})$.

The maximum pressure ratios of the compressor stages, Table 1, are plotted as a function of their impeller tip speeds (Figure 19).

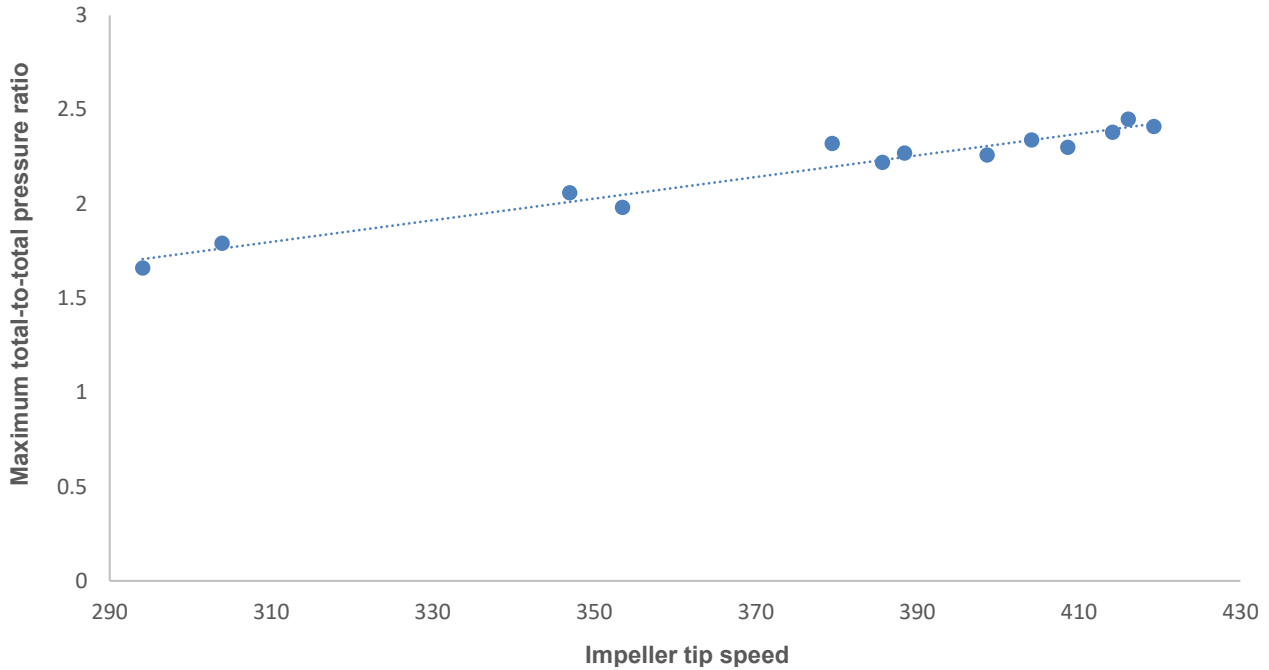


Figure 19: Stage maximum pressure ratio as a function of the impeller tip speed

For the compressors considered in this thesis, the stage maximum pressure ratio depicts a linear function of the impeller tip speed with the form:

$$\Pi_{\max, i} = 0.0057U_{2, i} + 0.0204 \quad (3.4)$$

The linear relationship between the maximum pressure ratio and impeller tip speed indicates the ratio of the relative inlet velocity and tip speed velocity at the compressor surge flow rate assumes an approximately constant value for all the compressor stages considered $(W_1 / U_2) \big|_{\Delta\dot{m}=0} = c$. Since this ratio remains constant, it is assumed the rest of the impellers' tip flow conditions are also similar at this flow rate.

3.2.3. Head coefficient curves

The performance curves of Compressor 3 illustrate parameterizing the stage head coefficient curves (Figure 20).

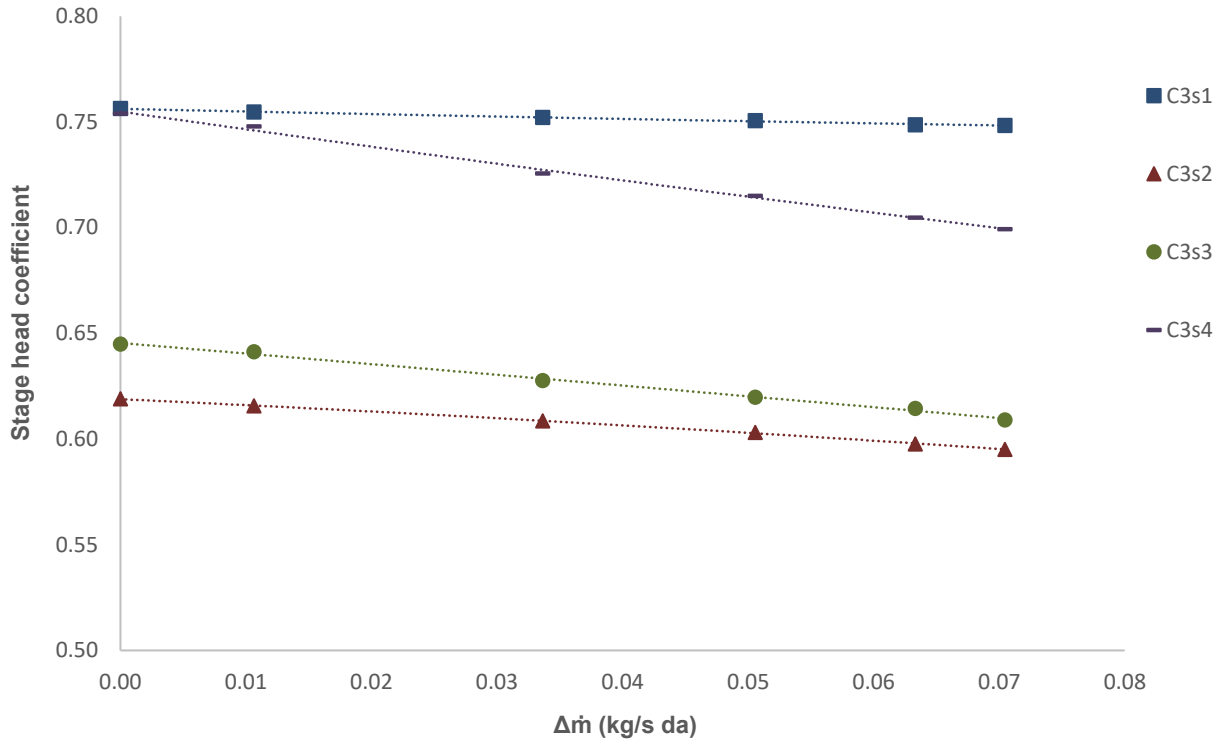


Figure 20: Compressor 3, stage head coefficient as a function of dry air mass flowrate

Similar to the pressure ratio, the stage head coefficient is parameterized as a second-order polynomial with the form:

$$\psi_i = d_i \Delta \dot{m}^2 + e_i \Delta \dot{m} + \psi_{\max,i} \quad (3.5)$$

where d_i and e_i represent the coefficients of the polynomial that have to be determined for each stage.

3.2.4. Maximum head coefficient

In section 3.2.2, the similarity concept is used to relate the maximum pressure ratio of each stage to the tip speed Mach number and finally to the impeller tip speed (equation 3.4). No clear relationship between stage head coefficient and other non-dimensional parameters is observed from the obtained compressor performance data (Appendix B-2).

The impeller is the only component of the compressor stage performing work on the fluid; therefore, the stage head coefficient is exclusively a property of the impeller. The isentropic head coefficient of the stage is a function of the entire stage, related to the head coefficient through the isentropic efficiency (equation 2.18). One requirement for similarity, as per section 2.3.2, is to have scaled velocity triangles at similar points in the flow path of each stage. Although this requirement can be

satisfied at the impeller tip, the amount of work required to produce the velocity triangle varies between impellers, as evident from the variation in efficiencies of the impellers.

The performance data for this study comes from compressors designed and manufactured between 1975 and 2010. The impellers of a multi-stage compressor were all manufactured and designed in the same era, and therefore it would be expected the stage efficiencies of a single compressor could be determined as a function of a non-dimensional parameter, such as the stage inlet flow coefficient and tip speed Mach number. However, for the performance data, no clear relationship between efficiency and non-dimensional parameters are observed (Appendix B-2).

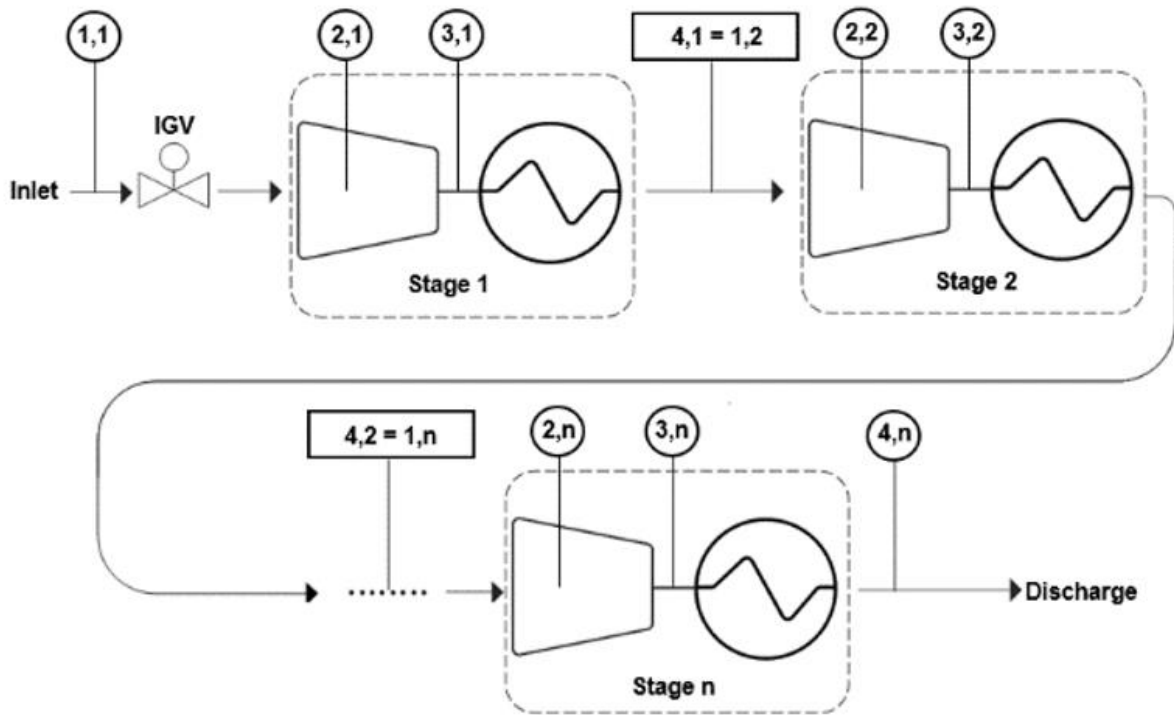
Compressor manufacturers typically use a family of pre-designed stages combined into an existing casing to yield a pressure ratio and flow rate based on the end-user requirement (Simon, 1987). The impeller tip speed is the main property manufacturers can vary to produce the required operating conditions, and hence, the impeller tip speeds are chosen to produce the required pressure and flow rate at an acceptable efficiency rather than maximum efficiency. It is assumed this practice of combining stages is the reason no clear observable relationship exists between the head coefficient and other non-dimensional parameters for the data obtained.

Implementing the modified stage stacking procedure requires the relative maximum stage head coefficient of each stage. The stage head equals the impeller head, and thus an impeller for each stage is first designed and then assessed at the compressor's surge flow rate, using a simplified version of Aungier's (2000) impeller analysis model.

Chapter 4 describes how the relative stage head coefficients of the impellers are obtained.

3.3. Stage stacking

Stage stacking mathematically combines individual stage performance to attain overall compressor performance. The equations Mathioudakis and Stamatis (1994) used (equations 2.21–2.23) to implement stage stacking remain valid for a multi-stage compressor operating with an ideal gas without intercooling between stages. This section provides the procedure used to implement stage stacking for a multi-stage compressor employing intercooling between stages. The stage stacking procedure implements equations of state developed for real gas behaviour (Appendix A-1). Figure 21 outline the stations used to implement stage stacking.



Compressor station no.	Compressor station description
1	Stage inlet
2	Impeller outlet
3	Intercooler inlet
4	Intercooler outlet

Figure 21: Compressor stations when implementing the stage stacking procedure

3.3.1. Discharge pressure

The stage stacking procedure is initiated by obtaining initial values for the maximum pressure ratios and coefficients of equation 3.3. An initial value for the maximum pressure ratio of each stage, Π_{max} , is calculated using equation 3.4. Initial values for the coefficients a_i and b_i of equation 3.3 are chosen to generate the parameterised stage pressure ratio curve. Due to the shape of the pressure ratio curves, the a_i coefficient assumes a negative value while the value of the b_i coefficient can be either positive or negative.

The initial pressure ratio curve for each stage is used in conjunction with the stage's inlet pressure to calculate the stage total discharge pressure at various flow rates. The discharge pressure of each stage is then stacked on top of each other to produce an overall compressor total discharge pressure curve using equation 3.6. To account for pressure losses across the intercoolers, a pressure loss term, Δp_{cooler} , is defined:

$$p_{0c,calc} = \prod_{i=1}^n [p_{04,calc,i} - \Delta p_{cooler}] \quad (3.6)$$

From measurements, the observable pressure loss across the stage intercoolers of new compressors remains nearly constant throughout the compressor's flow range. The pressure loss across the intercooler is thus calculated as the average value of the measurements obtained (Table B-1).

The difference between the derived and measured compressor performance at various flow rates, k , is computed as a cost function.

$$F_{p_{0c}} = \sum_{k=1}^m [p_{0c,meas}(\Delta \dot{m}_k) - p_{0c,calc}(\Delta \dot{m}_k)]^2 \quad (3.7)$$

Using a numerical search algorithm, the curve coefficients and maximum pressure ratios of each stage (equation 3.3) are updated until the cost function is minimized. The numerical search algorithm used is the Nelder Mead Simplex method (Press *et al.*, 1989), implemented through the Engineering Equation Solver (EES[®]) software interface.

Based on performance data, the following limits are imposed on the search algorithm when the curve coefficients and maximum pressure ratio values are being updated:

- The maximum pressure ratio of each stage occurs at the compressor's surge point, and all subsequent pressure ratios are equal to or smaller than this value, $\Pi \leq \Pi_{max}$.
- An upper and lower limit is set for the maximum stage pressure ratio as: $1.5 \leq \Pi_{max} \leq 2.5$.

The process of deriving stage pressure ratio curves through stage stacking is displayed in Figure 22.

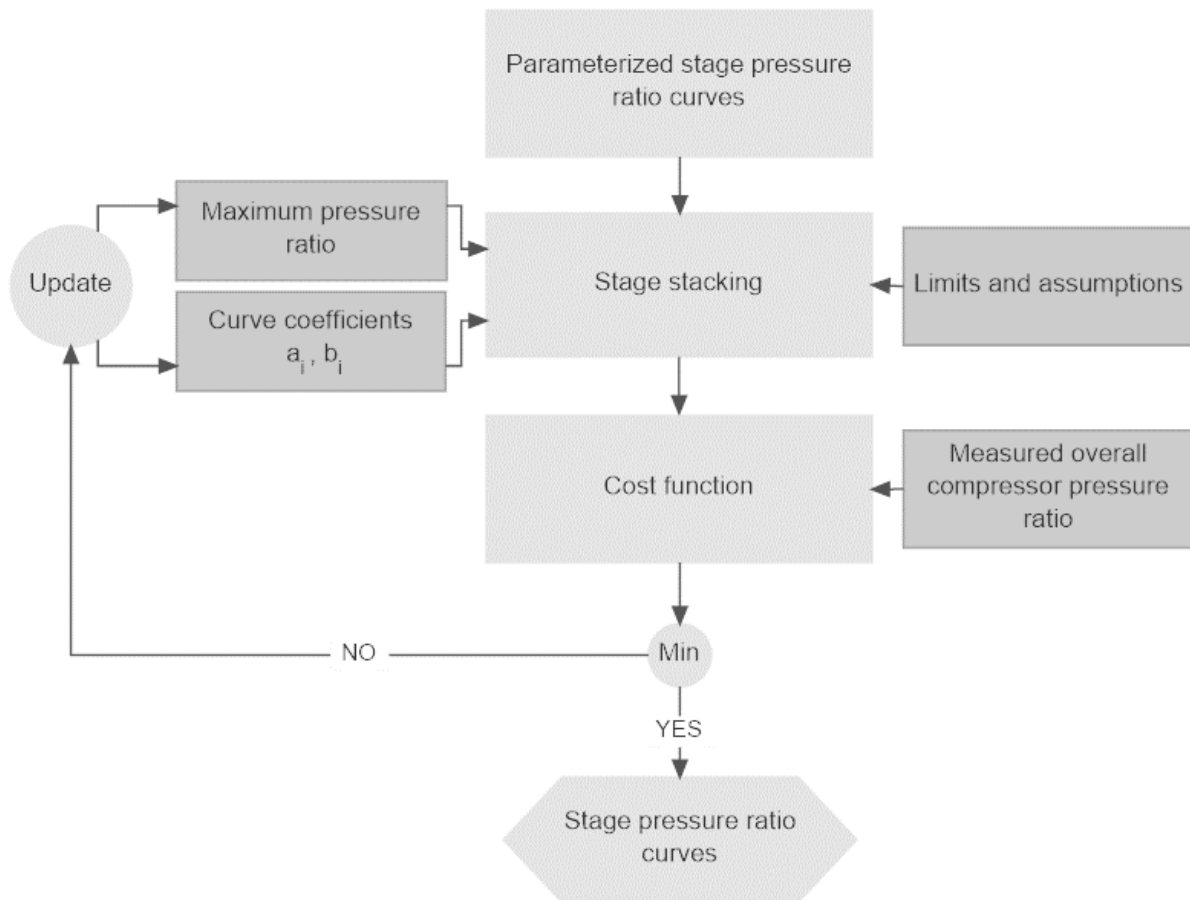


Figure 22: Pressure ratio stage stacking procedure

3.3.2. Head coefficient

Implementing the head coefficient stage stacking procedure requires the relative head coefficient of each stage, compared to each other. These values are obtained from the 1-dimensional impeller design through the process discussed in Chapter 4. To facilitate the discussion of the subsequent section, assumedly, the relative maximum head coefficients are obtained for each stage.

With the known relative maximum stage head coefficient, the curve coefficients d_i and e_i are chosen to produce the parameterized stage head performance curve (equation 3.5). Due to the shape of the stage head coefficient curves, the d_i coefficient assumes a negative value while the value of the e_i coefficient could be either positive or negative.

With an initial curve produced for each stage, the curves are stacked on top of each other to generate a compressor coupling power curve. Coupling power refers to the power input of the compressor measured at the coupling and is defined as (Standards, 2005):

$$P_{calc} = \sum_{i=1}^n P_{g,i} - P_{mech} \quad (3.8)$$

with the gas-power of each stage, P_g , calculated as:

$$P_{g,i} = \dot{m} \psi_i U_{2,i}^2 \quad (3.9)$$

The mechanical power losses, P_{mech} , denotes the losses occurring in bearings, shaft seal, gearboxes and lubrication pumps, and they do not affect the compression process. Based on the measurements, the mechanical power loss is defined as a fixed percentage of the compressors' maximum coupling power (Table B-1).

The inlet temperatures to each stage except the first stage remain unknown and are computed using a cold temperature difference.

$$T_{01} = T_{cw} + \overline{CTD} \quad (3.10)$$

Since the intercooler design data remains unknown and no clear relationship between the CTD of the stages and the compressors' performance could be observed, the cold temperature difference is calculated as the average value of the measurements (Appendix B, Table B-1).

The difference between the measured coupling power and derived coupling power at various flow rates, k , is once again determined using a cost function.

$$F_P = \sum_{k=1}^m [P_{meas}(\Delta \dot{m}_k) - P_{calc}(\Delta \dot{m}_k)]^2 \quad (3.11)$$

The curve coefficients and maximum stage head coefficients of each stage (equation 3.5) use a numerical search algorithm, Nelder Mead Simplex method (Press *et al.*, 1989), implemented through the EES® interface, to update until the cost function is minimized.

The following limits are imposed on the search algorithm when updating the curve coefficients and maximum stage head values:

- Maximum stage head is obtained at the compressor's surge point, and all subsequent stage head values are smaller than or equal to this value: $\psi \leq \psi_{max}$.
- An upper and lower limit is set for the stage isentropic efficiency as: $0.7 \leq \eta_{04s} \leq 0.9$

The process of deriving the stage head coefficient curves through stage stacking is displayed in Figure 23.

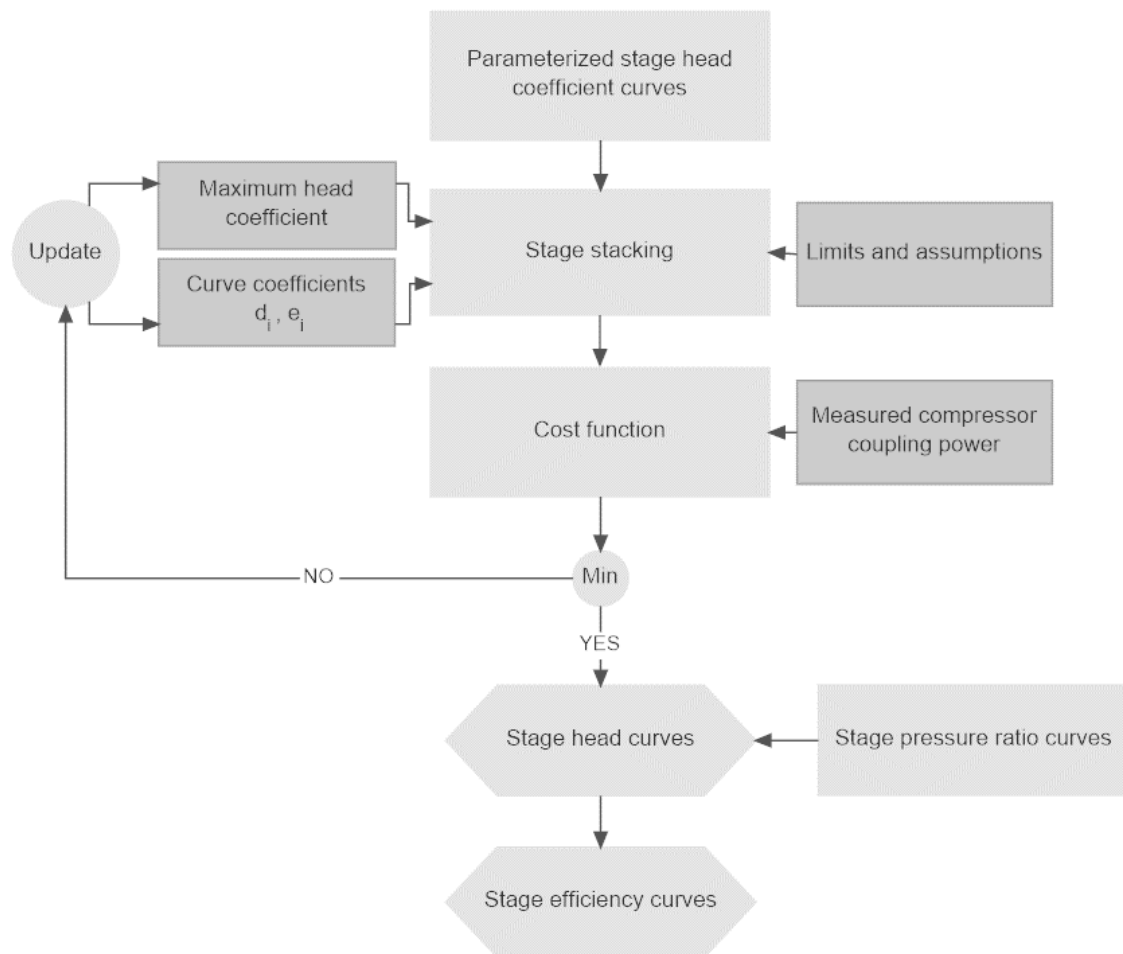


Figure 23: Head coefficient stage stacking procedure

3.4. CONCLUSION

This chapter discussed the method developed to obtain the stage performance curves from the overall performance curve of multi-stage compressors when only the compressor's overall performance curve in conjunction with the impellers' tip speeds and diameters are known. The method is based on a modified version of the stage stacking procedure used by Mathioudakis and Stamatis (1994). In contrast to the Mathioudakis and Stamatis (1994) stage stacking procedure, the proposed approach does not require a known operating point on each stage's performance curve, for it assesses the relative stage performance at the overall compressor surge flow rate. The relative maximum pressure ratio of each stage is acquired through the application of similarity principles while the relative maximum head coefficients are attained through a simplified 1-dimensional impeller design and

analysis model (Chapter 4). Practical consideration for the implementation of the stage stacking procedure, such as pressure losses across intercoolers and mechanical power losses, are discussed.

4

SIMPLIFIED 1-DIMENSIONAL IMPELLER ANALYSIS MODEL

4.1. INTRODUCTION

This chapter discusses the method developed to obtain the relative maximum stage head coefficients required during the stage stacking procedure of section 3.3.2. The method entails designing impellers and then assessing their relative performance using a simplified version of the impeller analysis model of Aungier (2000).

In section 4.2 a compressor impeller is designed and analysed using the COMPAERO[®] commercial software based on the theory of Aungier (2000). The impeller designed is of the semi-open kind, such as the ones found in the IGCCs used in the coal-fired power generation industry. COMPAERO[®] does not possess the capability to conduct an impeller design input sensitivity analysis, and hence the 1-dimensional compressor performance analysis model of Aungier (2000) is implemented using the EES[®] software. To ensure the integrity of the analysis model implemented in EES[®], the impeller designed using COMPAERO[®] is analysed using both COMPAERO[®] and EES[®], and the results are compared.

The simplified analysis model has to be implementable using only the impeller tip speed and diameters. In section 4.3, a sensitivity analysis is conducted to establish the relative impact of impeller design parameters on the prediction accuracy of the impeller analysis model of Aungier (2000).

Based on the results of the sensitivity analysis, section 4.4 illustrates the approach developed to design comparative impellers using only the impeller tip diameter.

4.2. VALIDATION OF 1-DIMENSIONAL ANALYSIS MODEL

4.2.1. Validation approach

Using COMPAERO®, a compressor stage was designed of which the complete geometry is tabulated in Appendix C-1. The software designed the stage based on user-defined inlet conditions (temperature, pressure and relative humidity) and operating parameters (pressure ratio, flowrate and efficiency), chosen to be similar to conditions encountered by IGCC's in the coal-fired power generation industry. Table 2 contains the specified stage inlet conditions and the required performance of the stage.

Table 2: Validation stage inlet conditions and required performance parameters

T_{01}	P_{01}	RH	N	U_2	Π	\dot{m}
300	100	0	28987	346.959	2.04	1.49

The impeller design is affected by the diffuser with which it is matched with (section 2.2). To ensure the designed impeller is represent the ones used in IGCCs, the stage designed using COMPAERO® consists of a semi-open impeller in combination with a wedge type vaned diffuser. Although an entire stage is modelled, the performance analysis is limited to the impeller since the stage head coefficients required for the stage stacking procedure of section 3.3.2 comprises an exclusive function of the impeller. Some of the main features of the designed impeller are shown in Figures 24 and 25, with the corresponding values provided in Table 3.

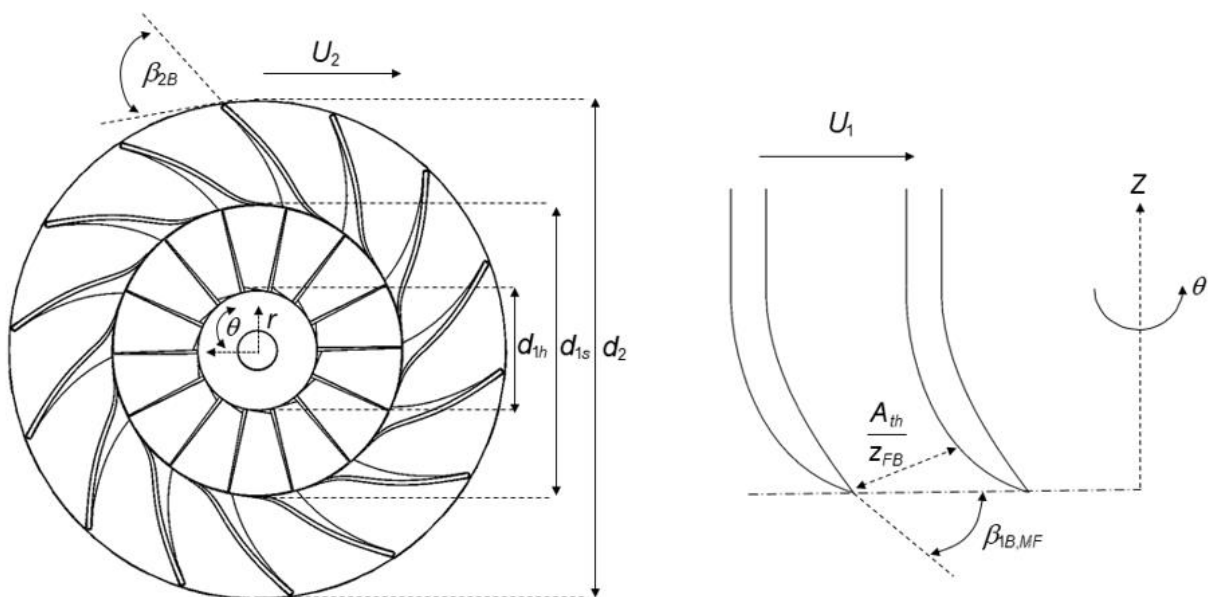


Figure 24: Impeller geometry in the $r-\theta$ plane (left) and impeller inlet geometry (right)

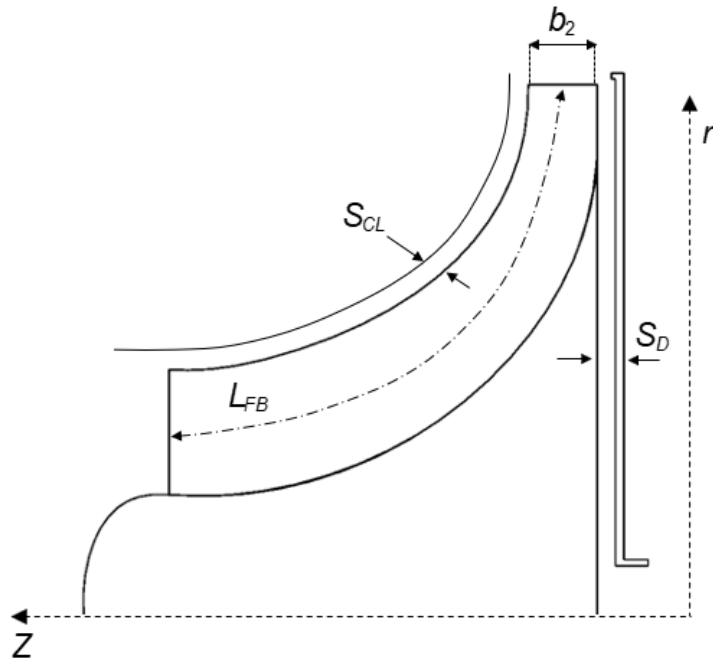


Figure 25: Impeller geometry in the r - Z plane

Table 3: Validation stage impeller geometry

Inlet	d_{1h} (mm)	40
	d_{1sh} (mm)	147
	$\beta_{1B,MF}$ ($^\circ$)	27.68
	z_1	21
	A_{th} (cm 2)	76.57
Tip	β_{2B} ($^\circ$)	63.01
	d_2 (mm)	22.86
	b_2 (mm)	0.1257
	z_2	21
Overall	L_{FB} (mm)	129
	S_{cl} (mm)	0.28
	S_D (mm)	1.7

4.2.2. Results and discussion

Using both COMPAERO[®] and the analysis model of Aungier (2000) implemented in EES[®], the impeller's pressure ratio and the head coefficient are analysed at eight mass flow rates between the stage's surge- and choke points. The complete stage analysis results obtained from COMPAERO[®] are provided in Appendix C-2.

The model of Aungier (2000) predicts a lower pressure ratio at all eight mass flow rates when compared to the values obtained with COMPAERO[®] (Figure 26). The maximum deviation between results was 1.84%, occurring at a mass flow rate of 1.34 kg/s (Table 4).

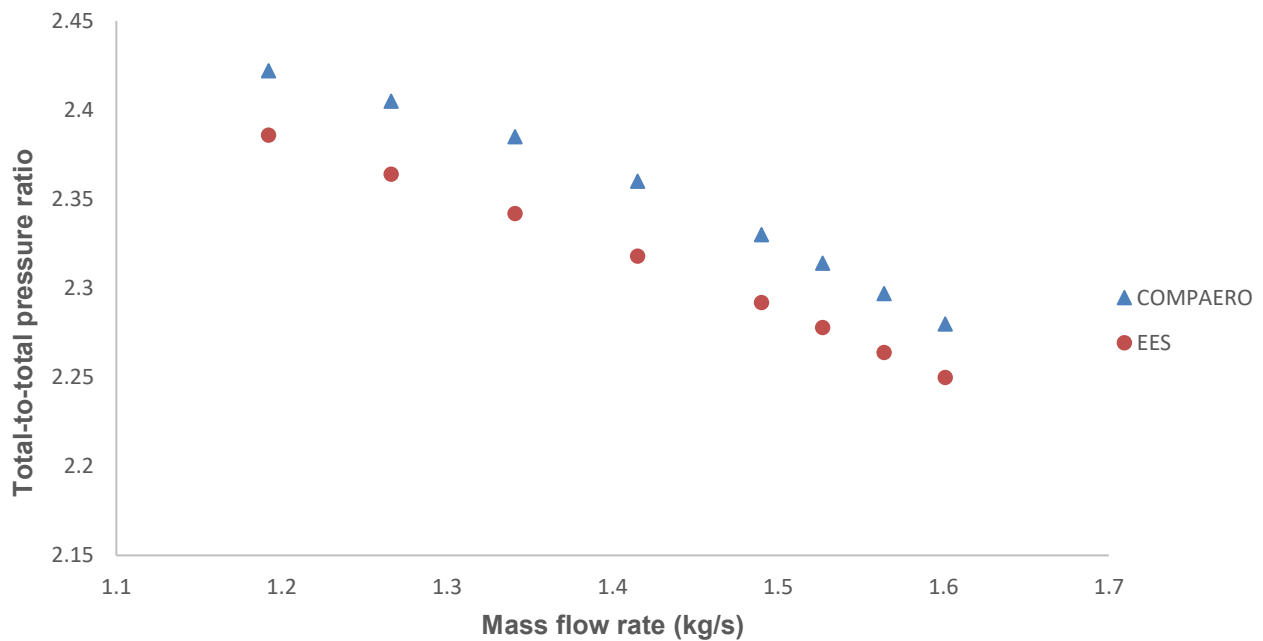


Figure 26: Impeller pressure ratio comparison

Table 4: Total-to-total pressure ratio comparison

POINT	1	2	3	4	5	6	7	8
\dot{m}	1.192	1.266	1.341	1.415	1.49	1.527	1.564	1.601
COMPAERO [®]	2.422	2.405	2.385	2.36	2.33	2.314	2.297	2.28
EES [®]	2.386	2.364	2.342	2.318	2.292	2.278	2.264	2.25
Relative percentage deviation (%)	1.51	1.73	1.84	1.81	1.66	1.58	1.46	1.33

Similar to the pressure ratio values, the head coefficient values calculated using the analysis model of Aungier (2000) were lower than the values obtained using COMPAERO® (Figure 27). For the head coefficients, the maximum deviation between results was 0.71%, occurring at a mass flow rate of 1.564 kg/s (Table 5).

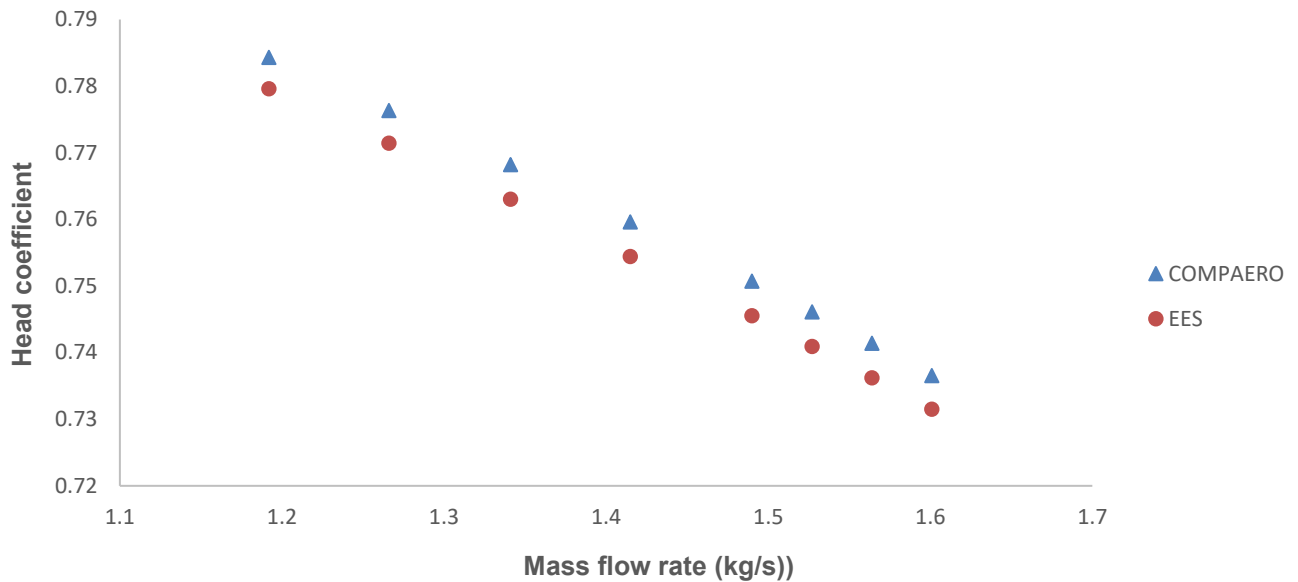


Figure 27: Impeller head coefficient comparison

Table 5: Head coefficient comparison

POINT	1	2	3	4	5	6	7	8
\dot{m}	1.192	1.266	1.341	1.415	1.490	1.527	1.564	1.601
COMPAERO®	0.7843	0.7763	0.7682	0.7596	0.7507	0.7461	0.7414	0.7365
EES®	0.7796	0.7714	0.763	0.7544	0.7455	0.7409	0.7362	0.7315
Relative percentage deviation (%)	0.60	0.64	0.68	0.69	0.70	0.70	0.71	0.68

The difference in analysis findings can be attributed to the fact, although the COMPAERO® software is based on the analysis strategy of Aungier (2000), it is not identical. COMPAERO® considers additional features such as blade fillets and shaft seal geometry while also using mean values for

inputs, such as the impeller tip diameter, when the performance analysis is conducted. Furthermore, the model implemented in EES® uses the equation of state developed for real gases by Lemmon *et al.* (2000) while the equation of state in COMPAERO® are calculated using a modified version of the equation developed by Redlich and Kwong (1949).

4.3. SENSITIVITY ANALYSIS

The objective of this chapter is to develop a method based on a simplified 1-dimensional analysis model that could be used to produce the relative maximum stage head coefficients required during the stage stacking procedure of section 3.2.2. This simplified analysis model should be implementable with only the impeller tip diameters and speeds known. It is proposed, for this purpose, impellers could be designed with parameters scaled as a function of impeller' tip diameter.

Aungier (2000) stated several of the design parameters required for the preliminary design of an impeller have little effect on its performance and can thus be scaled with the impeller's tip diameter. However, Aungier (2000) did not detail which of the parameters could be scaled and which parameters should be sized correctly.

To determine the effect the different design parameters have on the prediction accuracy of the 1-dimensional model of Aungier (2000), a sensitivity analysis is conducted on the impeller designed in section 4.2. Hence, at the stage surge flow rate, only three design parameters, namely tip width, tip blade angle and number of blades at the impeller tip, significantly affect impeller performance, and all other parameters can be designed as a function of the impeller tip diameter.

4.3.1. Analysis approach

The sensitivity analysis is conducted with the uncertainty propagation feature of EES®. EES® calculates uncertainty propagation using the method described in the NIST Technical Note 1297 (Taylor and Kuyatt, 1994). The uncertainty of a variable, ΔF , is calculated through equation 4.1 as:

$$\Delta F = \sqrt{\left(\Delta u_1 \frac{\partial F}{\partial u_1}\right)^2 + \left(\Delta u_2 \frac{\partial F}{\partial u_2}\right)^2 + \dots + \left(\Delta u_n \frac{\partial F}{\partial u_n}\right)^2} \quad (4.1)$$

where, n , represents the number of input parameters considered. EES® determines the partial derivate of each parameter, $\frac{\partial F}{\partial u}$, numerically. The relative effect each parameter has on the

calculated parameter, ΔF , is expressed through the $\left(\Delta u \frac{\partial F}{\partial u}\right)$ term. To apply equation 4.1, the

amount with which each input parameter can reasonably vary, Δu , must be specified. The variation can be specified as either an absolute or a relative percentage value u .

To establish reasonable variations of input parameters, the design geometry of ten impellers used in IGCCs with a similar design and application to those used in the coal-fired power generation industry of South Africa were obtained (Appendix D-1). Relevant design parameters were scaled with their impeller tip diameters and their average values calculated (Appendix D-2). For each parameter, the value of the maximum outlier u_{\max} , was used in conjunction with the average value, \bar{u} , to compute the maximum percentage variation using equation 4.2.

$$\Delta u_{\max} = \left| \frac{\bar{u} - u_{\max}}{\bar{u}} \right| \quad (4.2)$$

Appendix D-3 provides the maximum variation values calculated for each of the parameters.

De Wet *et al.* (2012) noted the prediction accuracy of Aungier's (2000) analysis model is greatly dependent on the accurate calculation of the inducer throat area due to its relation to the choke loss (Appendix A-4, Equation A.4.7). Since the analysis is conducted at the impellers surge flowrate (1.192 kg/s), it is assumed the choke loss can be neglected. Furthermore, the impeller tip and disk clearances were kept constant throughout the analysis, as it is assumed these properties will be set to the same or similar values for all the stages that comprise an IGCC.

4.3.2. Results and discussion

The accuracy with which the 1-dimensional impeller analysis of Aungier (2000) predicts the impeller pressure ratio and head coefficient when inputs are varied was calculated. A maximum variation value was computed for each parameter and used in conjunction with the geometry of the impeller designed in section 4.2. The resulting change in prediction accuracy is shown in Table 6.

Table 6: Effect of varying input parameters on the prediction accuracy of Aungier's (2000) impeller analysis model

Calculated parameter	Value	Absolute uncertainty	Relative uncertainty (%)
Π_{\max}	2.386	± 0.221	± 9.3
ψ_{\max}	0.7796	± 0.0988	± 13.0

The complete sensitivity analysis output data is provided in Appendix E with the main variables affecting the total uncertainty and their contribution to this uncertainty shown in Table 7.

Table 7: Impeller design input parameter contribution to total calculation uncertainty

Input parameter	% of relative Π_{\max} uncertainty	% of relative ψ_{\max} uncertainty
β_{2b}	48.75	55.20
$\frac{b_2}{d_2}$	34.53	33.61
z_2	14.17	11.07
Total	97.45	99.88

Results of the sensitivity analysis illuminate the performance of the impeller at the compressor's surge flow rate is predominantly a function of the impellers' tip design. The three parameters influencing the performance the most entail the impeller tip exit blade angle, impeller tip width and number of blades at the impeller tip.

Table 8 shows the change in the derived values of Π_{\max} and ψ_{\max} if the average parameter values of Table D-3 are used to replace all the design parameters of the impeller designed in section 4.2, except for the impeller's tip exit blade angle, the impeller tip width and the number of blades at the impeller tip.

Table 8: Effect on prediction accuracy using average values for all parameters excluding the main tip parameters

Calculated parameter	Original Value	New value	Relative percentage difference (%)
Π_{\max}	2.38	2.3514	1.45
ψ_{\max}	0.7796	0.7639	2.01

Table 8 portrays designing an impeller with average scaled inputs has a minimal effect on the prediction accuracy of Aungier's (2000) impeller analysis model as long as the three tip parameters listed in Table 8 are modelled correctly.

4.4. COMPARATIVE IMPELLER DESIGN

The aim of reproducing impellers is not to design the true impeller geometry, but rather to produce geometries, which can be used to compare relative performance. When designing comparative impellers, it is assumed the impellers comprising an IGCC were all designed and manufactured in the same era using the same available technology. Moreover, it is assumed any prediction error associated with the 1-dimensional analysis model would be proportionally transferred to each impeller, thus not impacting the relative assessment result.

The sensitivity analysis conducted in section 4.3 demonstrated impeller performance at the surge flow rate predominantly reflects a function of the tip design parameters. The influence the three tip parameters have on impeller performance is attributed to their relationship to the blade work input factor (Equation 2.32), which is, amongst others, a function of the slip factor (Equation A.3.10). With the analysis model of Aungier (2000), the impeller discharge pressure is calculated as a function of the impeller blade work. The impeller head is computed as the sum of the blade work and external losses. However, the external losses typically remain small; therefore, the stage head and pressure ratio are principally a function of the impeller blade work: $\Pi, \psi \approx f(I_B) \approx f(\beta_{2B}, b_2, z)$.

4.4.1. Design approach

The sensitivity analysis conducted in section 4.3 illustrated the impeller tip blade angle and width accounted for 83.28% and 88.81% of the prediction uncertainty when calculating impeller discharge pressure and head coefficient, respectively (Table 7). Thus, at the compressor surge flow rate, ($\Delta \dot{m} = 0$), all impeller design parameters, excluding the tip blade angle and width, is reflected as average values (Table D-3). However, to assess impeller performance using the analysis model of Aungier (2000), two design inputs, namely the tip blade angle and width are still required. Instead of using these inputs, the design approach specifies a discharge pressure and tip flow coefficient.

Employing this approach means the designed impeller tip will not represent the true geometry of the impeller. However, the goal is to assess relative impeller performance for which the approach is assumed sufficient. The process followed to acquire impeller discharge pressure, and tip flow coefficient is discussed in sections 4.4.2.1 and 4.4.2.2.

4.4.2. Design inputs

4.4.2.1. Impeller discharge pressure

An approximate impeller discharge pressure is calculated using the stage discharge pressure in conjunction with the minimum expected isentropic stage efficiency. Through the implementation of the stage stacking procedure of section 3.3.1, the stage's discharge pressures are known. With the discharge pressure of one stage representing the inlet pressure of the subsequent stage, all stage inlet pressures are also known. The stage inlet temperature is calculated as a function of a cold temperature difference through Equation 3.10. The inlet entropy of each stage is computed as a function of the inlet pressure and temperature and used in conjunction with the stage's discharge pressure to calculate the isentropic discharge enthalpy: $h_{04s} = f(s_1, P_{04})$. The process of deriving an approximate impeller discharge pressure is illustrated in Figure 28.

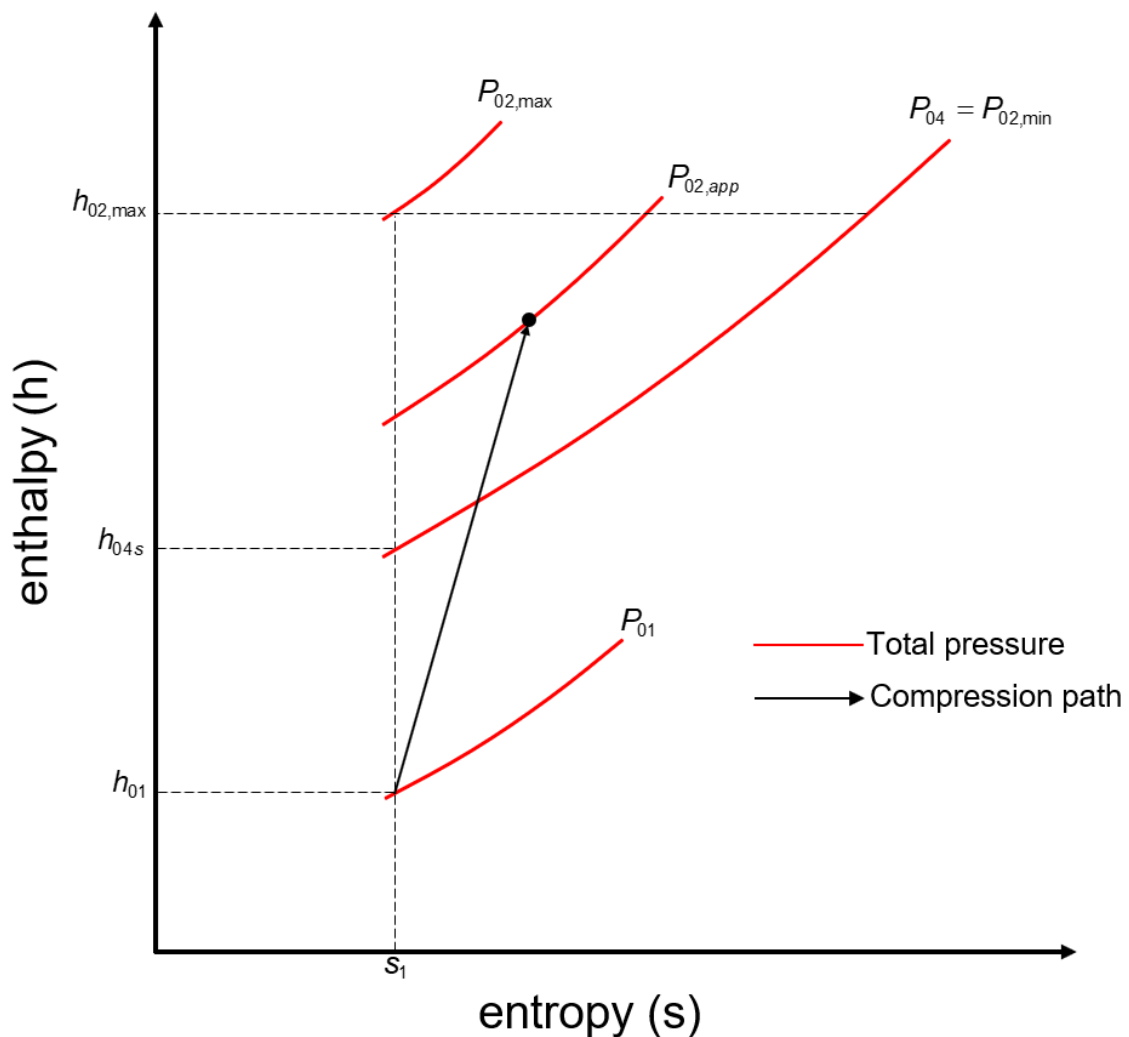


Figure 28: Impeller discharge pressure approximation

From measured data (Appendix B-2, Figure B-11 and B-12), the isentropic stage efficiencies at the compressor surge flow rate varied between a minimum of 70% and a maximum of 90%. Hence, for an ideal compression process, the maximum possible impeller discharge pressure ($P_{02,max}$) corresponds to the enthalpy ($h_{02,max}$) that would result in the minimum isentropic stage efficiency. The maximum enthalpy is derived through equation 4.3 as:

$$h_{02,max} = h_{01} + \frac{h_{04s} - h_{01}}{\eta_{04s,min}} \quad (4.3)$$

From which, in conjunction with the inlet entropy, the maximum impeller discharge pressure is calculated as $P_{02,max} = f(s_1, h_{02,max})$. The minimum possible impeller discharge pressure is equal to the stage's discharge pressure, $P_{02,min} = P_{04}$. The approximate impeller discharge pressure is represented as the root mean square of the maximum and minimum impeller discharge pressure through equation 4.4.

$$P_{02,app} = \left(\frac{P_{02,max}^2 + P_{04}^2}{2} \right)^{0.5} \quad (4.4)$$

4.4.2.2. Impeller tip flow coefficients

Ludtke (2004) used non-dimensional impeller tip velocity diagrams to classify and categorize impeller designs at their best efficiency points (BEPs). Ludtke (2004) indicated the typical velocity diagram of an S-type impeller at its design point with the symbol S (Figure 29). In this section, the 1-dimensional

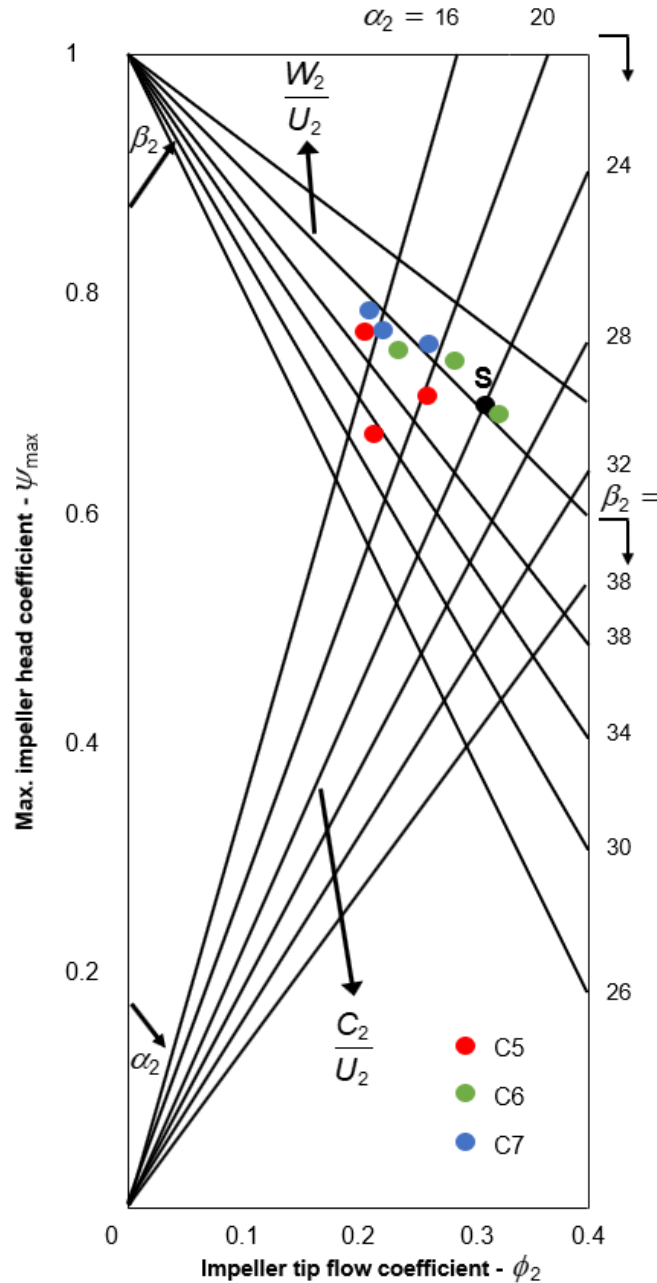


Figure 29: Non-dimensional impeller tip velocity diagrams at surge flow rate

analysis model of Aungier (2000) is used to illustrate the non-dimensional impeller tip velocity diagrams for the ten impellers of compressors 5, 6 and 7 (Appendix D-1). In contrast to the Ludtke (2004) diagram, the impeller tip velocity diagrams are assessed at the overall compressor’s surge flow rate. The resulting tip velocity diagrams are portrayed in Figure 29, with corresponding values provided in Table 9.

Table 9: Impeller non-dimensional tip values

Compressor no.	\dot{m}	Stage no.	ϕ_2	ψ_{\max}
C5	1.52	1	0.18	0.76
		2	0.24	0.70
		3	0.18	0.68
C6	0.92	1	0.21	0.77
		2	0.19	0.79
		3	0.19	0.78
C7	1.56	1	0.30	0.74
		2	0.26	0.66
		3	0.25	0.77
		4	0.28	0.73

A weakness of 1-dimensional analysis models entails no single rendition can produce optimum prediction accuracy for all compressors (section 2.5). This means the calculated tip flow coefficients of Table 9 may or may not represent the true impeller tip flow conditions. However, since the tip flow coefficients are calculated with the same analysis model that will be used to assess relative impeller performance, it is assumed any weakness in prediction accuracy will be distributed proportionally between impellers, thus not impacting the relative assessment result.

Based on the assessment result, an average value of 0.24 was specified for the impeller tip flow coefficient when comparative impellers are designed.

4.5. CONCLUSION

This chapter outlined how a simplified 1-dimensional analysis model could be used to model the relative performance of IGCC impellers. The integrity of the author's rendition of the analysis model of Aungier (2000) is illustrated in section 4.2. A sensitivity analysis, conducted at the stage surge flow rate, portrays the prediction accuracy of the 1-dimensional analysis model of Aungier (2000) is primarily based on the three impeller tip design parameters, particularly the blade angle, width and number of blades. Of these three parameters, the tip blade angle and width were responsible for 83.28% and 88.81% of the uncertainty associated with modelling impeller discharge pressure and head, respectively.

A design approach employing average values for all impeller design parameters, excluding the tip blade angle and width, is developed. Instead of specifying the tip blade angle and width of an impeller, the developed approach specifies the impeller discharge pressure and tip flow coefficient.

5

STAGE STACKING PROCEDURE ILLUSTRATION AND VALIDATION

5.1. INTRODUCTION

This chapter outlines and validates the stage stacking procedure developed in Chapters 3 and 4. In section 5.2, the procedure is demonstrated through modelling of Compressor 3's stage performance. Section 5.3 provides the results obtained when the developed stage stacking procedure is applied to compressors 1 to 4 (Table 1).

5.2. STAGE STACKING PROCEDURE ILLUSTRATED

Compressor 3's impeller tip diameters and speeds are provided in Table 1 with the compressor's overall performance curves portrayed in Figure 30. Compressor reference conditions are shown in Appendix B-1. Real gas equations of state (Appendix A-1) are used to calculate relevant properties.

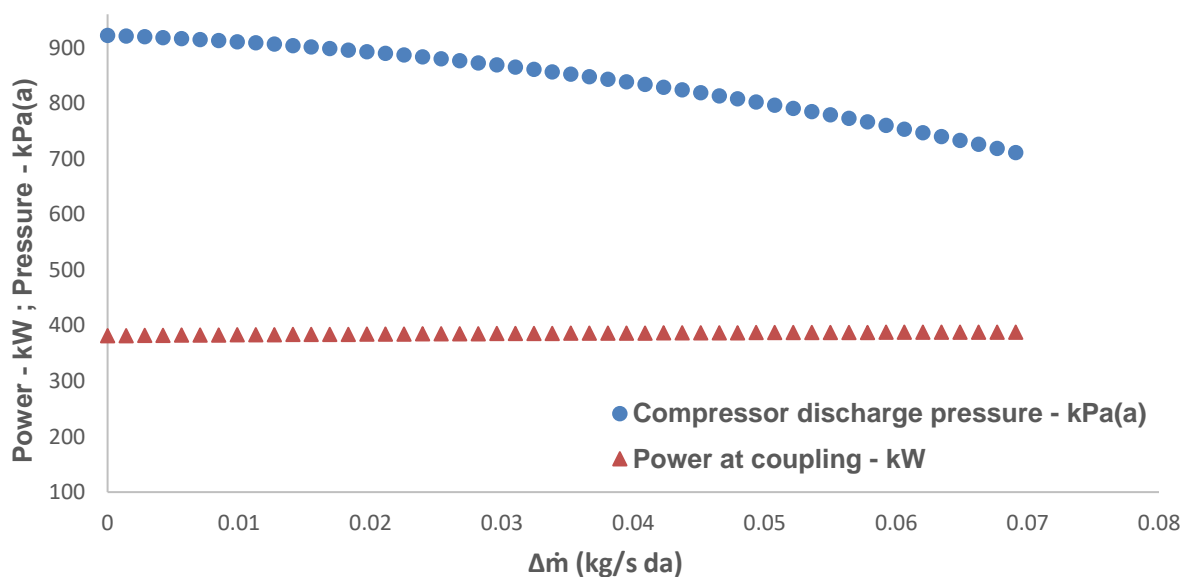


Figure 30: Overall performance curves of Compressor 3

5.2.1. Obtaining stage pressure curves

In section 3.2.2, the maximum total-to-total pressure ratio of a stage was approximated through a linear function (equation 3.4) of stage impeller tip speed. With Compressor 3's impeller tip speeds known, equation 3.4 can be used to compute an initial maximum pressure ratio value for each stage (Table 10).

Table 10: Calculated initial maximum pressure ratio values

Stage no.	Tip speed [m/s]	Maximum pressure ratio value (initial) $\Pi_{\max} = 0.0057U_2 + 0.0204$
1	346.96	2.00
2	353.60	2.04
3	294.10	1.70
4	303.97	1.75

From Table 11, the relative maximum pressure ratios to be imposed when the pressure cost function is minimized equal $2.5 > \Pi_{\max,2} > \Pi_{\max,1} > \Pi_{\max,4} > \Pi_{\max,3} > 1.5$. With the initial maximum pressure ratio values computed, the curve coefficients of equation 3.3 have to be set. The coefficients a_i and b_i are initially set to -1 and 0 for each stage, respectively.

Based on measured values (Appendix B-1, Table B-1), the pressure loss across each intercooler, Δp_{cooler} , is defined as an average value of 6.6 kPa. Using the stage's inlet pressures in conjunction with their parameterized pressure ratio curves, the initial discharge pressure curve for each stage is derived (Figure 31).

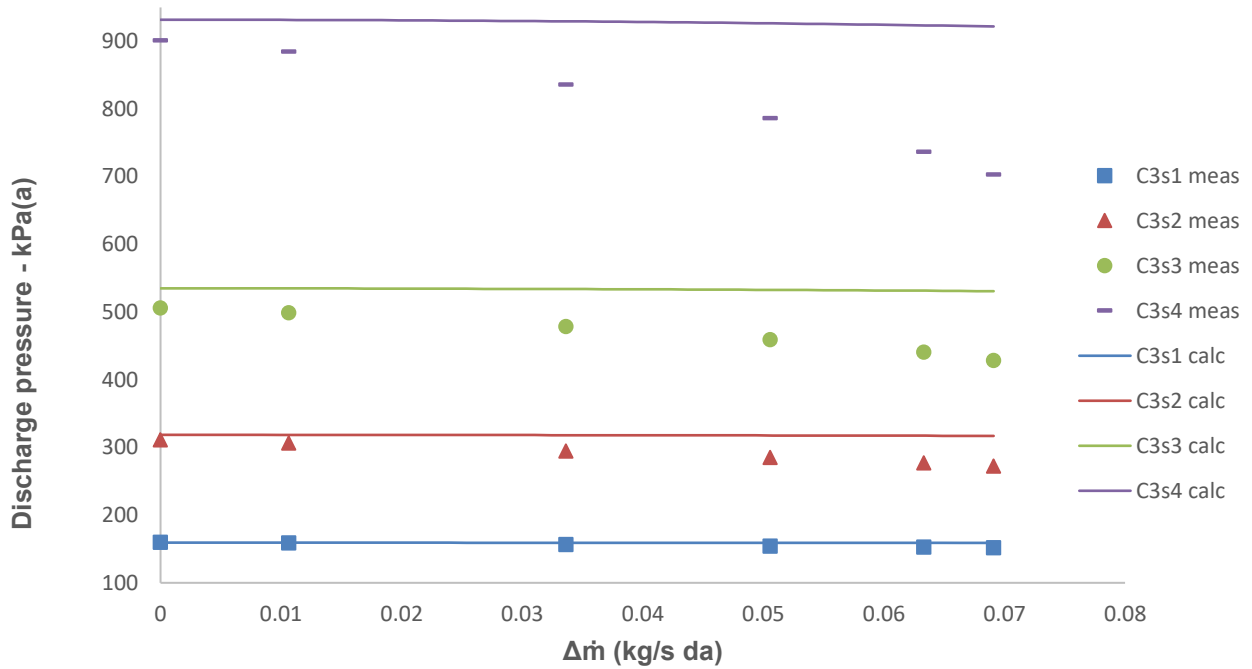


Figure 31: Stage discharge pressure before minimization of the pressure cost function

Noting the compressor’s overall discharge pressure curve (Figure 30) represents the performance of the last stage (Figure 31, stage 4), the overall compressor pressure cost function (equation 3.7) is minimized to obtain the remaining stage discharge pressure curves. Figure 31 presents even before the pressure cost function is minimized, relatively high prediction accuracy of the pressure curves are acquired, provided the maximum pressure ratios of each stage are calculated correctly. The Nelder-Mead Simplex optimization algorithm (Press *et al.*, 1989), implemented through the EES® interface, is employed to vary the parameters of equation 3.3 within upper and lower bounds until the cost function is minimized. Table 11 provides the initial value as well as the upper and lower bounds of each of the parameters of equation 3.3.

Table 11: Initial values and bounds of the pressure ratio curve parameters

Parameter	Stage no.				Lower bound	Upper bound
	1	2	3	4		
Π_{max}	2	2.04	1.7	1.754	1.5	2.5
a	-1	-1	-1	-1	-50	0
b	0	0	0	0	-1	1

Figure 32 demonstrates the stage's discharge pressure curves after the overall compressor pressure cost function (equation 3.7) has been minimized. Table 12 displays the final values of the pressure ratio curve parameters.

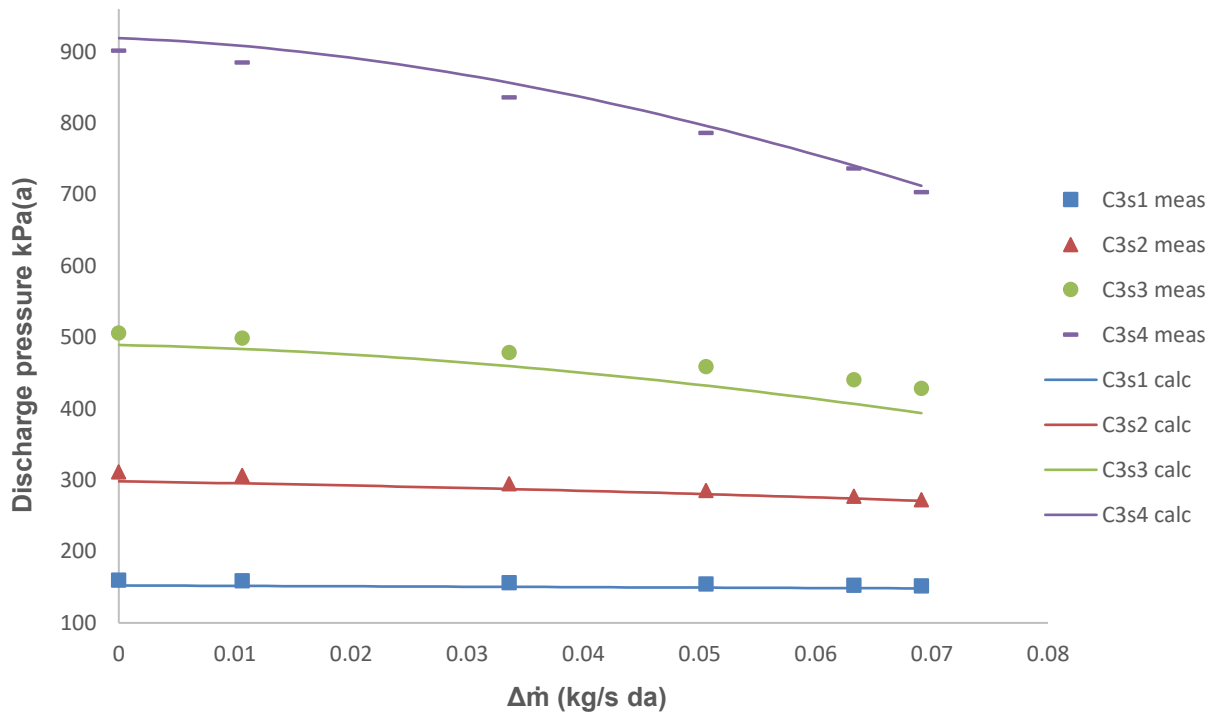


Figure 32: Stage discharge pressure after the minimization of the pressure cost function

Table 12: Final values of the pressure ratio curve parameters

Parameter	Stage no.			
	1	2	3	4
Π_{max}	1.92	2.0	1.663	1.9
a	-0.1469	-14.75	-40.99	-15.33
b	-0.7048	-0.8318	0.148	0.0938

Between the compressors surge, and operating flow rate, the relative error of derived pressures equaled approximately 1-5% for all compressor stages. The maximum error was approximately 8% and occurred near the choked flow region of stage 3.

To ascertain how employing an average pressure drop value across the coolers affects the accuracy of calculated stage discharge pressure, pressure curves were again calculated. However, this time, actual pressure drop values were implemented. Table 13 depicts the value of the pressure drop across each cooler, with Figure 33 illustrating the calculated pressure curves.

Table 13: Pressure loss across stage intercoolers

Impeller no.	Δp_{cooler}
1	12.0
2	7.0
3	3.5
4	5.7

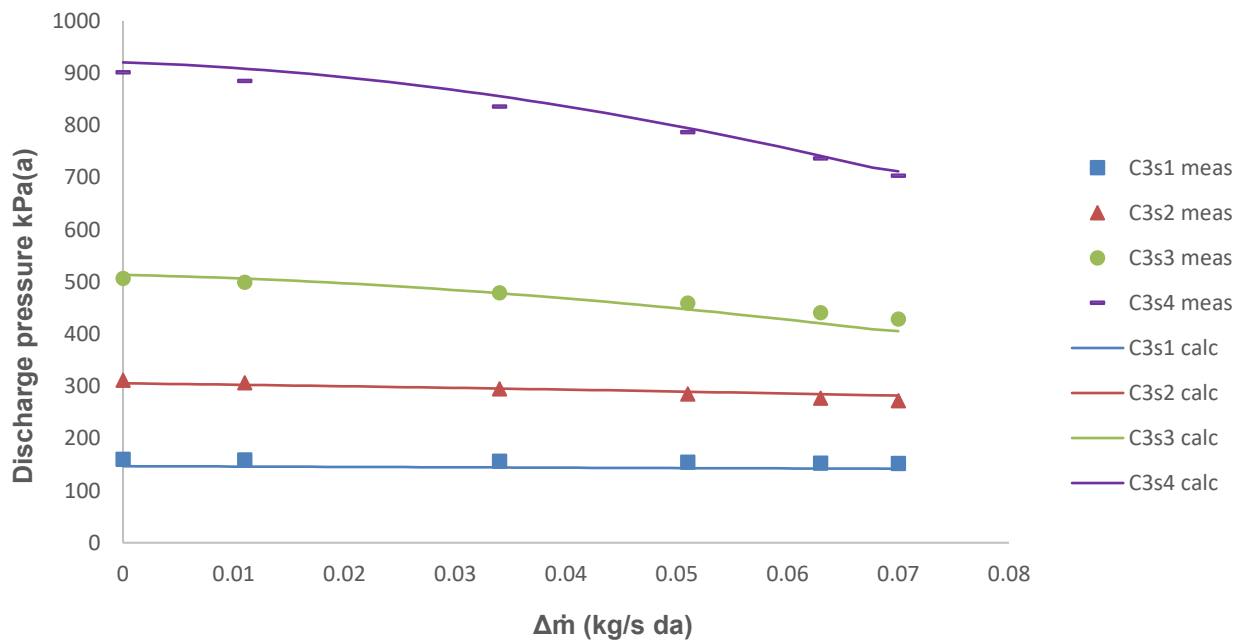


Figure 33: Stage discharge pressure calculated with known inter cooler pressure drop values

Similar to the results of Figure 32, the relative error of calculated pressures varied between 1-5% for all compressor stages. However, the maximum error associated with the choke flow region of stage 3 was reduced from 8% to 6%.

5.2.2. Obtaining stage efficiency curves

With the pressure curve of each stage calculated (Figure 32), the isentropic stage head coefficient curves were computed next. Equation 3.10 was used to determine the inlet temperature of each stage, with the cold temperature difference and cooling water temperature equaling 10.5 °C and 25 °C, respectively. The cold temperature difference is defined based on the average value of measurements obtained (Appendix B, Table B-1). Since the discharge pressure of one stage represents the inlet pressure of the subsequent stage, the inlet pressures of each stage are known. Stage inlet enthalpies and entropies are calculated as a function of the inlet temperatures and pressures: $h_{01}, s_1 = f(T_{01}, P_{01})$, with the isentropic discharge enthalpies representing a function of the inlet entropies and discharge pressures: $h_{04s} = f(s_1, P_{04})$. At each flow point, the stage's isentropic head coefficients are denoted through equation 2.16.

Figure 34 illustrates the isentropic head coefficient curves calculated for the stages of Compressor 3.

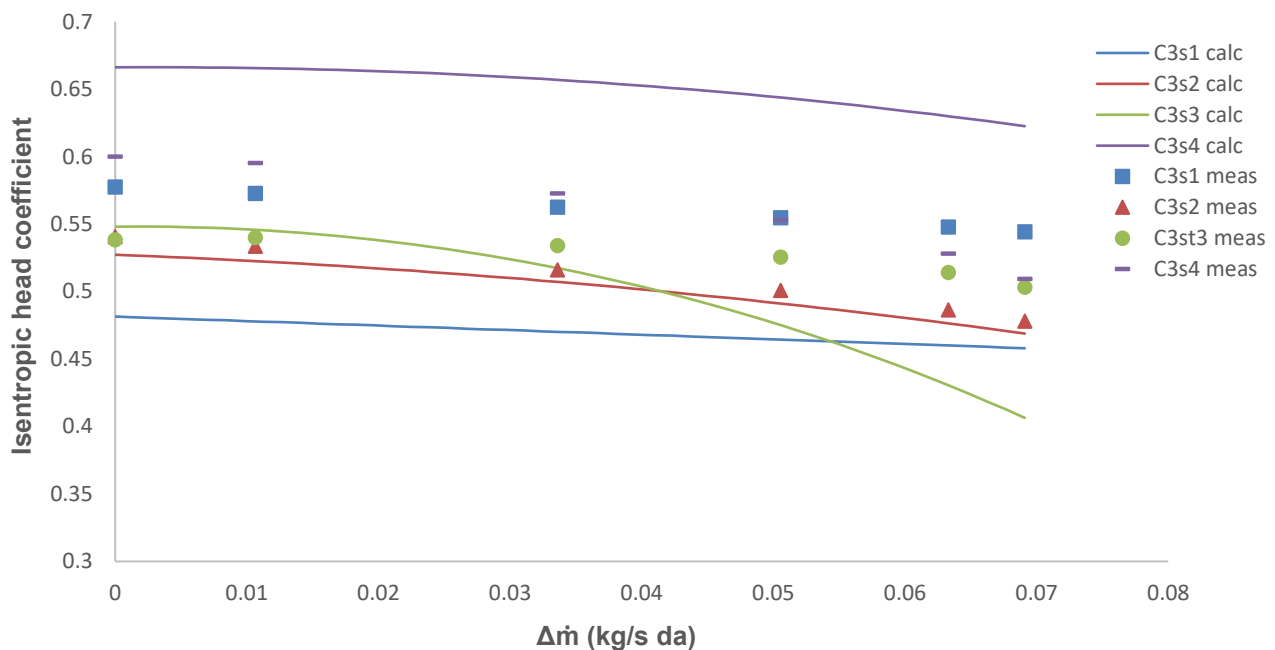


Figure 34: Isentropic head coefficient curves of Compressor 3

To evaluate the relative performance of each of the impellers in terms of their maximum head coefficient, a comparative impeller is designed and analysed for each stage at the compressor surge flow rate, employing the procedure detailed in section 4.4. Impeller parameters, excluding the tip blade angle and width, are designed using the average values listed in Appendix D, Table D-3. Instead of specifying the impeller's tip blade angles and widths, a tip flow coefficient and approximating discharge pressure is specified. Based on the results of section 4.2.2.2, an average tip flow coefficient value of 0.24 was derived for each impeller. Approximate impeller discharge pressures were

calculated through the procedure outlined in section 4.4.2.1. Stage 1’s estimated impeller discharge pressure is calculated to demonstrate this procedure.

Through equation 4.3, the maximum impeller discharge enthalpy is reflected as $h_{02,max} = 392.11$ kJ/kg. The corresponding maximum discharge pressure, $P_{02,max}$, is computed as a function of the stage inlet entropy and the maximum discharge pressure as $P_{02,max} = 210.41$ kPa. The minimum possible impeller discharge pressure equals stage discharge pressure: $P_{02,min} = P_{04} = 152.40$ kPa. Finally, the approximate impeller discharge pressure is denoted as the root mean square value of the maximum and minimum possible impeller discharge pressure through equation 4.4 as $P_{02,app} = 188.23$ kPa. The approximated impeller discharge pressures calculated for all four stages are shown in Table 14.

Table 14: Approximated impeller discharge pressure of Compressor 3

Impeller no.	$P_{02,app}$
1	188.29
2	341.34
3	543.94
4	1037.01

Using the analysis model of Aungier (2000), the relative performance of impellers in terms of their maximum head coefficients were examined. Table 15 presents the appraisal in comparison to the measured values.

Table 15: Relative impeller head coefficients of Compressor 3

Measured	Assessed
$\psi_{max,4} > \psi_{max,1} > \psi_{max,3} > \psi_{max,2}$	$\psi_{max,4} > \psi_{max,1} > \psi_{max,3} > \psi_{max,2}$

Stage efficiencies varied between 70-90% at the compressors’ surge flowrates (Figure B-11 and B-12), and based on these findings, a lower and upper bound was defined for the maximum stage head

coefficient of each impeller. The upper bound is calculated as a function of the isentropic stage head coefficient and the minimum stage efficiency, through equation 5.1.

$$\psi_{02,max} = \frac{\psi_{04s}}{\eta_{04,min}} \quad (5.1)$$

The lower bound is calculated as a function of the isentropic stage head coefficient and the maximum stage efficiency through equation 5.2.

$$\psi_{02,min} = \frac{\psi_{04s}}{\eta_{04,max}} \quad (5.2)$$

Initial values for each stage were chosen within the upper and lower bounds subject to the relative performance requirement of Table 15 ($\psi_{max,4} > \psi_{max,1} > \psi_{max,3} > \psi_{max,2}$). Table 16 presents the calculated initial values and bounds for the head coefficients used during the stage stacking procedure.

Table 16: Initial values and bounds calculated for stage head coefficients

ψ_{max}	Stage no.			
	1	2	3	4
Initial value	0.65	0.60	0.63	0.76
Lower bound	0.59	0.53	0.60	0.73
Upper bound	0.76	0.68	0.73	0.93

With relative performance in terms of maximum head coefficients known, the curve coefficients of equation 3.5 must be set. The coefficients c_i and d_i were initially set to -1 and 0, respectively. For the c_i curve coefficient, the lower and upper bounds were set as -50 and 0, respectively. The lower and upper bounds of the d_i curve coefficient were set as -1 and 1, respectively. Figure 35 shows the

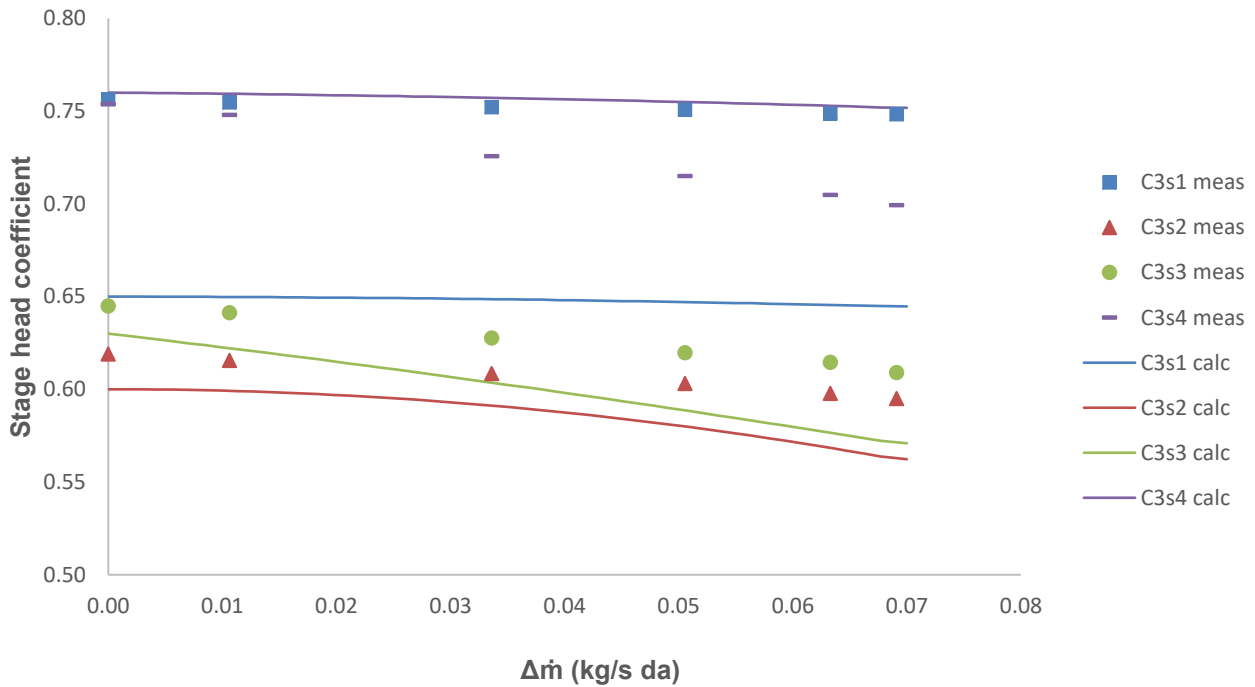


Figure 35: Head coefficients curves of Compressor 3 before minimization of the power cost function

calculated stage head coefficient curves before the coupling power cost function (equation 3.11) is minimized.

The gas power of each stage at various mass flow rates can be calculated using equation 3.9. Based on measurements obtained (Appendix B-1, Table B-1), the total mechanical loss of the compressor was defined as 11% of the compressor’s coupling power at its surge flowrate.

Finally, a derived coupling power curve is produced through the summation of the stages’ gas power curves. The coupling power curve computed before the minimization of the power cost function (equation 3.11) is portrayed in Figure 36.

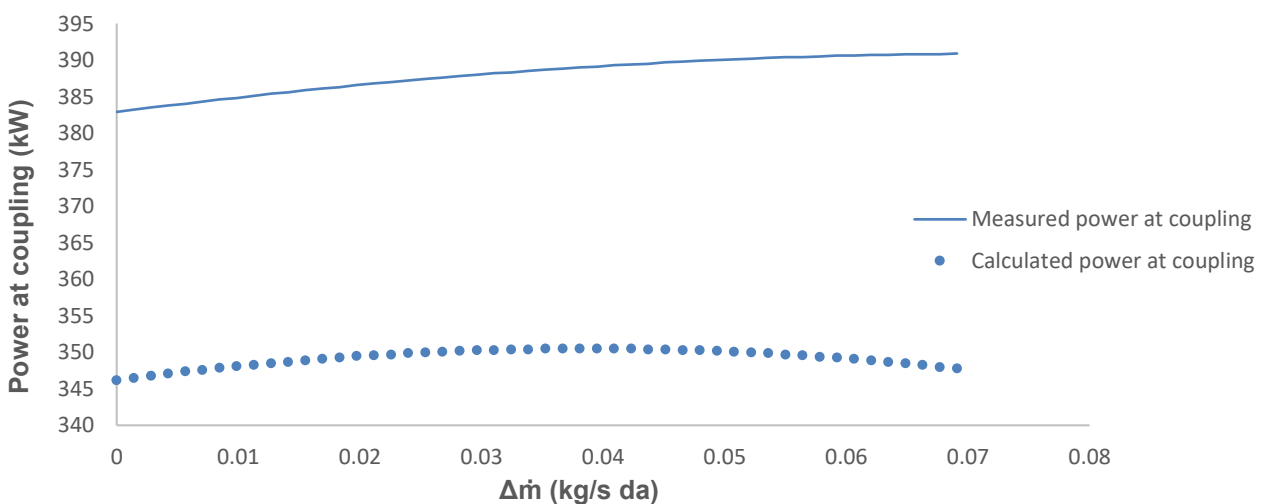


Figure 36: Calculated coupling power before minimization of the cost function

With the initial head coefficient curves calculated for each stage, the Melder Mead simplex optimization algorithm (Press *et al.*, 1989) was implemented through the EES® interface to minimize the power cost function (equation 3.11).

Figure 37 demonstrates the derived power curve compared to the measured power curve when the power cost function has been minimized. Table 17 illustrates the updated values of the stage head curve parameters, and Figure 38 portrays the updated stage head coefficient curves.

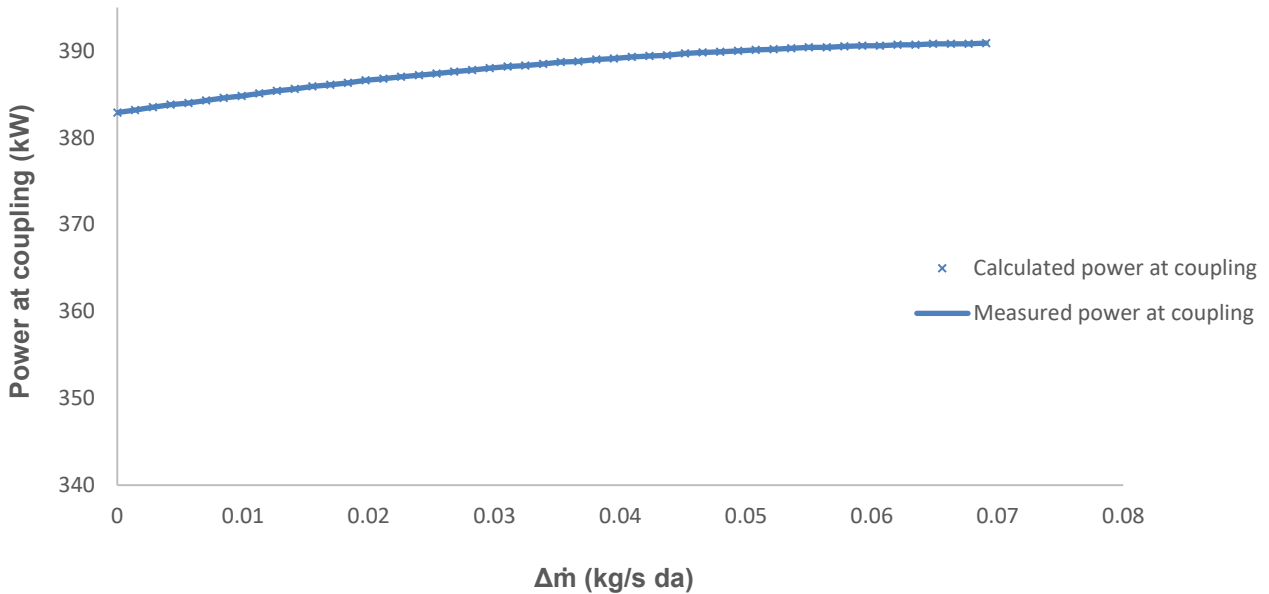


Figure 37: Calculated coupling power after the minimization of the power cost function

Table 17: Final values of the head coefficient curve parameters

Parameter	Stage no.			
	1	2	3	4
ψ_{max}	0.64	0.60	0.62	0.80
c	0	-5.57	-1.98	-0.86
d	-0.002	0.003	-0.620	-0.065

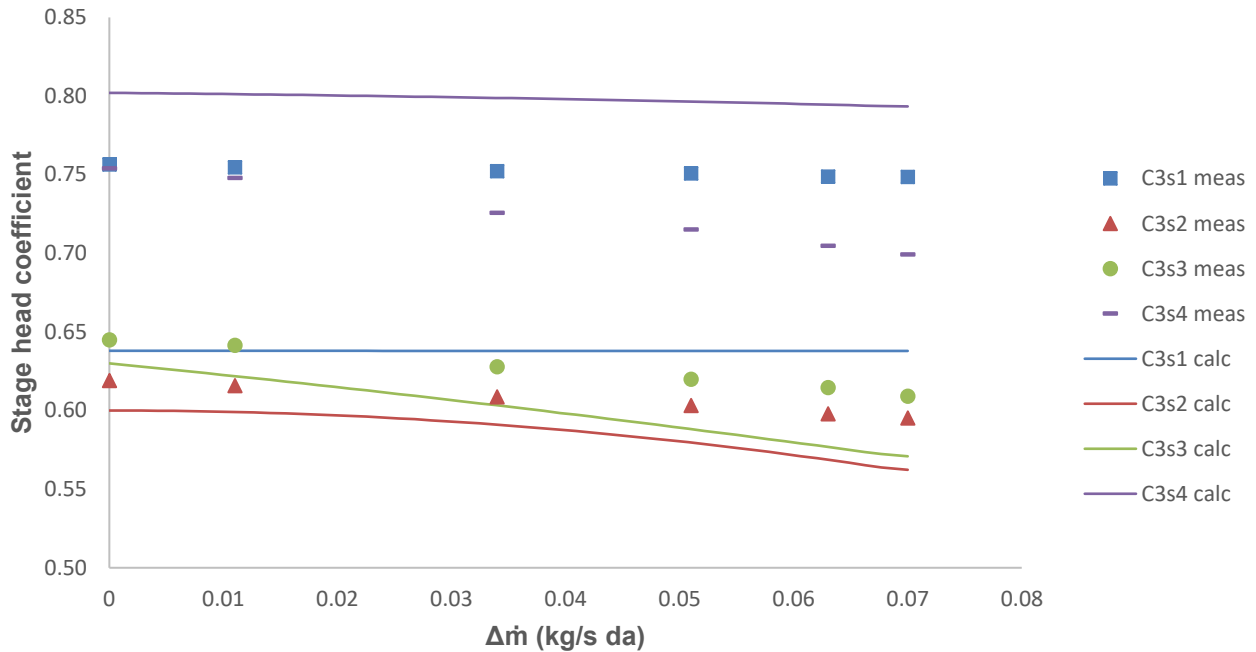


Figure 38: Head coefficient curves of Compressor 3 after minimization of the power cost function

Figure 38 reveals the head coefficient values of stage 1 are much lower than the measured values while the values of stage 4 are much higher than the measured values. When the coupling power cost function is minimized, the head coefficient values are limited to values that will produce isentropic efficiencies ranging between 70% - 90%. Hence, if the isentropic head coefficient values calculated (Figure 34) are lower or higher than the measured values, the head coefficient values will then have to assume lower or higher values to ensure the stage isentropic efficiencies are calculated within the defined limits.

Although the stage stacking procedure (section 3.2.3) entails calculating stage head coefficient curves, compressor performance is typically assessed in terms of efficiency. The isentropic efficiency curve of each stage can be computed as a function of the stage head- (equation 2.15) and stage

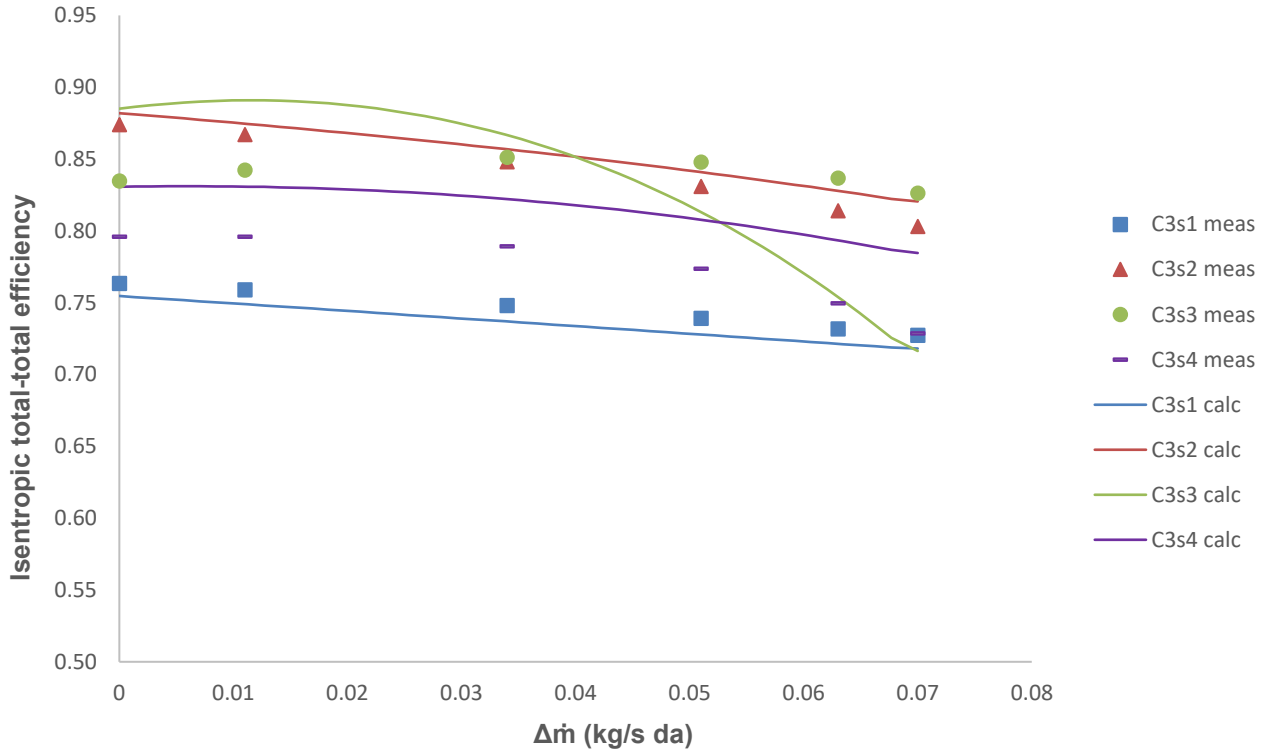


Figure 39: Stage isentropic efficiency curves

isentropic head (equation 2.16) coefficients through equation 2.18. Figure 39 depicts the measured versus calculated isentropic stage total-to-total efficiencies of Compressor 3.

The efficiencies of all the stages, excluding stage 3, were calculated within a 6% (absolute) error margin. The calculated efficiency for stage 3 remained within a 5% error margin between the compressor's surge and operating flow rates, with the error increasing to a maximum error of 8% between the operating and choke flow rates. This is due to the fact the isentropic head coefficient curve derived for stage 3 (Figure 34) also deviated from the measured values in the same flow region.

To ascertain how employing an average CTD value affects the accuracy of the derived efficiency curves, the curves were calculated again. This method employed the discharge pressures calculated with actual intercooler pressure drop values (Figure 33) in conjunction with the actual CTD across each stage intercooler (Table 18). Accuracy improved with the maximum prediction error reduced from 8% to 6% (Figure 40).

Table 18: CTD across intercoolers

Impeller no.	CTD
1	12.5
2	9.5
3	7.9
4	8.6

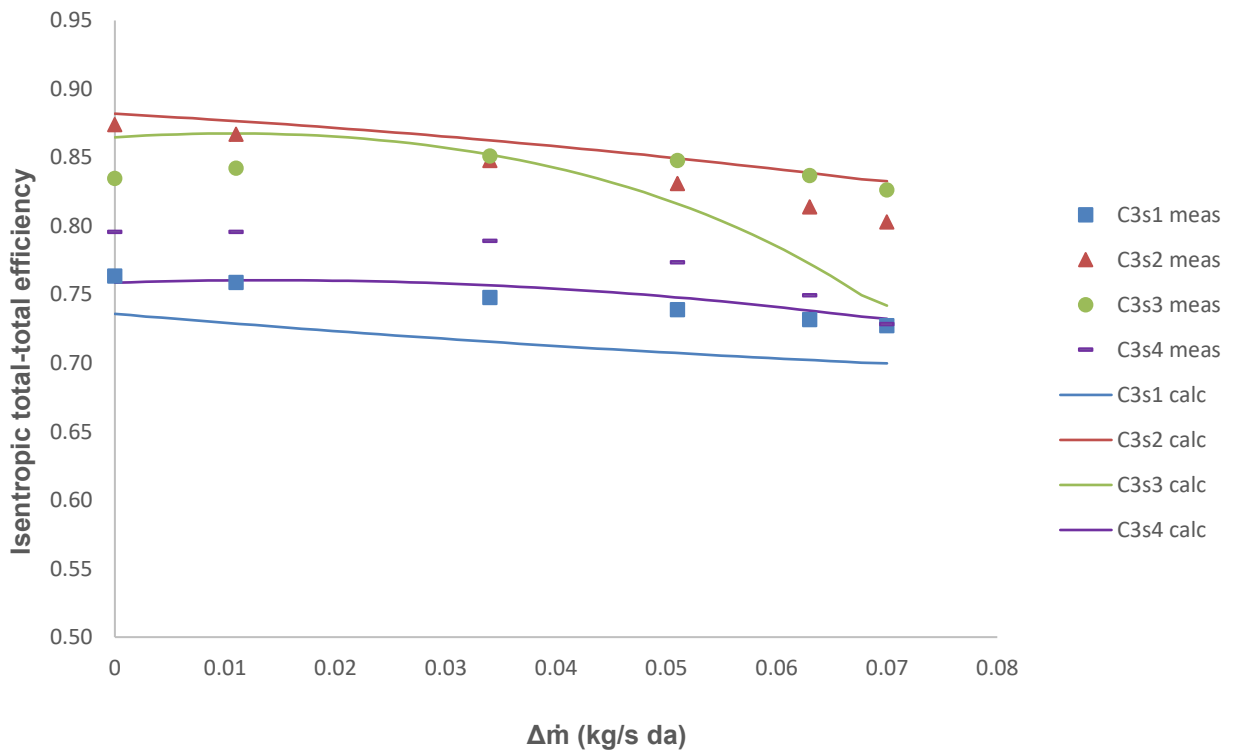


Figure 40: Stage isentropic efficiency calculated with known intercooler pressure drop and CTD values

5.3. VALIDATION RESULTS AND DISCUSSION

The modified stage stacking procedure was applied to all the compressors for which stage performance was known (Appendix F). Figures 41 and 42 illustrate the prediction error associated

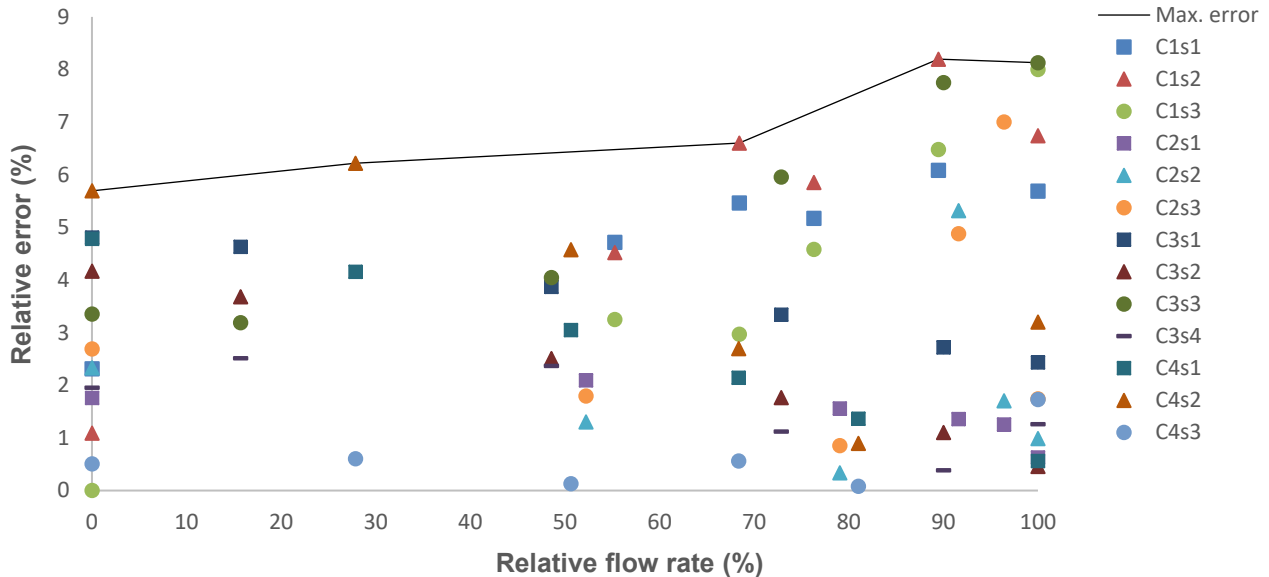


Figure 42: Relative error of calculated stage total discharge pressure

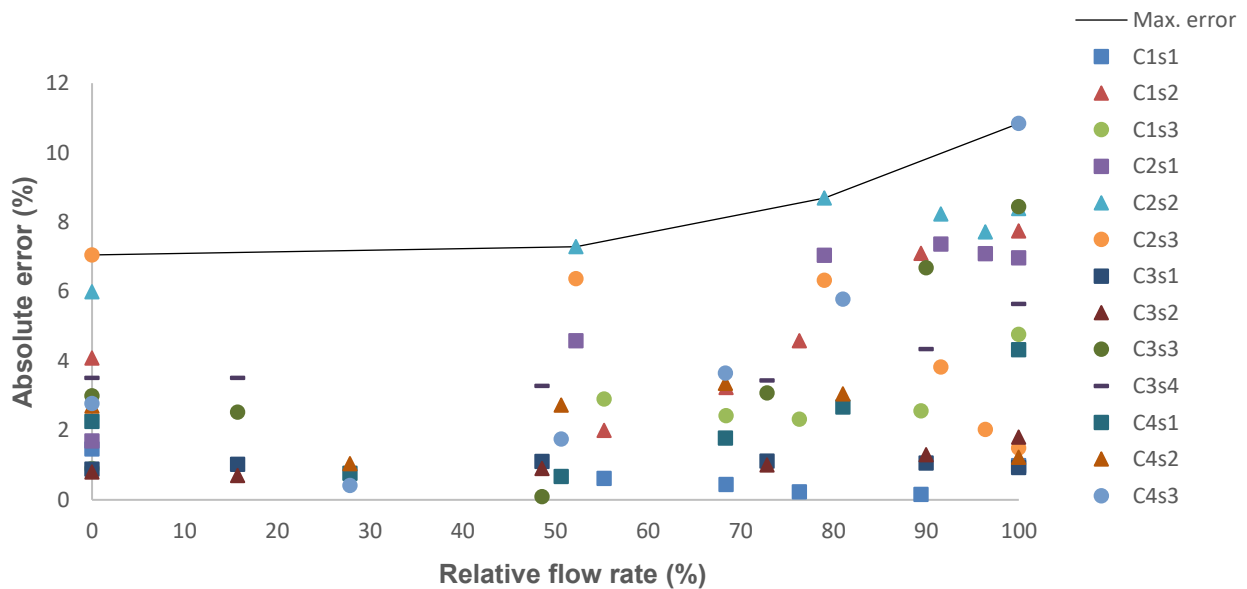


Figure 41: Absolute error of calculated stage isentropic efficiency

with each stage as a function of the relative flow rate. The 0% relative flow rate corresponds to the compressor’s surge point whereas the 100% relative flow rate relates to the compressor’s choke point. For all stages, the lowest error between the modelled and measured data occurred within the 0-60 % relative flow range. Generally, the stage performance curves remain linear in this flow range, and if the maximum pressure ratios and head coefficients are calculated accurately, the first section of the

curves will be accurate as well. In the 0-60 % flow range, the developed stage stacking procedure predicted the discharge pressure and efficiency of the stages within a maximum error of 6.22% and 7.23%, respectively. From the 60% flow range upwards, the maximum pressure and efficiency prediction errors equaled 8.20% and 10.84%, respectively.

The simplified 1-dimensional model accurately reflected the relative maximum head coefficients for all compressors (Table 19), except for compressor 4. However, the value of compressor 4's maximum

Table 19: Relative assessment of maximum impeller head coefficients

Compressor no.	Measured	Calculated
1	$\psi_{\max,3} > \psi_{\max,2} > \psi_{\max,1}$	$\psi_{\max,3} > \psi_{\max,2} > \psi_{\max,1}$
2	$\psi_{\max,3} > \psi_{\max,2} > \psi_{\max,1}$	$\psi_{\max,3} > \psi_{\max,2} > \psi_{\max,1}$
3	$\psi_{\max,4} > \psi_{\max,1} > \psi_{\max,3} > \psi_{\max,2}$	$\psi_{\max,4} > \psi_{\max,1} > \psi_{\max,3} > \psi_{\max,2}$
4	$\psi_{\max,1} > \psi_{\max,3} > \psi_{\max,2}$	$\psi_{\max,3} > \psi_{\max,2} > \psi_{\max,1}$

stage head coefficients were so similar (Appendix B, Figure B-8), an error assessing relative performance did not significantly affect the stage stacking results.

5.4. CONCLUSION

Odom and Muster (2009) unveiled map-based models hold accurate for +/- 5% at best. Brown and Rahman (2002) asserted if these models are used for performance monitoring, they generally accurately identify performance gaps of 10% and higher. Based on this, the results obtained with the developed stage stacking procedure, with a maximum prediction error of 8.20% and 10.84% for discharge pressure and isentropic efficiency, respectively, is deemed adequate for stage performance monitoring.

This study demonstrates prediction accuracy improves if actual values for the pressure drop and CTD's across intercoolers are used.

6

SUMMARY AND CONCLUSION

6.1. EXECUTIVE SUMMARY

The reliable operation of IGCCs used in the coal-fired power generation industry of South Africa is essential for economic, environmental and safety considerations (section 1.1). To maintain these compressors proactively, individual stage performance curves are required (section 1.2). The objective of this thesis (section 1.3) was to develop a methodology for compressor owners to model compressor stage performance using inputs reasonably available to them, namely the overall performance characteristic of the compressors in conjunction with stage impeller diameters and tip speeds. The developed technique had to be generic enough to be compatible with different IGCC models, manufactured between 1970-current, found in the coal-fired power generation industry of South Africa.

A literature study was conducted in Chapter 2, focusing on the design of IGCCs, compressor aerothermodynamics, map-based compressor performance models and 1-dimensional compressor performance models. Map-based models were an obvious choice in attaining the thesis objectives since they require the least amount of detailed stage design input. Of the models studied, the stage stacking procedure (section 2.4.1) Mathioudakis and Stamatis (1994) employed was identified as the most suitable for realising the thesis goal. However, the Mathioudakis and Stamatis (1994) model required a known operating point on each of the stage's performance curves, unknown to compressor owners. The approach taken in this thesis resulted in a modified version of the Mathioudakis and Stamatis (1994) stage stacking procedure, which instead of being based on known stage performance points, employed relative stage performance. Relative stage maximum discharge pressure was assessed through the application of similarity principles (section 2.3.1) with the relative stage maximum head coefficient assessed through a combination of similarity principles and a simplified version of the 1-dimensional impeller analysis model of Aungier (2000).

Chapter 3 illustrated the approach taken when the modified stage stacking procedure was developed. Parameterisation of the pressure and head coefficient curves for the stages of the IGCCs found in the coal-fired power generation industry of South Africa was illustrated in sections 3.2.1 and 3.2.3, respectively. Section 3.2.2 revealed how similarity principles were applied to relate the maximum stage discharge pressure to the impeller tip speed. The procedure of stage stacking implemented for discharge pressures and head coefficients was described in sections 3.3.1 and 3.3.2, respectively. Practical considerations, such as the effect of intercoolers and mechanical losses, are discussed.

Chapter 4 outlined how the 1-dimensional impeller analysis model of Aungier (2000) can be simplified so the relative maximum impeller head coefficients can be assessed, employing only the impeller diameters and tip speeds. To ensure the integrity of the researcher rendition of the 1-dimensional impeller analysis model of Aungier (2000), a verification process was followed whereby the results of the 1-dimensional model were compared to the results of a commercial compressor analysis software package (section 4.2). A sensitivity analysis was conducted to understand the influence of design parameters on the prediction accuracy of the 1-dimensional model (section 4.3). Section 4.4 portrayed how average values for design parameters were used in conjunction with similarity principles to obtain impeller designs for relative assessment.

The developed stage stacking procedure was applied to four compressors, for which the stage performance was known (Chapter 5). The resulting accuracy with which stage performance was predicted remained in the same range as similar models found in the literature. Stage discharge pressures and isentropic efficiencies were predicted with maximum errors of 8.20% and 10.84% (Figures 43 and 44), respectively. The simplified 1-dimensional model correctly predicted relative stage maximum head coefficients for three out of the four compressors assessed (Table 19). It was demonstrated how the prediction accuracy of the developed model improved when actual intercooler performance parameters were used instead of the assumed performance.

6.2. CONCLUSION

For the IGCCs used in the coal-fired power generation industry of South Africa, similarity principles can be employed in conjunction with a simplified 1-dimensional impeller analysis model to obtain stage performance from overall compressor performance. Stage performance can be obtained even with the limited stage design information (impeller diameter and tip speed). The accuracy of the modelled stage performance is similar to that of map-based models found in literature and deemed sufficiently accurate to be used for condition monitoring purposes.

6.3. RECOMMENDATIONS FOR FURTHER RESEARCH

The developed stage stacking procedure defines intercooler performance employing average values for performance parameters. It was illustrated in Sections 5.2.1 and 5.2.2 that the prediction accuracy of the developed stage stacking procedure could be improved if the actual intercooler performance parameters are used. It is proposed the prediction accuracy of the developed stage stacking procedure could be improved through the inclusion of an intercooler model.

This thesis dealt with the problem of obtaining stage performance curves when limited stage design data is available. With the means to obtain stage performance curves realized, further research should focus on the process of employing these curves to trend stage performance and identifying stage failure mechanisms. The research should consider the unique challenges site-based compressors pose, typically not being installed with all the instrumentation required to conduct comprehensive performance assessments. Furthermore, the effect that different IGV settings have on compressor and stage performance should be considered.

BIBLIOGRAPHY

- Aungier, R. (2000) *Centrifugal Compressors: A Strategy for Aerodynamic Design and Analysis*. New York: ASME Press.
- Balje, O. E. (1981) *Turbomachines - A guide to design, selection, and theory*. New York: John Wiley & Sons.
- Botha, B. W., and Moolman, A. (2005) 'Determining the Impact of the Different Losses on Centrifugal Compressor Design', *The SA mechanical Engineer*, 21(3), pp. 23–31.
- Boyce, M. P. (2003) *Centrifugal Compressors: A Basic Guide*. Tulsa: PennWell.
- Brown, R. and Rahman, K. (2002) 'Turbine/compressor performance monitoring software and flow capacity', in *PSIG Annual Meeting 2002*. Pipeline Simulation Interest Group.
- Busemann, A. (1928) 'The head ratio of centrifugal pumps with logarithmic spiral blades', *ZAMM*, (8 Oct.), pp. 372–384.
- Cicciotti, M. (2015) 'Adaptive Monitoring of Health-State and Performance of Industrial Centrifugal Compressors by Matteo Cicciotti', (June).
- Coppage, J.E., Dallenbach, F., Eichenberger, H.P., Hlavaka, G.E., Knoernschild, E.M., Van Lee, N. (1956) *Study of Supersonic Radial Compressors for Refrigeration and Pressurization on Systems*.
- Daily, J.W. and Nece, R. E. (1960) 'Roughness Effects on Frictional Resistance of Enclosed Rotating Disks', *Journal of Basic Engineering*, 82(3), p. 553.
- Dixon, S. and Hall, C. (2010) *Fluid Mechanics and Thermodynamics of Turbomachinery*. 5th edn, *Fluid Mechanics and Thermodynamics of Turbomachinery*. 5th edn. London: Elsevier-Butterworth-Heinemann.
- Fingerhut, U., Rothstein, E. and Sterz, G. (1991) 'Standardized Integrally Geared Turbomachines Tailor Made for the Process Industry', in *Proceedings of the 20th Turbomachinery Symposium*, pp. 131–143.
- Galvas, M. R. (1973) 'Fortran Program for Predicting off-Design Performance of Centrifugal Compressors'.

- Gong, X. and Chen, R. (2014) 'Total Pressure Loss Mechanism of Centrifugal Compressors', *Mechanical Engineering Research*, 4(2), pp. 45–59.
- GUTIÉRREZ VELÁSQUEZ, E. I. (2017) 'Determination of a suitable set of loss models for centrifugal compressor performance prediction', *Chinese Journal of Aeronautics*, 30(5), pp. 1644–1650.
- Lemmon, E. *et al.* (2000) 'Thermodynamic Properties of Air and Mixtures of Nitrogen, Argon, and Oxygen From 60 to 2000 K at Pressures to 2000 MPa', *Journal of Physical and Chemical Reference Data*, 29(3), pp. 331–385.
- Li, P. Y., Gu, C. W. and Song, Y. (2015) 'A new optimization method for centrifugal compressors based on 1D calculations and analyses', *Energies*, 8(5), pp. 4317–4334.
- Lieblein, S. (1959) 'Loss and Stall Analysis of Compressor Cascades', *Journal of Basic Engineering*, (Sept.), p. 387.
- Ludtke, K. H. (2004) *Klaus H. Ludtke Process Centrifugal Compressors*. Springer.
- Massardo, A. (1991) 'An analytical method for the fault diagnosis of axial multistage compressors', in *Proceedings of the ASME Turbo Expo*.
- Mathioudakis, K. and Stamatis, A. (1994) 'Compressor fault identification from overall performance data based on adaptive stage stacking', *Journal of Engineering for Gas Turbines and Power*, 116(1), pp. 156–164.
- Müller, M., Hendricks, E. and Sorenson, S. C. (1998) 'Mean value modelling of turbocharged spark ignition engines', in *SAE Technical Papers*, p. 23.
- Nece, R. E. (1960) 'Roughness Effects on Frictional Resistance of Enclosed Rotating Disks', *Journal of Basic Engineering*, 82(3), p. 553.
- Odom, F. M. and Muster, G. L. (2009) 'Tutorial on modeling of gas turbine driven centrifugal compressors', in *PSIG Annual Meeting 2009*. Pipeline Simulation Interest Group.
- Oh, H. W., Yoon, E. S. and Chung, M. K. (1997) 'An optimum set of loss models for performance prediction of centrifugal compressors', *Proceedings of the Institution of Mechanical Engineers, Part A: Journal of Power and Energy*, 211(4), pp. 331–338.
- Press, W. *et al.* (1989) 'Numerical recipes in Pascal', in *Numerical recipes in Pascal*. Cambridge University Press, p. 737.

- Redlich, O. and J., K. (1949) 'On the Thermodynamics of Solutions. V. An Equation of State. Fugacities of Gaseous Solutions.', *Chemical Reviews*, 44(1), pp. 233–244.
- Rogers, C. ; (1996) 'Gas Turbine Theory'. Harlow, England: Pearson Education Limited.
- Schlichting, H. (1979) *Boundary-Layer Theory*. 6th Ed. New York: Mcgraw- Hill.
- Sieros, G., Stamatis, A. and Mathioudakis, K. (1997) 'Jet Engine Component Maps for Performance Modeling and Diagnosis', *Journal of Propulsion and Power*, 13(5), pp. 665–674.
- Simon, H. (1987) 'Design Concept and Performance of a Multistage Integrally Geared Centrifugal Compressor Series for Maximum Efficiencies and Operating Ranges', *Turbomachinery*, 1, p. V001T01A012.
- Standards, B. (2005) *Turbocompressors - Performance test code*.
- Taylor, B. and Kuyatt, C. (1994) 'Guidelines for evaluating and expressing the uncertainty of NIST measurement results'.
- de Wet, A. L., von Backström, T. W. and van der Spuy, S. J. (2012) 'Performance Investigation of a Turbocharger Compressor', *Turbomachinery*, Volume 8, pp. 939–953.
- Wiesner, F. J. (1967) 'A review of slip factors for centrifugal impellers', *Journal of Engineering for Gas Turbines and Power*, 89(4), pp. 558–566.
- Ziegler, K. (2003) 'Centrifugal Compressor "Radiver" with MTU Impeller - Test Case CD-Rom Readme'. Aachen University.

APPENDIX A: IMPELLER PERFORMANCE MODELLING

This appendix provides the correlations employed to implement the 1-dimensional model of Aungier (2000), as discussed in section 2.5. Figures A-1 and A-2 display the impeller design parameters required for model implementation.

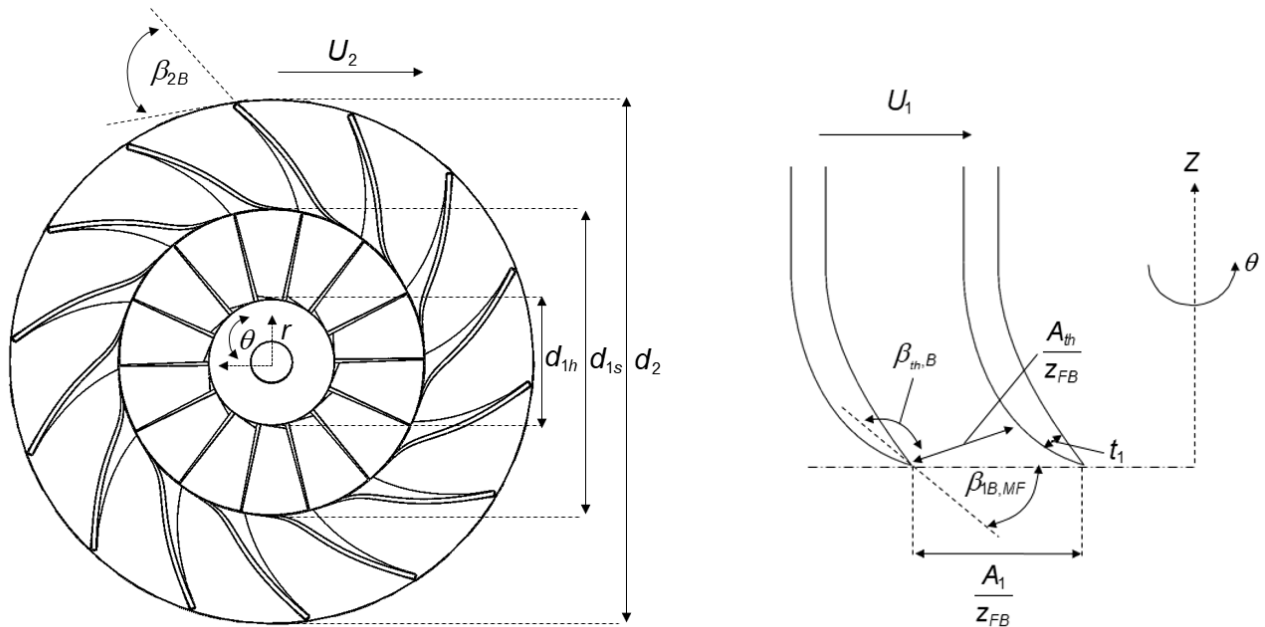


Figure A-1: Impeller frontal view in the $r-\theta$ plane (left) and inlet blade geometry (right)

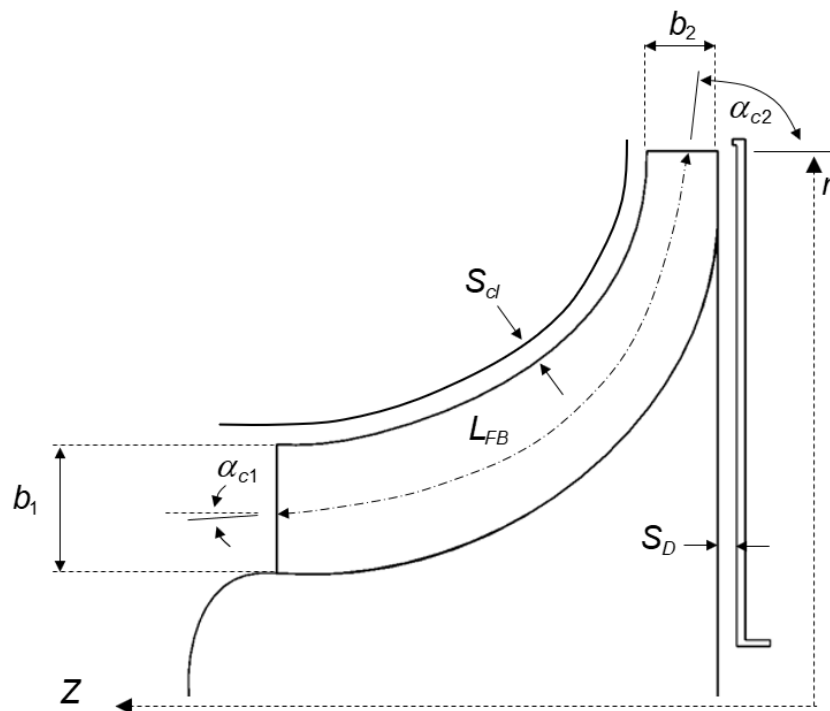


Figure A-2: Cross-sectional view of a impeller in the $r-z$ plane

A-1 EQUATIONS OF STATE FOR REAL GASES

Aerodynamic analysis requires thermodynamic state equations in addition to fundamental equations of fluid dynamics and thermodynamics (Aungier, 2000). This thesis employs the 1-dimensional model of Aungier (2000) using the EES® software. EES® calculates dry air properties using the fundamental equations of state developed for real gases by Lemmon (2000), valid for temperatures between 60 K – 2000 K at pressures up to 2000 MPa.

A-2 SKIN FRICTION COEFFICIENT

To demonstrate skin friction effects on impeller performance, a general formulation considering laminar and turbulent flow regimes in conjunction with impeller surface finish impact is needed (Aungier, 2000). Aungier (2000) used three well-established skin friction models by Schlichting (1979). For rough surfaces, Aungier (2000) developed correlations for each flow regime (laminar and turbulent), computed as a function of the valley to peak surface roughness. However, for this study, the impeller surfaces are assumed to be smooth, and only the relevant correlations will be discussed further.

The relevant flow regime is determined through the Reynolds number, Re_d , with representing a laminar flow, $2000 < Re_d < 4000$ representing transitional flow, and $Re_d > 4000$ signifies a turbulent flow. The Reynolds number is denoted as:

$$Re_d = \frac{\rho \bar{W} d_h}{\mu} \quad A.2.1$$

with d_h illustrating the hydraulic diameter of an impeller passage presented as:

$$d_H = \frac{4(A_{cs})}{wp} \quad A.2.2$$

The hydraulic diameter depicts the mean value of the impeller inlet and discharge passage and is used in conjunction with a mean relative velocity to compute the Reynolds number. For a laminar flow regime, the skin friction coefficient is as:

$$C_{f_l} = \frac{16}{Re_d} \quad A.2.3$$

For a transitional flow regime, the skin friction coefficient is rendered as:

$$c_f = c_{ff} + (c_{ft} - c_{ff}) \left(\frac{Re_d}{2000} - 1 \right) \quad A.2.4$$

whereas for a turbulent flow regime, the skin friction coefficient is represented as:

$$\frac{1}{\sqrt{c_{ft}}} = -2 \log_{10} \left[\frac{2.51}{Re_d \sqrt{4c_{ft}}} \right] \quad A.2.5$$

A-3 IMPELLER WORK INPUT MODELING

The impeller comprises the stage component doing work on the fluid, and the enthalpy rise it imparts to the fluid indicates the impeller work input. The enthalpy difference across the impeller rendered non-dimensional with the tip speed illustrating the work input factor. For the ideal impeller, the work input factor consists of the blade work only, but in practice, additional parasitic work inputs must be considered. The parasitic work inputs Augnier (2000) discussed include disc friction-, leakage- and recirculation losses.

$$I = \frac{\Delta h_0}{U_2^2} = I_B + I_{DF} + I_L + I_R \quad A.3.1$$

The blade work input factor is calculated as:

$$Re_d < 2000 \quad I_B = \frac{C_{U_2}}{U_2} - \frac{U_1 C_{U_1}}{U_2^2} \quad A.3.2$$

with the second term on the right-hand side of the equation falling away if no pre-whirl exists at the inlet.

$$I_B = \frac{C_{U_2}}{U_2} \quad A.3.3$$

If no slip is present at the impeller tip (ideal case) equation A.3.3 could be written as:

$$I_B = \frac{C_{U_2}}{U_2} = 1 - \lambda \phi_2 \cot \beta_2 \quad A.3.4$$

where λ represents the tip distortion factor.

$$\lambda = \frac{1}{1 - B_2} \quad A.3.5$$

Since in practice slip is always present, equation A.3.4 is modified to include the slip factor:

$$I_B = \sigma(1 - \lambda\phi_2 \cot \beta_2) \quad \text{A.3.6}$$

Slip Factor

The slip factor (Aungier,2000) used is the approximated Busemann (1928) slip factor at zero flow by Wiesner (1967) and is shown in equation A.3.7.

$$\sigma = 1 - \frac{\sqrt{\sin \beta_2 \sin \alpha_{C2}}}{z^{0.7}} \quad \text{A.3.7}$$

Busemann (1928) uncovered the slip factor could be treated as a constant up to a limiting radius ratio. Aungier (2000) denoted his limiting ratio as:

$$\varepsilon_{LIM} = \frac{\sigma - \sigma^*}{1 - \sigma^*} \quad \text{A.3.8}$$

With

$$\sigma^* = \sin(19^\circ + 0.2\beta_2) \quad \text{A.3.9}$$

When the limiting factor is reached, a corrected slip factor is calculated as:

$$\sigma_{COR} = \left[1 - \left(\frac{\varepsilon - \varepsilon_{LIM}}{1 - \varepsilon_{LIM}} \right)^{\sqrt{\frac{\beta_2}{10}}} \right] \quad \text{A.3.10}$$

The Impeller Distortion/Blockage Factor

Blockage is due to boundary layer growth along the blade passage between the throat and the tip, and it affects impeller performance, effectively reducing the cross-sectional area along the blade passage. Aungier (2000) derived the tip blockage correlation by inverting the work input equation and then deriving the blockage factor from experimental work input curves.

$$B_2 = \varpi_{SF} \frac{\rho_{v1}}{\rho_{v2}} \sqrt{\frac{W_1 d_H}{W_2 b_2}} + \left[0.3 + \frac{b_2^2}{L_{FB}^2} \right] \frac{A_R^2 \rho_2 b_2}{\rho_1 L_{FB}} + \frac{S_{CL}}{2b_2} \quad \text{A.3.11}$$

The throat tip area ratio is illustrated as:

$$A_R = \frac{A_2 \sin \beta_{2B}}{A_1 \sin \beta_{th,B}} \quad \text{A.3.12}$$

Clearance Gap Flows

For open impellers, such as the ones considered in this study, flow leakage occurs between the blade and housing surfaces through the clearance gap. The flow is driven by the pressure gradient between the blades pressure and suction sides, and this leakage flow velocity is reflected as:

$$U_{CL} = 0.816 \sqrt{\frac{2\Delta P_{CL}}{\rho_2}} \quad \text{A.3.13}$$

Using the change in fluid angular momentum, Aungier (2000) computes the average pressure difference across the clearance gap as:

$$\Delta P_{CL} = \frac{\dot{m}(r_2 C_{U_2} - r_1 C_{U_1})}{zr b L_{FB}} \quad \text{A.3.14}$$

With the average radius and hub to shroud passage width given in equations A.3.15 and A.3.16, respectively:

$$\bar{r} = \frac{(r_1 + r_2)}{2} \quad \text{A.3.15}$$

$$\bar{b} = \frac{(b_1 + b_2)}{2} \quad \text{A.3.16}$$

To account for a impeller which includes splitter blades, Aungier (2000) defines an effective number of blades as:

$$z = z_{FB} + z_{SB} L_{SB} / L_{FB} \quad \text{A.3.17}$$

Finally, the clearance gap mass flow is calculated as:

$$\dot{m}_{CL} = \rho_2 z S_{CL} L_{FB} U_{CL} \quad \text{A.3.18}$$

Windage and Disk Friction Work

Windage and disk friction work results from the friction between the impeller disc and the compressor housing. The impeller disks in this study are assumed to be smooth, and thus only the applicable loss models will be discussed. Aungier (2000) used Daily and Nece (1960) as a starting point to calculate the windage and disc friction work. The disk torque coefficient is defined as:

$$C_M = \frac{2\tau}{\rho\omega^2 r^5} \quad \text{A.3.19}$$

Four flow regimes are considered, and for each regime, a torque coefficient is rendered, namely: laminar, merged boundary layers,

$$C_{M1} = \frac{2\pi}{(S_D / r)\text{Re}} \quad \text{A.3.20}$$

laminar, separated boundary layers,

$$C_{M2} = \frac{3.7\left(\frac{S_D}{r}\right)^{0.1}}{\sqrt{\text{Re}}} \quad \text{A.3.21}$$

turbulent, merged boundary layers,

$$C_{M3} = \frac{0.08}{\left(\frac{S_D}{r}\right)^{\frac{1}{6}} \text{Re}^{\frac{1}{4}}} \quad \text{A.3.22}$$

And turbulent, separated boundary layers,

$$C_{M4} = \frac{0.102\left(\frac{S_D}{r}\right)^{0.1}}{\text{Re}^{0.2}} \quad \text{A.3.23}$$

The Reynolds number in equations A.3.20-A.3.23 is calculated as:

$$\text{Re} = \frac{\rho\omega r_2^2}{\mu} \quad \text{A.3.24}$$

The four torque coefficients reflect the flow regime. The correct flow regime corresponds to the largest of the four torque coefficients. Aungier (2000) imposed a clearance gap flow to the ideal torque coefficients listed in equation A.3.20-A.3.23 as:

$$C_M = C_{Mo} \frac{(1-K)^2}{(1-K_0)^2} \quad \text{A.3.25}$$

C_{Mo} denotes the Daily and Nece (1960) torque coefficient, and K and K_0 is determined through equation A.3.26 and A.3.27, respectively.

$$K = \frac{C_{U_2}}{U_2} \quad \text{A.3.26}$$

$$K_0 = \frac{0.46}{\left(1 + 2 \frac{S_D}{d_2}\right)} \quad \text{A.3.27}$$

Daily and Nece (1960) defined torque coefficients from both disc sides, and Aungier (2000) enforced a factor of 0.75 to this value for the single disc of an open impeller (equation A.3.28).

$$C_{MD} = 0.75C_M \quad \text{A.3.28}$$

Finally, the disc work coefficient equals:

$$I_{DF} = \frac{\rho_2 U_2 r_2^2 C_{MD}}{2\dot{m}} \quad \text{A.3.29}$$

Impeller Leakage Loss

This flow leakage loss results from the impeller clearance gaps to the impeller inlet, where the impeller reenergizes it (Aungier, 2000). Portraying this loss, Aungier (2000) assumed the impeller inlet re-entrains half the clearance gap flows. Experimental work with open impellers helps derive this empirical postulation. The impeller leakage loss is illustrated as:

$$I_L = \frac{\dot{m}_{CL} U_{CL}}{2U_2 \dot{m}_{CL}} \quad \text{A.3.30}$$

with U_{cl} and \dot{m}_{cl} calculated using equations A.3.13 and A.3.18, respectively.

Recirculation work

Aungier (2000) professed for very high head coefficients impellers with excessive blade loading and low tip relative flow angles, the work input increased dramatically at low mass flow rates. Aungier (2000) asserted the rise in work input results from flow back recirculation into the impeller tip at low flow rates. Demonstrating the losses associated with recirculation, Aungier (2000) used a conditional requirement based on a generalized version of the compressor equivalent diffusion factor, D_{eq} , Lieblein (1959) used for axial compressors. If the condition $D_{eq} > 2$ is met, a recirculation loss is computed from equation A.3.31.

$$I_R = \frac{\frac{D_{eq}}{2} - 1}{\frac{W_{U_2}}{C_{m_2}} - 2 \cot \beta_2} \quad \text{A.3.31}$$

The compressor equivalent diffusion factor is derived as:

$$D_{eq} = \frac{W_{max}}{W_2} \quad \text{A.3.32}$$

with the maximum impeller blade velocity difference between the blade's pressure and suction sides being calculated as:

$$W_{max} = \left(\frac{W_1 + W_2 + \Delta W}{2} \right) \quad \text{A.3.33}$$

with the average blade velocity difference, ΔW , calculated as:

$$\Delta W = \frac{2\pi d_2 U_2 l_B}{z L_{FB}} \quad \text{A.3.34}$$

A-4 IMPELLER INTERNAL LOSS CORRELATIONS

Traditionally losses are computed as a total head loss, however, for convenience, when used in conjunction with the model discussed in section 2.5, Aungier (2000) expressed these losses as a pressure loss coefficient defined as:

$$\varpi = \frac{\Delta p_0}{p_0 - p} \quad \text{A.4.1}$$

Inducer Incidence loss

Incidence losses occur when the relative velocity of the fluid entering the inducer is at a different flow angle than the relative inlet blade impeller angle. The effects of incidence loss are most prominent at off-design operating conditions. The correlation for inducer incidence equals:

$$\varpi_{inc} = 0.8 \left[1 - \frac{C_{M_i}}{W_1 \sin \beta_{1B}} \right]^2 + \left[\frac{z_{FB} t_1}{2\pi r_1 \sin \beta_{1B}} \right]^2 \quad \text{A.4.2}$$

The incidence coefficient is calculated at the hub, mean and shroud surfaces. The overall incidence coefficient is defined as the weighted average of these values with the mean values weighed ten times more than the hub and shroud values.

Entrance diffusion loss

As the flow moves from the inducer leading edge to the impeller throat, the negative pressure gradient in the boundary layer results in boundary layer growth, potentially leading to flow separation and eventually inducer stall (GUTIÉRREZ VELÁSQUEZ, 2017). The diffusion loss is given as:

$$\varpi_{DIF} = 0.8 \left[1 - \frac{W_{th}}{W_1} \right]^2 - \varpi_{inc} \quad A.4.3$$

with the requirement $\varpi_{DIF} \geq 0$. For some impellers, losses associated with inducer diffusion is more prominent than incidence losses (Aungier, 2000).

Choking Loss

When the relative velocity component at the impeller inlet reaches sonic conditions, shock wave associated losses drastically reduce impeller efficiency. Aungier (2000) defines a contraction ratio, equation A.4.4, to represent the aerodynamic blockage in the throat area:

$$C_r = \sqrt{\frac{A_1 \sin \beta_1}{A_{th}}} \quad A.4.4$$

The contraction ratio in conjunction with the critical inlet area calculated as:

$$A^* = \frac{\dot{m}}{\rho^* V^*} \quad A.4.5$$

conditionally imposing a choke loss based on the value defined for X :

$$X = 11 - \frac{10C_r A_{th}}{A^*} \quad A.4.6$$

with the choke loss coefficient assuming a value of:

$$\varpi_{CH} = \begin{cases} 0 & ; X \leq 0 \\ \frac{0.05X + X^7}{2} & ; X > 0 \end{cases} \quad A.4.7$$

Skin Friction loss

Skin friction losses are due to the shear forces exerted on the fluid inside of the boundary layer as it moves across the impeller, diffuser and channel walls. The skin friction loss coefficient is calculated as:

$$\varpi_{SF} = 4c_f \left(\frac{\bar{W}}{W_1} \right)^2 \frac{L_{FB}}{d_H} \quad \text{A.4.8}$$

Aungier (2000) professed since the flow throughout the impeller varies substantially, a skin friction coefficient, C_f , is required. The friction coefficient is discussed in appendix A-2.

Blade loading loss

Blade loading losses, similar to inducer diffusion losses, are due to boundary layer growth and flow separation resulting in secondary circulation between the pressure and suction sides of the impeller vanes (GUTIÉRREZ VELÁSQUEZ, 2017). Aungier (2000) used equation A.4.9 to defined blade loading loss.

$$\varpi_{BL} = \left(\frac{\Delta W}{W_1} \right)^2 / 24 \quad \text{A.4.9}$$

The average blade velocity difference, ΔW , is calculated using equation A.3.34.

Hub to shroud loading loss

The pressure gradient between the blade-to-blade and hub-to-shroud surfaces causes this loss, producing secondary flows in the impeller passage (Aungier, 2000). The loss is computed as:

$$\varpi_{HS} = \left(\frac{\bar{k}_m \bar{b} \bar{W}}{W_1} \right)^2 / 6 \quad \text{A.4.10}$$

with the mean streamline curvature, \bar{k}_m , represented as:

$$\bar{k}_m = \frac{(\alpha_{C2} - \alpha_{C1})}{L_{FB}} \quad \text{A.4.11}$$

and the mean relative velocity denoted as:

$$\bar{W} = \frac{(W_1 + W_2)}{2} \quad \text{A.4.12}$$

Supercritical Mach Number Loss

Shock losses when the blade surfaces reach sonic conditions generate these losses (Gong and Chen, 2014). Aungier (2000) expressed these losses as:

$$\varpi_{cr} = 0.4 \left[\frac{(Ma_{1,r}^* - Ma_r^*) W_{max}}{W_1} \right]^2 \quad A.4.13$$

The critical relative Mach number, $Ma_{CR,rel}$, is calculated as:

$$Ma_r^* = Ma_1 W^* / W_{max} \quad A.4.14$$

W_{max} is calculated through equation A.3.32 and W^* represents the relative velocity at the impeller mid passage.

Clearance loss

A pressure difference exists between the pressure and suction face of a rotating impeller blade. The least resistant path the fluid moving along the blade pressure side can take to neutralise the pressure gradient is between the rotary impeller and stationary casing (Aungier, 2000). The correlation Aungier (2000) used to portray this loss is:

$$\varpi_{CL} = \frac{2\dot{m}_{CL}\Delta p_{CL}}{\dot{m}\rho_1 W_1^2} \quad A.4.15$$

Mixing loss

This loss results from mixing jet and wake profiles at the impeller exit (Botha and Moolman, 2005). Aungier (2000) calculated this loss through equation A.4.16.

$$\varpi_{mix} = \left[\frac{(C_{m,wake} - C_{m,mix})}{W_1} \right]^2 \quad A.4.16$$

Abrupt expansion loss

Similar to the mixing loss, this loss is due to distorted flow mixing with the free stream (Aungier, 2000) and is defined as:

$$\varpi_{\lambda} = \left[\frac{(\lambda - 1) C_{m_2}}{W_1} \right]^2 \quad A.4.17$$

with the impeller tip distortion factor, λ , derived through equation A.3.5.

APPENDIX B: MEASURED COMPRESSOR PERFORMANCE DATA

In this appendix, the compressor stage manufacturer performance data is provided. Performance data for four IGCCs consisting of 13 stages between them was obtained and is shown in Table B-1. Inlet conditions at which the performance data were obtained entail $T_{01} = 303.14$ K, $P_{01} = 83$ kPa and $RH = 0$. The compressors were all manufactured in the early 2000s, excluding compressor 4, manufactured in the 1970s. The performance data were acquired following the specifications of the Turbocompressor-Performance test code (Standards, 2005). Appendix B-1 provides the measured stage performance (total-to-total pressure ratio and stage head coefficient) for compressors 1 to 4. Appendix B-2 displays the graphs obtained when the maximum head coefficient and isentropic efficiency are plotted as a function of non-dimensional parameters.

B-1 Measured compressor performance data

Table B-1: Measured compressor performance data

Compressor no.	Stage no.	Average pressure loss across intercooler (kPa)	Average cold temperature difference (K)	Maximum coupling power (kW)	Mechanical power loss (kW)	Percentage of max coupling power (%)
1	1	5.0	7.9	759.4	85.8	11.3
	2	4.2	8.9			
	3	7.4	13.3			
2	1	6.2	13.9	535.3	61.7	11.2
	2	6.3	13.9			
	3	6.4	13.9			
3	1	10.0	12.5	387.5	47.3	12.2
	2	5.0	9.5			
	3	0.66	7.9			
	4	3.76	8.6			
4	1	9.0	11.1	1136.8	133.9	11.2
	2	12.5	6.3			
	3	9.1	8.6			
Average		6.6	10.5	-	-	11.5

Compressor 1

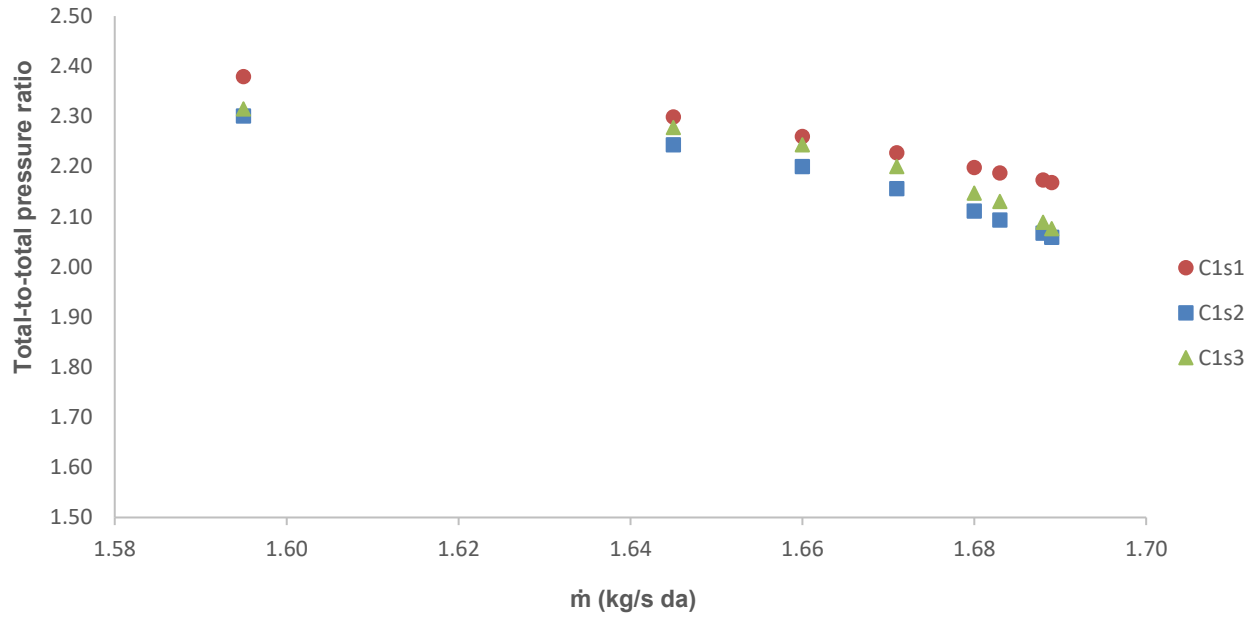


Figure B-1: Compressor 1, stage total-to-total pressure ratio

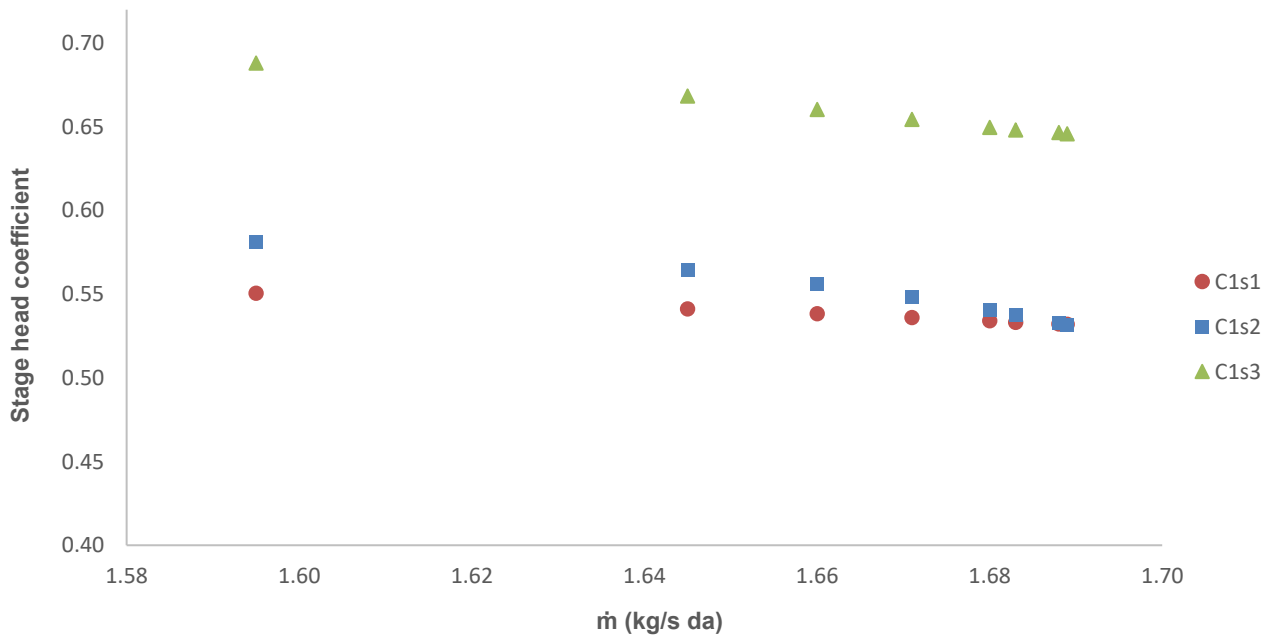


Figure B-2: Compressor 1, head coefficients

Compressor 2

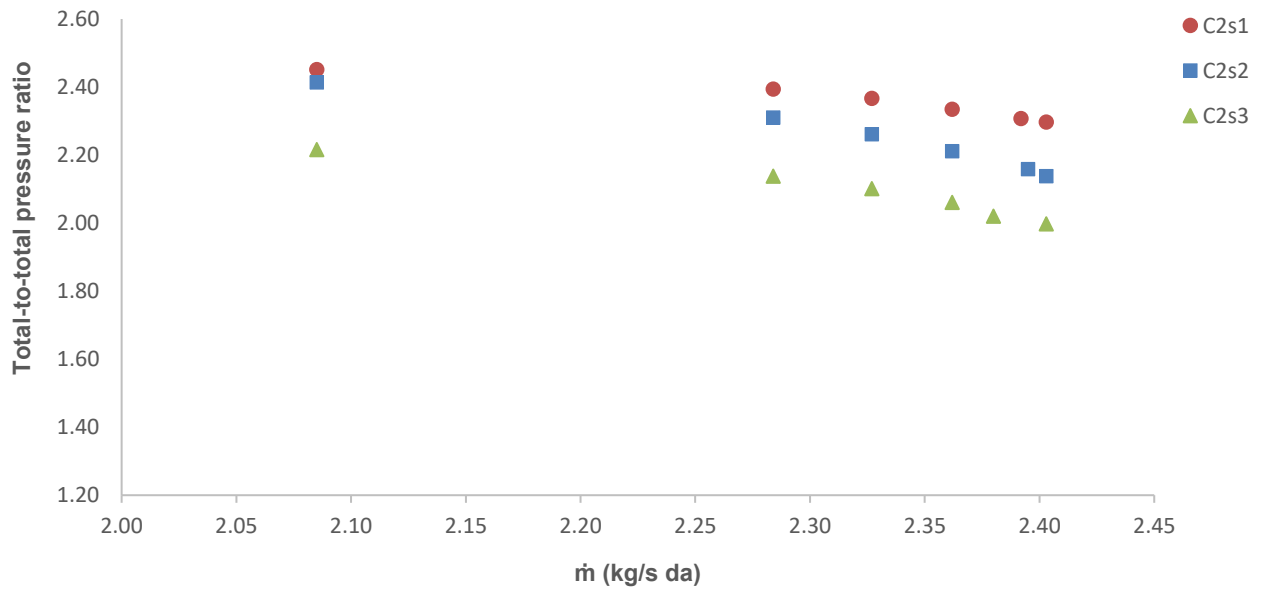


Figure B-3: Compressor 2, stage total-to-total pressure ratio

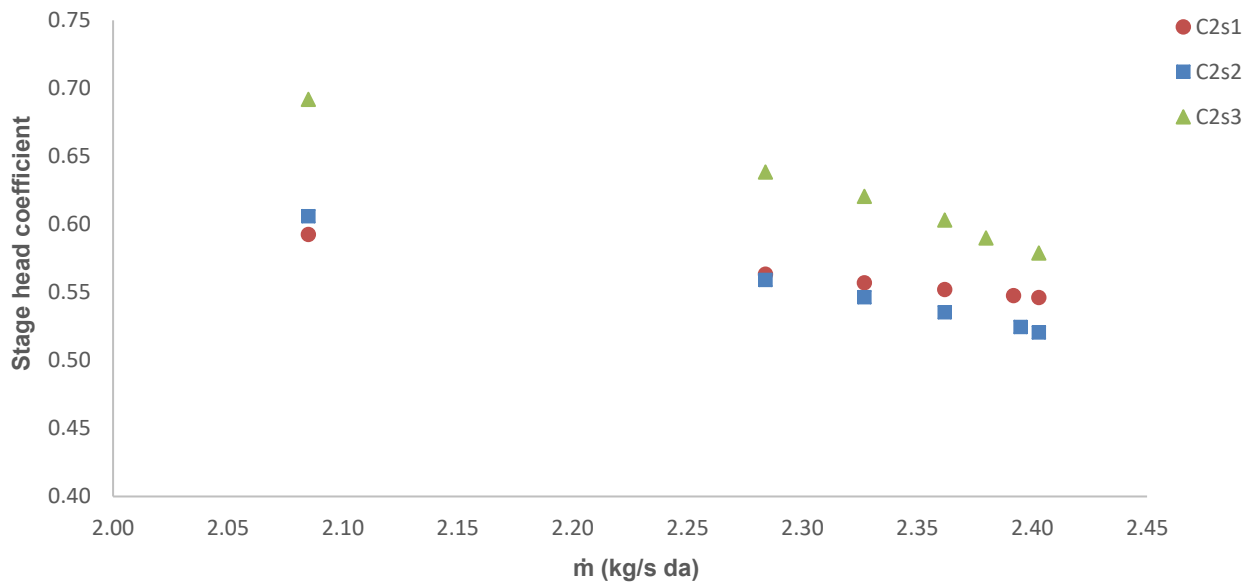


Figure B-4: Compressor 2, head coefficients

Compressor 3

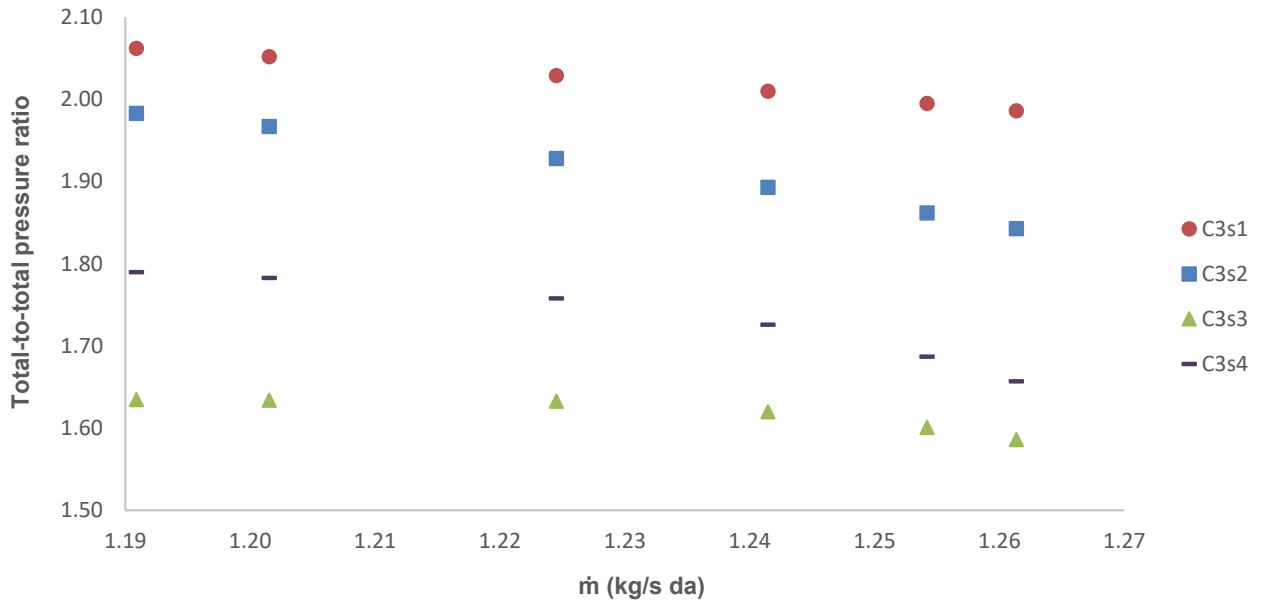


Figure B-5: Compressor 3, stage total-to-total pressure ratio

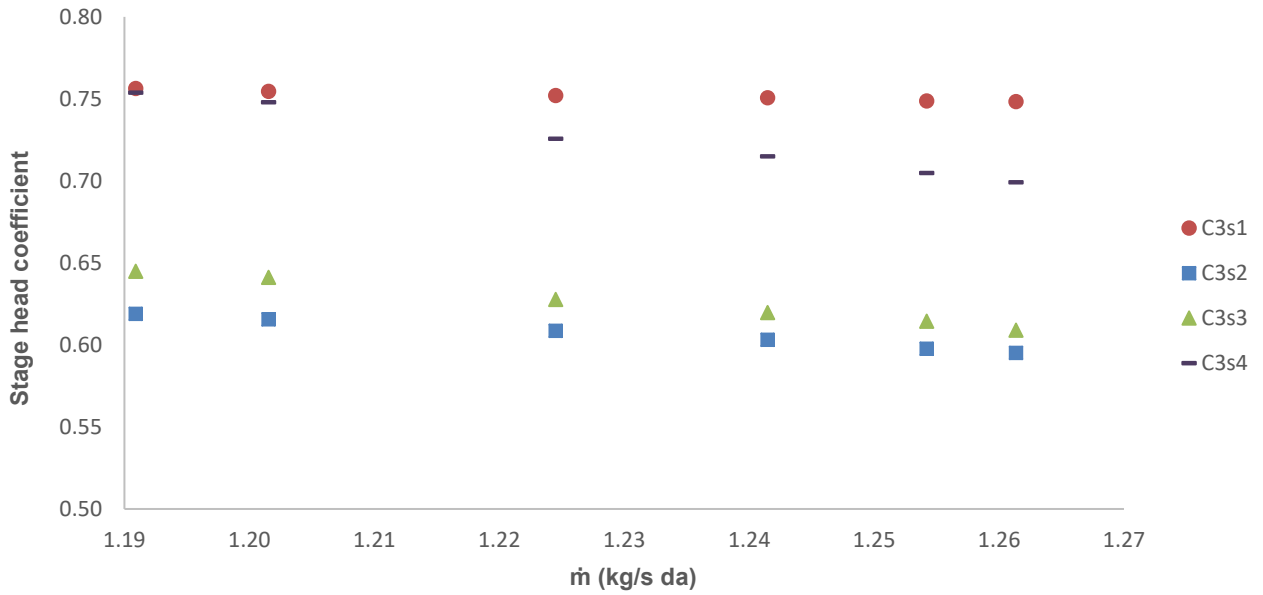


Figure B-6: Compressor 3, head coefficients

Compressor 4

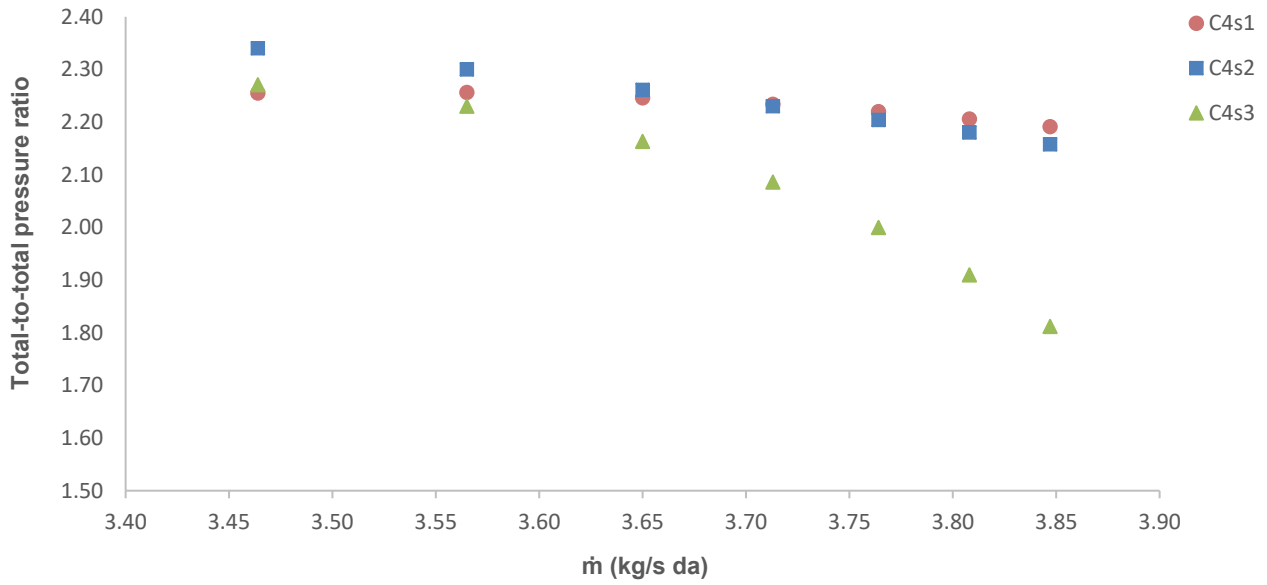


Figure B-7: Compressor 4, stage total-to-total pressure ratio

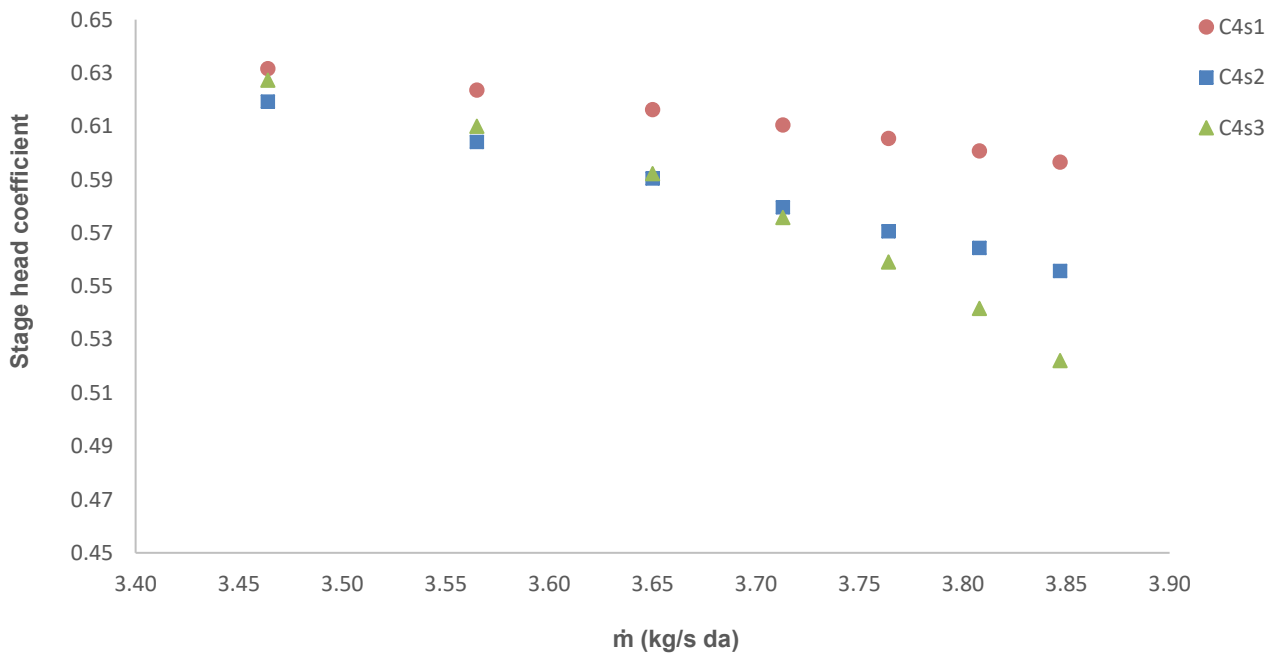


Figure B-8: Compressor 4, head coefficients

B-2 Maximum head coefficient and isentropic efficiency modelled as a function of non-dimensional parameters

In this appendix, the maximum head coefficient and isentropic efficiency of the 13 stages for which data were obtained (Table 1) are plotted as a function of their non-dimensional flow rates (equation 2.13) and tip speed Mach numbers (equation 2.19).

The maximum stage isentropic efficiency represents the actual maximum and is not defined at the compressors surge flow rate, as is the case for the maximum pressure ratio and head coefficient (Figure 17). Figures B-9 to B-14 reveal no observable relationship exists between these parameters and the maximum stage head or the maximum isentropic efficiency.

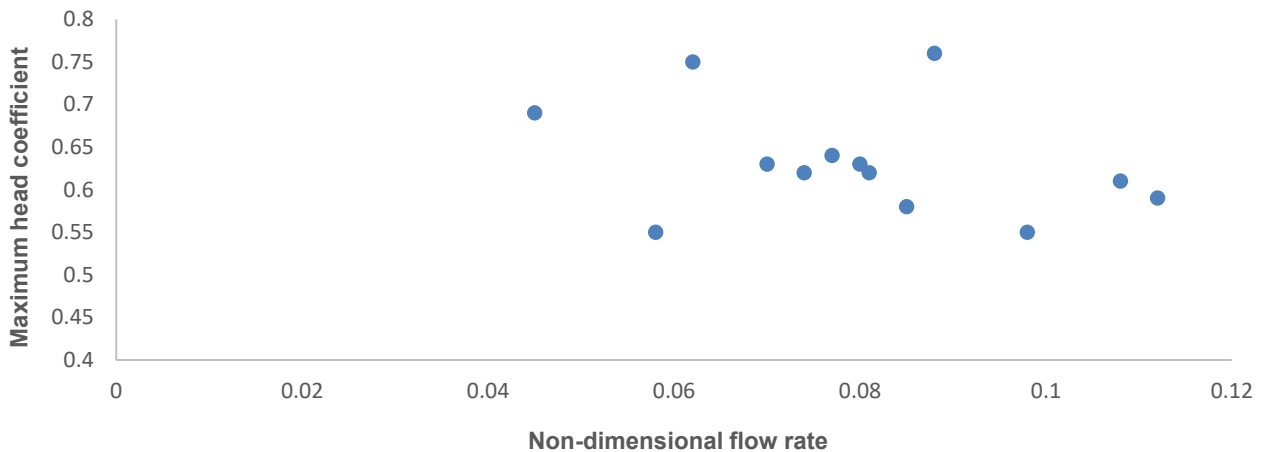


Figure B-9: Maximum stage head coefficient as a function of the non-dimensional flow rate

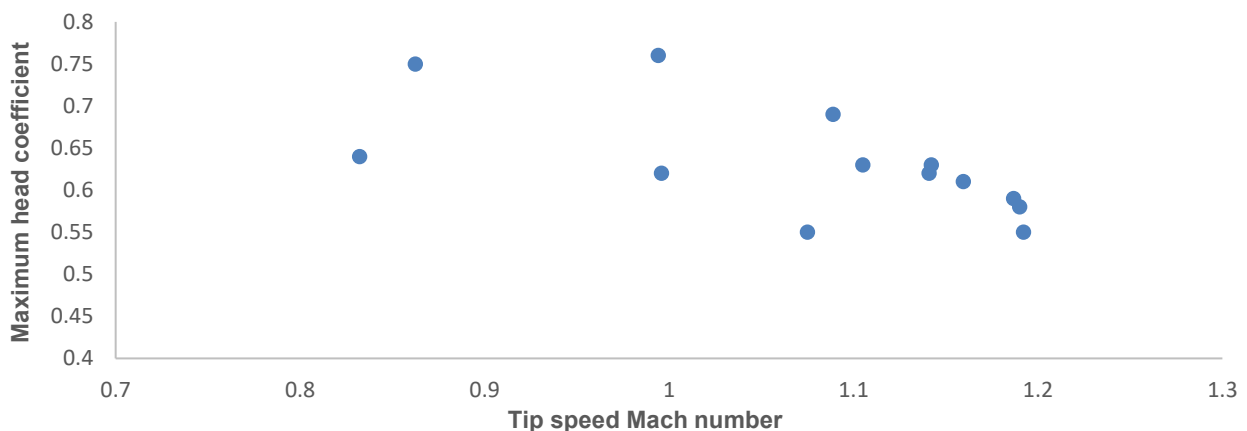


Figure B-10: Maximum stage head coefficient as a function of the Tip speed Mach number

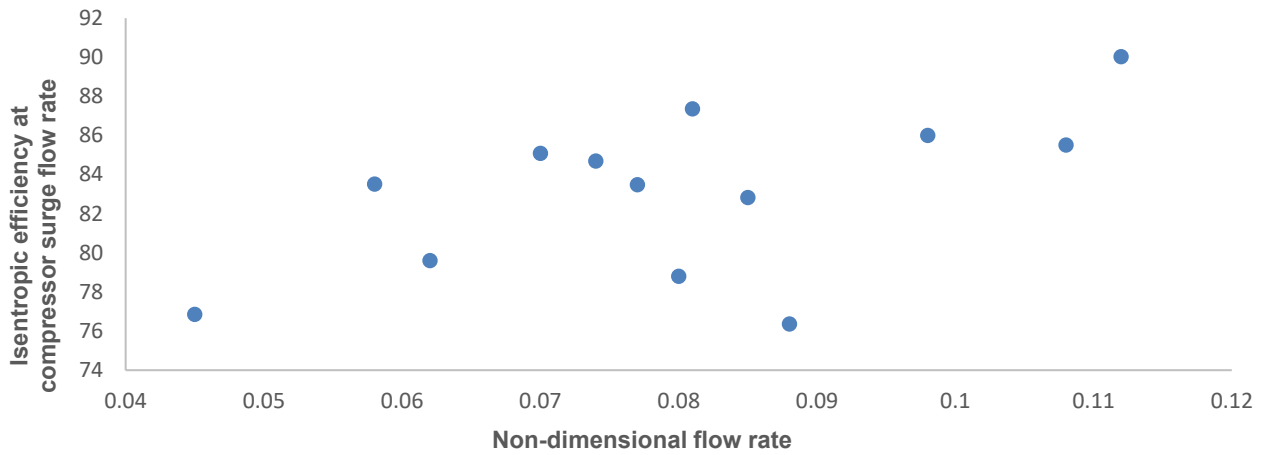


Figure B-11: Stage isentropic efficiency as a function of the non-dimensional flow rate at the compressor's surge flow rate

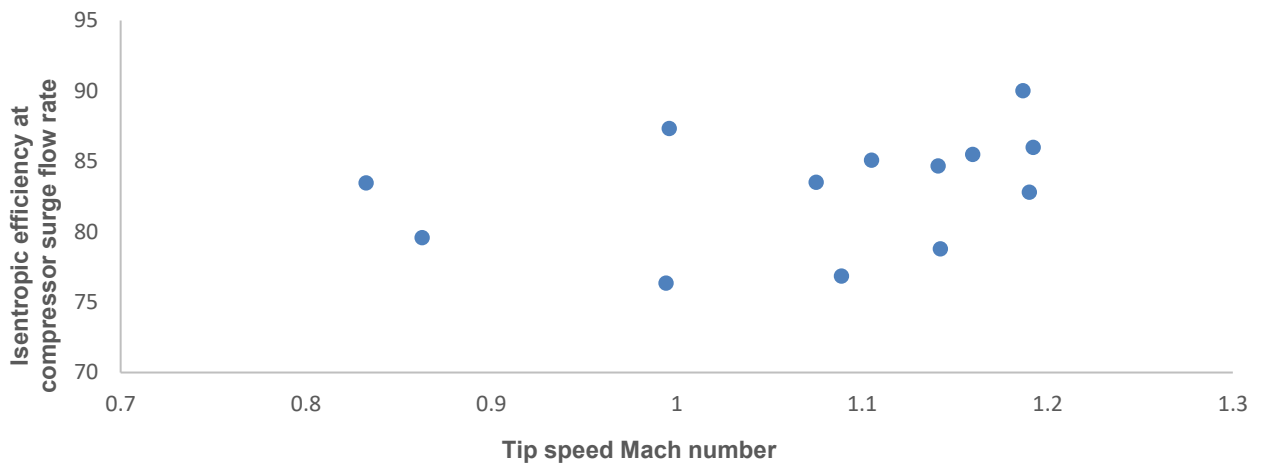


Figure B-12: Stage isentropic efficiency as a function of the tip speed Mach number at the compressor's surge flow rate

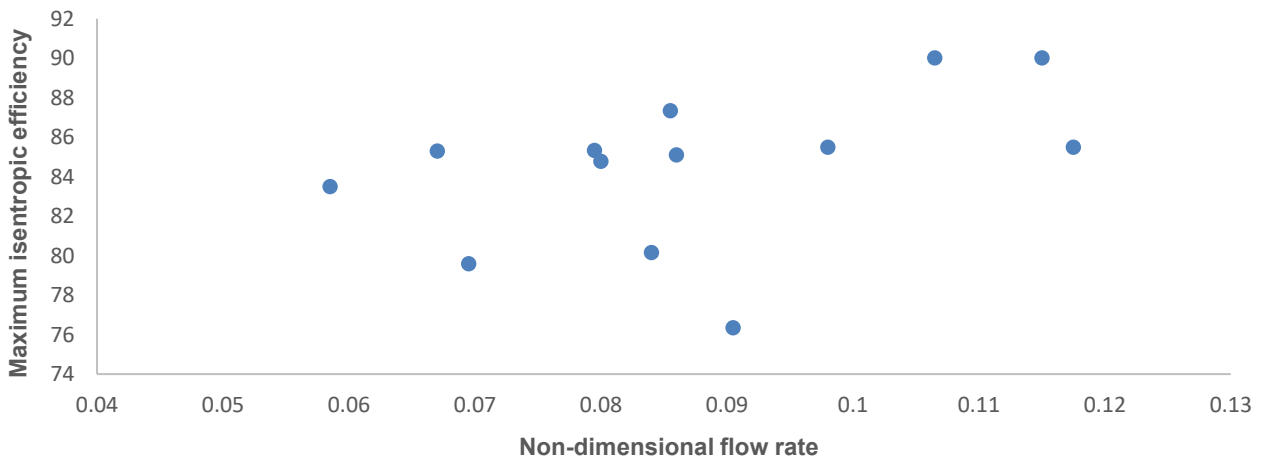


Figure B-13: Maximum stage isentropic efficiency as a function of the non-dimensional flowrate at the compressor's surge flow rate

APPENDIX B: MEASURED COMPRESSOR PERFORMANCE DATA

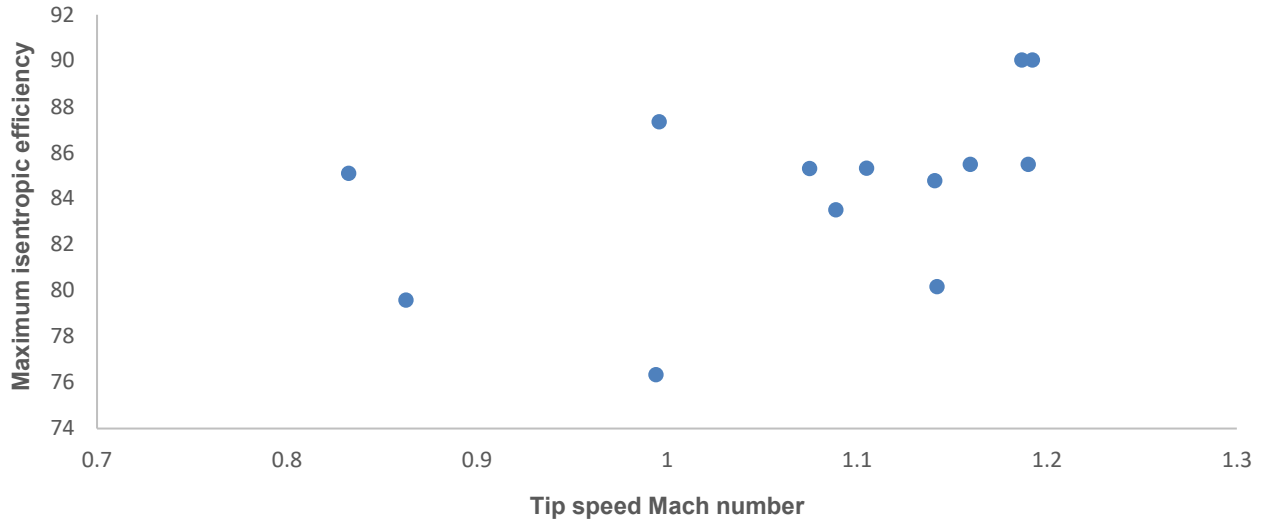


Figure B-14: *Maximum stage isentropic efficiency as a function of the tip speed Mach number at the compressor's surge flow rate*

APPENDIX C: COMPAERO[®] STAGE DESIGN AND ANALYSIS

This appendix provides the output parameters of the stage design and performance analysis conducted using the COMPAERO[®] software (section 4.2). Appendix C-1 provides the complete design geometry of the assessed impeller, and Appendix C-2 portrays the analysis output results of the COMPAERO[®] software.

C-1 Stage design outputs

I M P E L L E R D E S I G N S U M M A R Y

Inlet rms Diameter	10.74117	Tip rms Diameter	22.86000
Inlet rms Blade Angle	27.68266	Tip rms Blade Angle	63.01363
Inlet Passage Width	5.327101	Tip Passage Width	1.299654
Normal Inlet Passage Width .	5.327101	Normal Tip Passage Width ...	1.295685
Inlet rms Cone Angle	0.526939	Tip rms Cone Angle	85.37341
Inlet Hub Diameter	4.000000	Number Of Full Blades	21
Inlet Shroud Diameter	14.65420	Number Of Splitter Blades ..	0
Inlet Hub Blade Angle	48.63807	Blade Meridional Length	10.04257
Inlet Shroud Blade Angle ...	19.18930	Splitter Meridional Length .	0.000000
Inlet Blade Thickness	0.062865	Tip Blade Thickness	0.125730
Inlet Blade Rake Angle	-1.61169	Tip Blade Rake Angle	1.611691
Inlet Net Area	141.3617	Tip Net Area	89.03013
Inlet Metal Blockage	0.094384	Tip Metal Blockage	0.046143
Eye Hub Diameter	4.000000	Eye Passage Area	156.0945
Eye Shroud Diameter	14.65420	Est. Throat Area	76.57449
Inlet rms Mach no.	0.273339	Tip rms Mach No.	0.736746
Inlet rms Rel. Mach No.	0.546593	Tip rms Rel. Mach No.	0.360880
Inlet Shroud Rel. Mach No. .	0.701288	Tip Flow Angle	21.53000
Blade Loading, (Ws-Wp)/Wav .	0.769159	Rel. Velocity Ratio, W2/W1 .	0.719593
Inlet rms Flow Angle	30.00511	Inlet rms Incidence Angle ..	-2.32245
Inlet Hub Incidence Angle ..	-8.54475	Inlet Shroud Incidence Angle	-3.75223
Tip width/meridional length	0.129019	Impeller Distortion Factor .	1.132469
Impeller axial length	6.575565	Leakage-to-inlet flow ratio	0.000000

APPENDIX C: COMPAERO^R STAGE DESIGN AND ANALYSIS

V A N E D D I F F U S E R D E S I G N S U M M A R Y

Vane Inlet Diameter	24.83022	Vane Discharge Diameter	35.49463
Inlet Passage Width	1.295259	Discharge Passage Width	1.295259
Inlet Vane Angle	21.25428	Discharge Vane Angle	37.48980
Inlet Vane Thickness	0.062076	Discharge Vane Thickness ...	0.124151
Vane Inlet Net Area	96.60253	Vane Discharge Net Area	139.1495
Inlet Metal Blockage	0.043904	Discharge Metal Blockage ...	0.082463
Est. Throat Area	40.02348	Vaneless Space Width Ratio .	0.996618
Number Of Vanes	20.00000	Vaneless Space Radius Ratio	1.086186
Vane Inlet Flow Angle	21.75428	Vane Discharge Flow Angle ..	34.16722
Vane Mean Blade Angle	29.78394	Effectiveness Parameter, E .	1.618366
Vane Area Ratio	2.400000	Equivalent Divergence Angle	10.29997
Vane Radius Ratio	1.429493	Vane Loading Parameter	0.279700
Incidence Angle	-.500000		

C R O S S O V E R B E N D D E S I G N S U M M A R Y

Inlet Diameter	37.26936	Exit Diameter	37.26936
Inlet Passage Width	1.295259	Discharge Passage Width	2.018063
Outer Wall Total Axial Length	6.454633	Outer Wall Radial Height ...	2.865914
Inner Wall Arc Radius	1.570656	Overall Area Ratio	1.558039

R E T U R N C H A N N E L D E S I G N S U M M A R Y

Inlet Vane Angle	29.31415	Discharge Vane Angle	90.00000
Inlet Vane Thickness	0.251460	Discharge Vane Thickness ...	0.251460
Maximum Vane Thickness	1.005840	Vane Mean Blade Angle	72.21324
Inlet Passage Width	2.018063	Discharge Passage Width	3.981382
Vane Inlet Net Area	217.6284	Vane Discharge Net Area	125.5664
Throat Area	105.1998	Throat Vane-To-Vane Width ..	2.896060
Vane Exit Hub Diameter	8.664480	Vane Exit Shroud Diameter ..	14.29500
Number Of Vanes	18.00000	Incidence Angle	4.000000
Stage Exit Hub Diameter	4.000000	Stage Exit Passage Width ...	3.981383
Stage Exit Shroud Diameter ..	11.96277	Stage Exit Area	99.83019
Stage Axial Length	15.71632	Stage Maximum Diameter	43.00119
Stage Minimum Diameter	4.000000		

C-2 Stage performance analysis outputs

Stage Operating Conditions - Speed = 28987 rpm, Tip Speed = 347 m/s

Inlet Flow Coeff	0.0720	0.0765	0.0810	0.0855	0.0900	0.0923	0.0945	0.0968
Inlet Mass Flow	1.1916	1.2661	1.3406	1.4150	1.4895	1.5268	1.5640	1.6012
Inlet Volume Flow	3691.1	3921.8	4152.5	4383.2	4613.9	4729.2	4844.6	4959.9
Inlet Total Pressure	100.00	100.00	100.00	100.00	100.00	100.00	100.00	100.00
Inlet Total Temperature	300.00	300.00	300.00	300.00	300.00	300.00	300.00	300.00
Inlet Cu	0.0000	0.0000	0.0000	0.0000	0.0000	0.0000	0.0000	0.0000

Impeller Performance

Inlet Flow Coeff	0.0720	0.0765	0.0810	0.0855	0.0900	0.0923	0.0945	0.0968
Rotational Mach No.	1.0000	1.0000	1.0000	1.0000	1.0000	1.0000	1.0000	1.0000
Equivalent Tip Speed	347.18	347.18	347.18	347.18	347.18	347.18	347.18	347.18
rms Incidence	3.1624	1.7544	0.3655	-1.004	-2.354	-3.022	-3.685	-4.343
Inducer Stall (If > 1)	0.9916	0.9320	0.8780	0.8281	0.7817	0.7595	0.7377	0.7161
W2/W1 (rms)	0.6429	0.6658	0.6888	0.7126	0.7374	0.7499	0.7625	0.7756
Deq	1.7994	1.7446	1.6928	1.6427	1.6152	1.5917	1.5687	1.5460
Loading Parameter, DW/W	0.8175	0.7897	0.7621	0.7344	0.7188	0.7051	0.6915	0.6778
Throat A/A*	1.5803	1.4873	1.4047	1.3308	1.2642	1.2334	1.2040	1.1760
Throat Blockage	0.0748	0.0748	0.0748	0.0748	0.0748	0.0748	0.0748	0.0748
Inlet rms Cm	74.364	79.260	84.205	89.205	94.263	96.815	99.384	101.97
Inlet rms Cu	0.0000	0.0000	0.0000	0.0000	0.0000	0.0000	0.0000	0.0000
Inlet rms C	74.364	79.260	84.205	89.205	94.263	96.815	99.384	101.97
Inlet rms W	179.18	181.27	183.49	185.83	188.32	189.61	190.93	192.29
Inlet rms M'	0.5188	0.5252	0.5320	0.5392	0.5468	0.5508	0.5549	0.5591
Inlet rms Pt	100.00	100.00	100.00	100.00	100.00	100.00	100.00	100.00
Inlet rms P	96.823	96.397	95.940	95.452	94.931	94.658	94.377	94.087
Shroud Incidence	-5.154	-6.555	-7.937	-9.300	-10.64	-11.31	-11.97	-12.63
Inlet Shroud Cm	100.63	107.25	113.94	120.71	127.55	131.01	134.48	137.98
Inlet Shroud W	244.12	246.92	249.90	253.06	256.39	258.13	259.91	261.74
Inlet Shroud M'	0.7096	0.7186	0.7282	0.7384	0.7492	0.7548	0.7606	0.7666
Hub Incidence	10.248	8.4578	6.7407	5.0939	3.5145	2.7493	1.9997	1.2656
Inlet Hub Cm	48.102	51.268	54.467	57.701	60.973	62.624	64.285	65.958

Inlet Flow Coeff	0.0720	0.0765	0.0810	0.0855	0.0900	0.0923	0.0945	0.0968
Inlet Hub W	77.456	79.462	81.562	83.756	86.043	87.221	88.421	89.645
Inlet Hub M'	0.2237	0.2295	0.2357	0.2421	0.2488	0.2522	0.2557	0.2593
Tip Flow Coeff	0.2303	0.2457	0.2616	0.2783	0.2952	0.3042	0.3135	0.3230
Tip Cm	76.579	81.685	86.935	92.459	98.267	101.26	104.33	107.48
Tip Cu	263.96	261.53	259.00	256.32	253.46	251.99	250.48	248.92
Tip C	274.85	273.99	273.20	272.49	271.84	271.57	271.34	271.13
Tip M	0.7284	0.7267	0.7254	0.7242	0.7233	0.7231	0.7230	0.7229
Tip Flow Angle	16.178	17.345	18.554	19.835	21.192	21.893	22.613	23.353
Tip Pt	242.24	240.50	238.50	235.95	232.95	231.35	229.68	227.93
Tip Tt	393.88	392.92	391.95	390.92	389.86	389.31	388.74	388.16
Tip P	170.24	169.27	168.07	166.45	164.47	163.38	162.22	160.99
Tip V	0.5979	0.6003	0.6034	0.6079	0.6138	0.6172	0.6207	0.6246
Distortion Factor	1.2242	1.2105	1.1986	1.1880	1.1818	1.1775	1.1734	1.1695
Work Coeff	0.7843	0.7763	0.7682	0.7596	0.7507	0.7461	0.7414	0.7365

APPENDIX C: COMPAERO^R STAGE DESIGN AND ANALYSIS

Blade Work Coeff	0.7608	0.7538	0.7465	0.7388	0.7305	0.7263	0.7219	0.7174
Disk Fric Work Coeff ..	0.0120	0.0112	0.0106	0.0099	0.0094	0.0091	0.0088	0.0086
Recirc. Work Coeff	0.0000	0.0000	0.0000	0.0000	0.0000	0.0000	0.0000	0.0000
Leakage Work Coeff	0.0115	0.0113	0.0111	0.0109	0.0109	0.0107	0.0106	0.0105
Inlet LC	0.0000	0.0000	0.0000	0.0000	0.0000	0.0000	0.0000	0.0000
Incidence LC	0.0419	0.0437	0.0527	0.0682	0.0898	0.1027	0.1170	0.1324
Inducer Diff LC.....	0.0338	0.0193	0.0050	0.0000	0.0000	0.0000	0.0000	0.0000
Choke LC	0.0000	0.0000	0.0000	0.0000	0.0000	0.0000	0.0000	0.0000
Skin Friction LC	0.2060	0.2073	0.2087	0.2104	0.2118	0.2128	0.2139	0.2151
Blade Loading LC	0.0306	0.0293	0.0281	0.0268	0.0261	0.0255	0.0248	0.0242
Hub-Shroud Loading LC .	0.0436	0.0449	0.0461	0.0474	0.0482	0.0489	0.0496	0.0503
Crit. Mach No. LC	0.0000	0.0000	0.0000	0.0000	0.0000	0.0000	0.0000	0.0000
Wake Mixing LC	0.0005	0.0006	0.0006	0.0007	0.0008	0.0008	0.0008	0.0009
Blockage LC	0.0025	0.0027	0.0028	0.0030	0.0025	0.0027	0.0028	0.0030
Clearance LC	0.0564	0.0561	0.0556	0.0550	0.0552	0.0548	0.0543	0.0539
Total LC	0.4152	0.4038	0.3997	0.4116	0.4344	0.4481	0.4633	0.4797
Impeller Mass Flow	1.1916	1.2661	1.3406	1.4150	1.4895	1.5268	1.5640	1.6012
ASME Re x 10 ⁻⁵	2.8325	2.8325	2.8325	2.8325	2.8325	2.8325	2.8325	2.8325
Static Ad Head Coeff ..	0.4107	0.4059	0.4000	0.3920	0.3821	0.3766	0.3708	0.3645
Adiabatic Head Coeff ..	0.7193	0.7127	0.7050	0.6952	0.6836	0.6773	0.6707	0.6638
Adiabatic Efficiency ..	0.9172	0.9181	0.9178	0.9153	0.9105	0.9078	0.9047	0.9013
Polytropic Head Coeff .	0.7269	0.7200	0.7122	0.7025	0.6910	0.6849	0.6785	0.6717
Polytropic Efficiency .	0.9268	0.9275	0.9272	0.9248	0.9205	0.9179	0.9151	0.9120

APPENDIX D: IMPELLER GEOMETRY

This appendix outlines the measured geometry of impellers used in IGCCs similar to those used in the coal-fired power generation industry of South Africa. The measurements were taken at a manufacturer workshop of impellers available on that specific day. The impellers do not correspond to the stages for which performance data were obtained (Appendix B).

Appendix D-1 Table D-1 presents the measured design parameters. Appendix D-2 reveals the values of applicable design parameters when scaled using the impeller tip diameter. Appendix D-3 depicts average values for all design parameters as well as the maximum calculated deviation of each parameter.

D-1 Measured Impeller geometry

Table D-1 displays the measurements of the ten impellers used in three IGCCs (2 x 3 stage and 1 x 4 stage IGCCs). The compressor stages all consist of a semi-open impeller in conjunction with a vaned diffusor, such as the ones used in the coal-fired power generation industry of South Africa. Compressor 5 was manufactured in the 2000s with compressors 6 and 7 manufactured in the 1980s and 1970s, respectively.

Table D-1: Measured impeller geometry

Parameter	C5			C6			C7			
	s1	s2	S3	s1	s2	s3	s1	s2	s3	s4
α_{c1}	0.04	0.05	0.05	0.05	0.06	0.06	0.04	0.06	0.06	0.04
α_{c2}	1.49	1.48	1.49	1.49	1.48	1.48	1.48	1.49	1.48	1.48
$\beta_{1B,h}$	35	24	15	40	35	45	35	40	30	26
$\beta_{1B,sh}$	35	28	20	23	35	45	35	20	30	20
β_{2B}	55	55	43	60	65	65	62	47	65	60

APPENDIX D: MEASURED IMPELLER GEOMETRY

b_2	18	12	7.8	11.3	8.6	4	6.1	5.2	3	2.35
d_{1h}	40	27	26	40	40	28	50	50	43	30
d_{1sh}	140	100	80	115	85	55	135	100	75	65
d_2	221	150	140	188	155	125	240	175	135	124
L_{FB}	110	70	71	85	70	45	105	60	50	45
L_{SB}	0	0	45	0	0	35	0	0	0	0
t_{1h}	1.5	2	2	1.2	1.2	2.3	2.2	2.2	2.2	2.2
t_{1sh}	1.5	1	1	1.2	1.2	2.3	1.2	1.2	1.3	1.3
t_{2h}	5.5	3.8	4.3	5	3.3	4	6.1	5.2	3	2.35
t_{2sh}	2	2	1.5	2	2	1.5	2	2.6	2	1.5
z_{FB}	16	16	18	17	17	9	19	15	14	17
z_{SB}	0	0	11	0	0	0	0	0	0	0
z	16	16	18	17	17	9	19	15	14	17

D-2 Scaled impeller design parameters

Table D-2 portrays the values of applicable impeller design parameters when scaled as a function of its tip diameter.

Table D-2: Value of scaled impeller parameters (x100)

Parameter	C5			C6			C7			
	s1	s2	s3	s1	s2	s3	s1	s2	s3	s4
$\frac{b_2}{d_2}$	8.14	8.00	5.57	6.01	5.55	3.20	4.08	4.20	2.88	4.83
$\frac{d_{1h}}{d_2}$	18.09	18.00	18.57	21.27	25.80	22.40	20.83	28.57	31.85	24.19
$\frac{d_{1sh}}{d_2}$	63.34	66.66	57.14	61.17	54.84	44.04	56.25	57.14	55.55	52.41
$\frac{L_{FB}}{d_2}$	49.77	46.66	50.71	45.21	45.16	36.00	43.75	34.29	37.03	36.29
$\frac{t_{1h}}{d_2}$	0.67	1.33	1.42	0.63	0.77	1.84	0.91	1.25	1.62	1.77
$\frac{t_{1sh}}{d_2}$	0.67	0.66	0.70	0.60	0.74	1.42	0.85	1.21	1.05	1.12
$\frac{t_{2h}}{d_2}$	2.52	2.34	3.12	2.73	2.14	3.20	2.51	3.01	2.24	1.93
$\frac{t_{2sh}}{d_2}$	0.90	0.13	1.07	1.06	1.29	1.20	0.833	1.49	1.48	1.21

D-3 Average and maximum design parameter variation

The average values of the impeller design parameters are calculated through Equation D.3.1

$$\bar{u}_n = \frac{\sum_{j=1}^{10} u_{n,j}}{10} \quad \text{D.3.1}$$

with n representing the parameter considered and j the stage to which the parameter corresponds. The maximum variation of a parameter is computed as the difference between the average value and the maximum outlier through equation D.3.2.

$$\Delta u_{n,\max} = \left| \frac{\bar{u}_n - u_{n,\max}}{\bar{u}_n} \right| \quad \text{D.3.2}$$

Table D-3: Value of average and maximum design parameter deviation (x100)

Parameter u	Average value \bar{u}	Maximum variation from average value u_{\max}	Maximum relative variation from average value (%) Δu_{\max}
$\frac{b_2}{d_2}$	5.25	2.88 (C7s3)	45
$\frac{d_{1h}}{d_2}$	22.95	31.85 (C7s3)	28
$\frac{d_{1sh}}{d_2}$	56.85	44.04 (C6s3)	23
$\frac{L_{FB}}{d_2}$	42.49	34.29 (C7s2)	19
$\frac{t_{1h}}{d_2}$	1.22	0.63 (C6s1)	48

APPENDIX D: MEASURED IMPELLER GEOMETRY

$\frac{t_{1sh}}{d_2}$	0.935	1.42 (C6s3)	52
$\frac{t_{2h}}{d_2}$	2.57	1.93 (C7s4)	25
$\frac{t_{2sh}}{d_2}$	1.75	0.83 (C7s1)	53
α_{c1}	0.06	0.04 (C5s1)	33
α_{c2}	1.48	1.49 (C5s1)	0.6
$\beta_{1B,h}$	33	15.00 (C5s3)	55
$\beta_{1B,sh}$	29.1	45.00 (C6s3)	55
β_{2B}	57.5	43.0 (C5s3)	25
z	16.5	9.0 (C6s3)	45

APPENDIX E: IMPELLER PERFORMANCE MODEL SENSITIVITY ANALYSIS

In this appendix, the importance of different input parameters in terms of their effect on the prediction accuracy of the 1-dimensional impellers analysis model of Aungier (2000) is assessed. For the stage designed in section 4.2 for which the complete design geometry is shown in Appendix C-1, a sensitivity analysis was conducted at the stage surge flow rate (1.192 kg/s).

E-1 Pressure ratio and head coefficient sensitivity analysis

The sensitivity analysis procedure is discussed in section 4.3. Table E-1 provides the outputs of the sensitivity analysis procedure.

Table E-1: Pressure ratio sensitivity analysis

u	$\frac{\partial(\Pi_{\max})}{\partial(u)}$	$\frac{\partial(\psi_{\max})}{\partial(u)}$	Δu_{\max} (%)	% contribution to the total prediction accuracy of uncertainty for max. pressure ratio	% contribution to the total prediction accuracy uncertainty for max. head coefficient
α_{c1}	0.0600	0.0028	45	0	0
α_{c2}	-0.0600	-0.0028	28	0.06	0
$\beta_{1B,h}$	-8.35 E-04	-3.96 E-05	23	1.01	0.01
$\beta_{1B,sh}$	-9.16 E-04	-4.34 E-05	19	0.19	0
β_{2B}	0.0981	0.0046	48	48.75	55.20
$\frac{b_2}{d_2}$	5.5350	2.3570	52	34.53	33.61

APPENDIX E: IMPELLER PERFORMANCE MODEL SENSITIVITY ANALYSIS

$\frac{d_{1h}}{d_2}$	0.0966	0.0049	25	0.08	0
$\frac{d_{1sh}}{d_2}$	-9.24 E-09	-3.107 E-10	53	0	0
$\frac{L_{FB}}{d_2}$	0.2679	0.0159	33	1.10	0.02
t_{1h}	0.6018	-0.0042	0.6	0	0
t_{1sh}	0.6019	-0.0042	55	0	0
t_{2h}	-2.178	-0.8715	55	0.02	0.02
t_{2sh}	-2.166	-0.8667	25	0.09	0.07
z	0.0088	0.0035	45	14.17	11.10

APPENDIX F: STAGE STACKING PROCEDURE VALIDATION

This appendix provides the results of the developed stage stacking procedure used to model stage performance for compressors 1-4 (Table 1).

F-1 Compressor 1

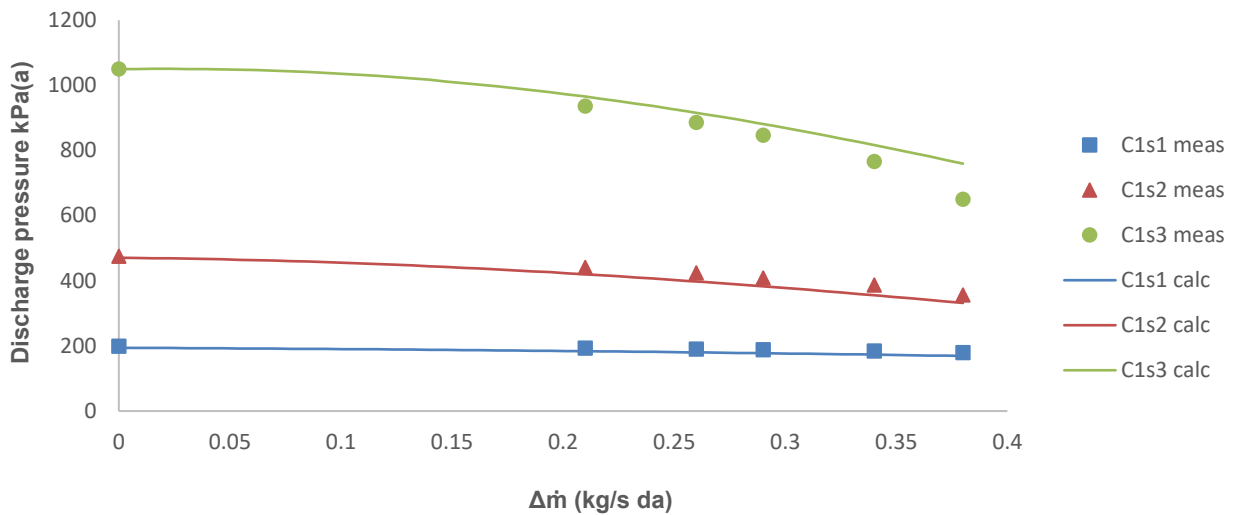


Figure F-1: Compressor 1, calculated versus measured stage total discharge pressure

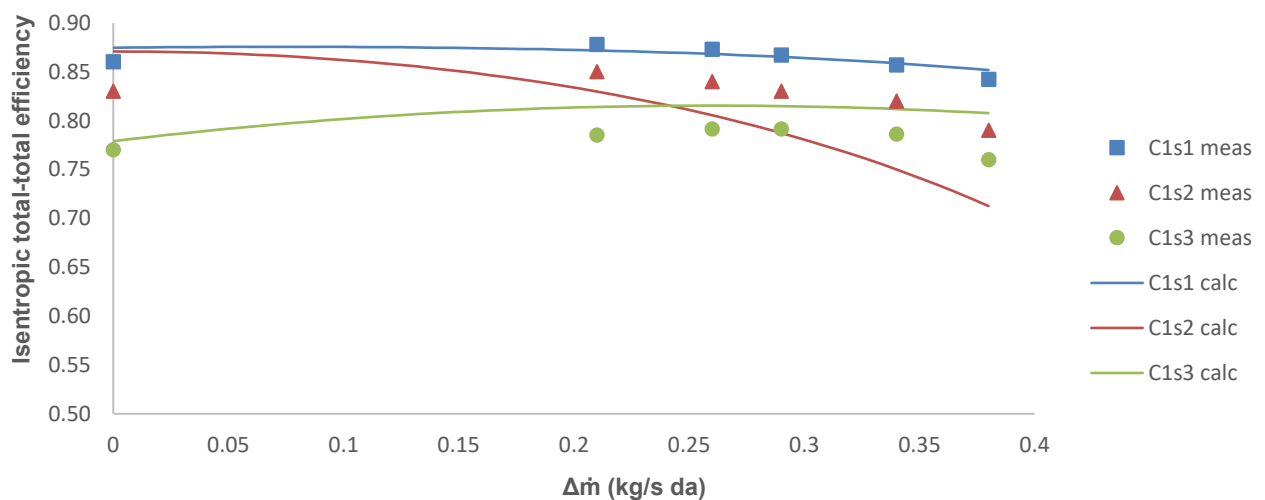


Figure F-2: Compressor 1, calculated versus measured stage isentropic efficiency

APPENDIX F: STAGE STACKING PROCEDURE VALIDATION RESULTS

Table F-1: Compressor 1, stage discharge pressure calculation results

Stage no.	$\Delta\dot{m}$	0	0.21	0.26	0.29	0.34	0.38
1	Measured	198.72	193.11	190.22	187.62	184.17	179.32
	Calculated	194.12	183.91	179.83	177.95	172.95	169.15
	Relative percentage deviation (%)	2.32	4.72	5.47	5.17	6.08	5.69
2	Measured	475.47	440.12	424.15	408.46	386.71	355.93
	Calculated	470.21	420.23	396.15	384.51	355.42	331.91
	Relative percentage deviation (%)	1.09	4.52	6.60	5.85	8.20	6.74
3	Measured	1050.00	935.52	885.51	846.27	765.67	650.34
	Calculated	1050.05	965.91	911.82	885.05	815.21	702.32
	Relative percentage deviation (%)	1.17	3.70	3.06	2.93	3.26	6.26

APPENDIX F: STAGE STACKING PROCEDURE VALIDATION RESULTS

Table F-2: Compressor 1, stage isentropic efficiency calculation results

Stage no.	$\Delta\dot{m}$	0	0.21	0.26	0.29	0.34	0.38
1	Measured	0.860	0.878	0.873	0.867	0.857	0.842
	Calculated	0.875	0.872	0.869	0.865	0.859	0.852
	Absolute percentage deviation (%)	1.500	0.600	0.400	0.200	0.200	1.000
2	Measured	0.831	0.852	0.845	0.836	0.823	0.794
	Calculated	0.871	0.830	0.808	0.784	0.749	0.713
	Absolute percentage deviation (%)	4.000	2.200	3.700	5.200	7.400	8.100
3	Measured	0.770	0.785	0.791	0.792	0.786	0.760
	Calculated	0.779	0.814	0.815	0.815	0.812	0.808
	Absolute percentage deviation (%)	0.900	2.900	2.400	2.300	2.600	4.800

F-2 Compressor 2

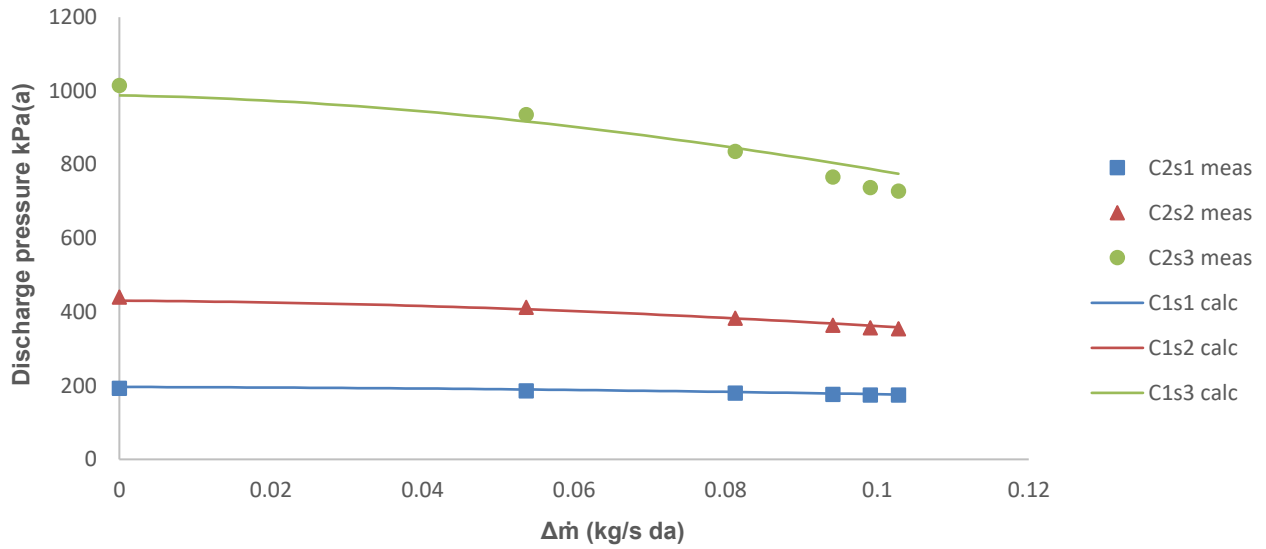


Figure F-3: Compressor 2, calculated versus measured stage total discharge pressure

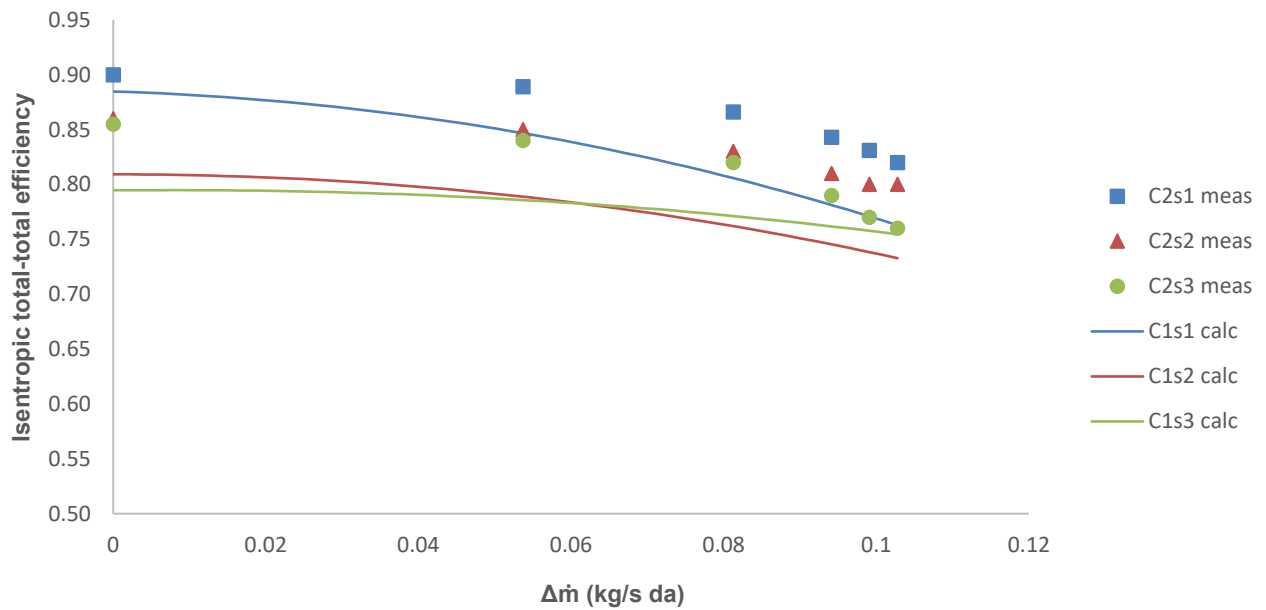


Figure F-4: Compressor 2, calculated versus measured stage isentropic efficiency

APPENDIX F: STAGE STACKING PROCEDURE VALIDATION RESULTS

Table F-3: Compressor 2, stage discharge pressure calculation results

Stage no.	$\Delta\dot{m}$	0	0.054	0.081	0.094	0.010	0.103
1	Measured	193.10	186.03	179.84	176.32	175.14	174.72
	Calculated	196.51	189.93	182.64	178.75	177.33	175.81
	Relative percentage deviation (%)	1.76	2.10	1.60	1.36	1.26	0.63
2	Measured	441.01	413.45	383.42	364.63	357.48	354.92
	Calculated	430.75	408.06	382.12	384.03	363.52	358.43
	Relative percentage deviation (%)	2.34	1.30	0.34	5.32	1.71	0.99
3	Measured	1015.02	935.61	836.02	766.37	737.95	728.24
	Calculated	987.71	918.82	843.15	803.74	789.63	715.51
	Relative percentage deviation (%)	2.69	1.80	0.86	4.88	7.00	1.74

APPENDIX F: STAGE STACKING PROCEDURE VALIDATION RESULTS

Table F-4: Compressor 2, stage isentropic efficiency calculation results

Stage no.	$\Delta \dot{m}$	0	0.054	0.081	0.094	0.099	0.103
1	Measured	0.900	0.889	0.866	0.843	0.831	0.820
	Calculated	0.885	0.848	0.805	0.781	0.772	0.763
	Absolute percentage deviation (%)	1.520	4.070	6.100	6.210	5.890	5.710
2	Measured	0.861	0.852	0.834	0.812	0.801	0.800
	Calculated	0.809	0.790	0.762	0.745	0.739	0.733
	Absolute percentage deviation (%)	5.160	6.210	7.250	6.680	6.180	6.710
3	Measured	0.855	0.840	0.823	0.792	0.774	0.766
	Calculated	0.795	0.787	0.771	0.762	0.758	0.755
	Absolute percentage deviation (%)	6.030	5.350	5.200	3.030	1.570	1.140

F-3 Compressor 3

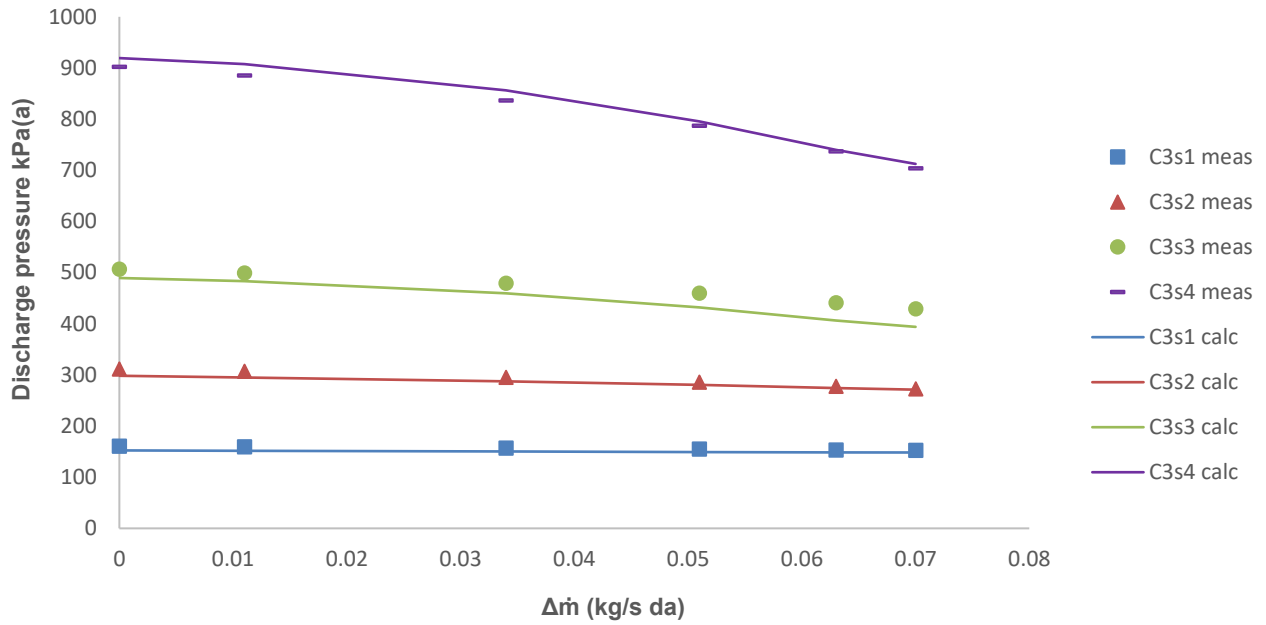


Figure F-5: Compressor 2, calculated versus measured stage total discharge pressure

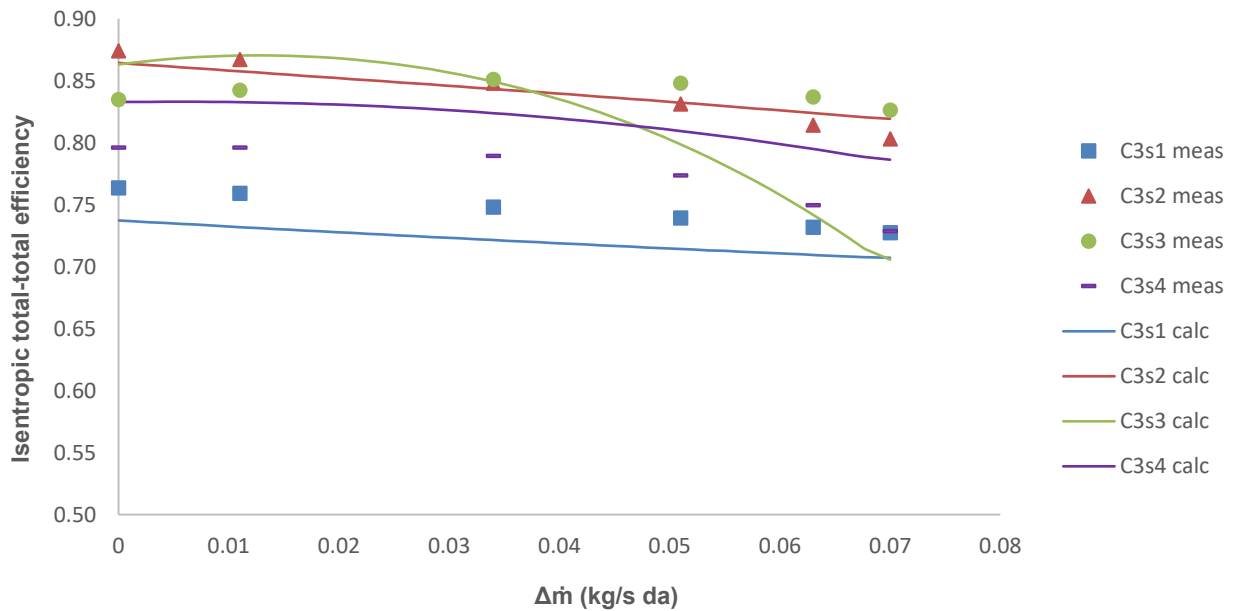


Figure F-6: Compressor 3, calculated versus measured stage isentropic efficiency

APPENDIX F: STAGE STACKING PROCEDURE VALIDATION RESULTS

Table F-5: Compressor 3, stage discharge pressure calculation results

Stage no.	Δm	0	0.011	0.034	0.051	0.063	0.07
1	Measured	160.12	159.20	156.53	154.58	152.92	152.03
	Calculated	152.42	151.83	150.47	149.41	148.76	148.33
	Relative percentage deviation (%)	4.81	4.53	3.90	3.30	2.75	2.43
2	Measured	311.32	306.56	294.91	285.37	277.23	272.41
	Calculated	298.33	295.26	287.51	280.32	274.17	271.16
	Relative percentage deviation (%)	4.18	3.69	2.51	1.75	1.12	0.48
3	Measured	506.41	499.26	478.84	459.37	440.73	428.76
	Calculated	489.41	483.32	459.46	432.01	406.56	393.9
	Relative percentage deviation (%)	3.40	3.19	4.05	5.94	7.76	8.12
4	Measured	901.72	885.16	836.23	786.71	736.95	703.57
	Calculated	919.33	907.41	856.04	795.56	739.81	712.43
	Relative percentage deviation (%)	1.95	2.52	2.37	1.12	0.39	1.27

APPENDIX F: STAGE STACKING PROCEDURE VALIDATION RESULTS

Table F-6: Compressor 3, stage isentropic efficiency calculation results

Stage no.	Δm	0	0.011	0.034	0.051	0.063	0.07
	Measured	0.764	0.759	0.748	0.739	0.732	0.727
	Calculated	0.755	0.749	0.737	0.728	0.721	0.718
	Absolute percentage deviation (%)	0.880	1.020	1.100	1.110	1.060	0.930
2	Measured	0.874	0.867	0.848	0.831	0.814	0.803
	Calculated	0.882	0.874	0.857	0.841	0.827	0.821
	Absolute percentage deviation (%)	0.800	0.700	0.900	1.000	1.300	1.800
3	Measured	0.8348	0.8423	0.8511	0.8478	0.8368	0.8263
	Calculated	0.865	0.868	0.852	0.817	0.770	0.742
	Absolute percentage deviation (%)	2.990	2.520	0.090	3.080	6.680	8.440
4	Measured	0.796	0.796	0.789	0.774	0.750	0.729
	Calculated	0.831	0.831	0.822	0.808	0.793	0.785
	Absolute percentage deviation (%)	3.510	3.510	3.280	3.440	4.340	5.640

F-4 Compressor 4

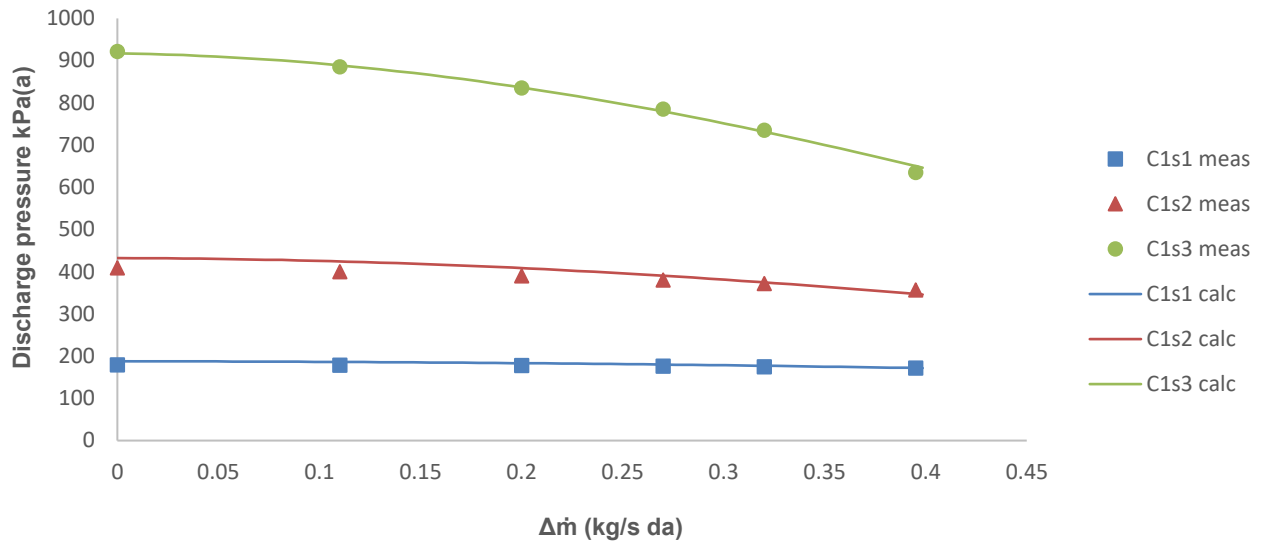


Figure F-7: Compressor 4, calculated versus measured stage total discharge pressure

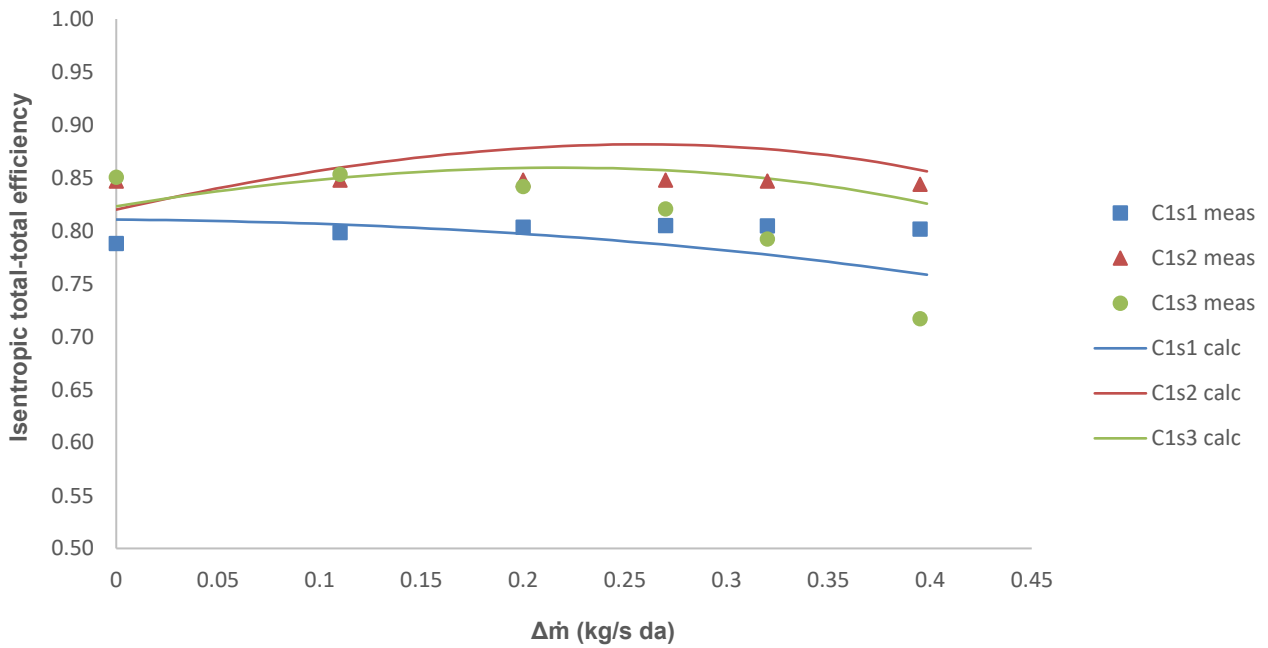


Figure F-8: Compressor 4, calculated versus measured stage isentropic efficiency

APPENDIX F: STAGE STACKING PROCEDURE VALIDATION RESULTS

Table F-7: Compressor 4, stage discharge pressure calculation results

Stage no.	Δm	0	0.11	0.20	0.27	0.32	0.40
1	Measured	179.31	178.94	177.71	176.36	174.92	172.05
	Calculated	187.93	186.42	183.21	180.15	177.32	171.72
	Relative percentage deviation (%)	4.80	4.19	3.10	2.16	1.37	0.17
2	Measured	409.01	400.12	389.93	380.76	372.34	357.02
	Calculated	432.32	425.04	407.83	391.02	375.71	345.82
	Relative percentage deviation (%)	3.19	1.23	3.22	3.95	3.60	1.45
3	Measured	921.92	885.23	835.23	785.01	735.12	635.34
	Calculated	917.21	890.76	834.12	781.26	734.64	646.34
	Relative percentage deviation (%)	0.511	0.605	0.133	0.565	0.083	1.730

APPENDIX F: STAGE STACKING PROCEDURE VALIDATION RESULTS

Table F-8: Compressor 4, stage isentropic calculation results

Stage no.	Δm	0	0.11	0.20	0.27	0.32	0.40
1	Measured	0.788	0.799	0.803	0.805	0.805	0.802
	Calculated	0.811	0.806	0.797	0.787	0.778	0.759
	Absolute percentage deviation (%)	2.260	0.760	0.670	1.780	2.670	4.320
2	Measured	0.847	0.848	0.848	0.848	0.847	0.844
	Calculated	0.820	0.858	0.875	0.882	0.878	0.856
	Absolute percentage deviation (%)	2.700	1.040	2.730	3.350	3.050	1.220
3	Measured	0.851	0.853	0.842	0.821	0.792	0.717
	Calculated	0.823	0.849	0.859	0.857	0.850	0.826
	Absolute percentage deviation (%)	2.770	0.410	1.750	3.650	5.780	10.840